Investigating New Physics with High Power Lasers

Konstantin Beyer

Merton College

University of Oxford

A thesis submitted for the degree of

Doctor of Philosophy

Trinity 2021

Acknowledgements

This doctoral project was made possible by funding by the EPSRC and the Oxford Center for High Energy Density Science (OxCHEDS), British Crown Copyright 2021/AWE. I am grateful to the Niels Bohr Institute in Copenhagen and the Instituto Superior Técnico in Lisbon for their hospitality.

I would like to thank my supervisor Gianluca Gregori for his tireless energy, his support and for pushing me to publish my work. Without his initiative, I might still be waiting for the 'right time'. Our collaboration has given me a thorough understanding of the work of a researcher and has put me a step closer to being one. I would like to thank my supervisor Subir Sarkar for his constant availability, enthusiasm and his guidance. His directedness came in the way of me developing many a gray hair, and his deep insights and critical eye made me grow as a scientist. Our discussions, too, provided me with countless insights, invaluable feedback, and a thorough education as a researcher.

My thanks go to all my collaborators during the years, Archie Bott, Colin Danson, Barry Dillon and Hye-Sook Park, who helped me on my journey, making it vastly more enjoyable. I thank Bob Bingham, for his enthusiasm and support during many discussions. Ben King, for his friendliness, advice and expertise when sharing his research and working together. Brian Reville, for his insights and introducing me to his research. Giacomo Marocco, for his hard work, his intuition for Physics and critical questions uprooting any shortcomings in our work.

I would like to thank Prateek Agrawal for his expertise and interest in my research and for providing a stimulating atmosphere in the Journal Club. Of course, I thank him for organising it in the first place!

My thanks go to Eleonora Rossi for proofreading this work, and her tireless hunt for all the commas I missed.

My deep gratitude goes to all my friends and family who supported me and made life in Oxford feel like home.

My deepest gratitude goes to Arianna Cinquatti for her tireless support, for being an anchor in my life and for letting a physicist into her world.

Abstract

This thesis presents theoretical studies of different aspects of axion physics. First, we review the origin of axions from the Peccei-Quinn (PQ) solution to the problem of charge-parity (CP) non-violation in the quantum chromodynamics (QCD) sector of the standard model (SM) of particle physics. An overview of the most common direct and indirect detection efforts is then presented before three distinct, new methods are presented and put in perspective.

Chapter 2 proposes a stimulated version of light shining through wall (LSW) type searches which utilises the large photon numbers in high power laser beams to achieve strong bounds around axion masses of $m_a \sim 1\,\mathrm{eV}$. The sensitivity is evaluated and special care is taken to consider stimulation effects stemming from the large number of photons present. In chapter 3 a new axion-photon parametric decay instability is found and analysed. The coupling of a strong pump and a weaker probe pulse is found to result in an exponentially growing axion mode. The prospect for direct detection experiments is discussed and put into perspective of ongoing searches. The axion's coupling to fermions is investigated in chapter 4 in which the decay of axions to electron-positron pairs in a strong background field is investigated. The chapter starts with a review of strong field quantum electrodynamics techniques and then proceeds by applying them to the axion coupling to identify different regimes based on the axion's mass and the background field strength.

The second part of the thesis investigates the cosmological implications of including axions into the SM. A review of the standard ΛCDM cosmology is followed by a discussion of the cosmological importance of the axion by an investigation of the energy density in a coherent axion field throughout the universe which could constitute the dark matter. An investigation of topological defects formed during the symmetry breaking stages of the axion then leads to the introduction of the domain wall problem. Chapter 6 is dedicated to the solution of the domain wall problem and finishes with a lookout onto avenues for future investigations and attempts at solutions.

In defence of this thesis I declare the following published articles by the author:

– [1] **K. A. Beyer**, B. Reville, A. Bott, H.-S. Park, S. Sarkar and G. Gregori *Analytical estimates of proton acceleration in laser-produced turbulent plasmas.* J. Plasma Phys., 84(6):905840608, 2018

– [2] B. King, B. M. Dillon, **K. A. Beyer**, and G. Gregori. *Axion-like-particle decay in strong electromagnetic backgrounds.* JHEP, 12:162, 2019

– [3] **K. A. Beyer**, G. Marocco, R. Bingham, and G. Gregori. *Axion detection through resonant photon-photon collisions.* Phys. Rev. D, 101(9):095018, 2020

– [4] **K. A. Beyer**, G. Marocco, C. Danson, R. Bingham, and G. Gregori. *Parametric co-linear axion photon instability.* arXiv: 2108.01489, submitted to SciPost

– [5] **K. A. Beyer**, G. Marocco, R. Bingham, and G. Gregori. *Light-shining-through-wall axion detection experiments with a stimulating laser.* Phys. Rev. D, 105(3):035031, 2022

Statement of Originality

I declare this thesis I am submitting is entirely my own work except where otherwise indicated. I have clearly indicated the presence of all material I have quoted from other sources.

Contents

Chapter 1

A brief Axion Review

The Standard Model (SM) of particle physics is among the most successful theories of fundamental physics and, to date, it has provided explanations for almost all terrestrial experiments. Yet, despite the copious successes, it is well known that the SM is incomplete. The strong sector, QCD, does not naturally preserve CP symmetry. The QCD Lagrangian explicitly violates CP through the vacuum angle θ

$$\mathcal{L}_{\mathrm{QCD}} = \bar{q}\left(i\gamma_\mu D^\mu - \mathcal{M}_q\right) q - \frac{1}{4} G^a_{\mu\nu} G^{a,\mu\nu} - \theta \frac{g^2}{32\pi^2} G^a_{\mu\nu} \tilde{G}^{a,\mu\nu}. \tag{1.1}$$

Here $\tilde{G}^{\mu\nu} \equiv 1/2\varepsilon^{\mu\nu\rho\sigma} G_{\rho\sigma}$ stands for the dual field strength. The existence of the term was known in the early days of QCD. However, it was traditionally ignored because it can be written as a total derivative [6]. Indeed, a total derivative in the Lagrangian does not enter to any order in perturbation theory.

Today we know that the term is of topological origin and cannot be ignored [7]. Given the QCD Lagrangian (1.1), the neutron would carry an electromagnetic dipole moment (edm) directly proportional to the QCD vacuum angle [8, 9, 10]

$$d_n\left(\bar{\theta}\right) = 2.4 \times 10^{-16} \bar{\theta} \mathrm{ecm}. \tag{1.2}$$

Note that here $\bar{\theta}$ sums up all contributions to CP violation in the SM and is defined in (1.11). The neutron edm can be probed very precisely and the current best bounds require [11]

$$\bar{\theta} \leq 3.3 \times 10^{-11}. \tag{1.3}$$

So why do we not just set $\bar{\theta}$ to a small value? After all, it hardly affects any other piece of physics. Solving the problem in this way is not natural, as the SM does not gain additional symmetry. We thus would not expect this parameter to be small. The fine tuning that is required for this solution is, in fact, worse than what an initial evaluation might indicate. Let us investigate this by a careful analysis of the origin of the term and the additional contributions to the CP violation.

1.1 The Strong CP problem

The QCD Lagrangian (1.1) admits a set of global symmetry transformations. Reducing our analysis to the two lightest quark flavours $q = (u, d)$ and taking the massless limit for a second, we find classical QCD to be invariant under global $SU(2)_L \times SU(2)_R \times U(1)_V \times U(1)_A$. The left- and right-handed quark fields do not mix in this limit, hence the independent $SU(2)_L$ and $SU(2)_R$, respectively. For later convenience we can write the symmetry transformations in terms of the diagonal isospin subgroup $SU(2)_I$ and axial rotations $SU(2)_P$

$$q \to e^{i\alpha_I^a \tau^a} q, \qquad q \to e^{i\alpha_P^a \gamma^5 \tau^a} q, \qquad q \to e^{i\alpha_V} q, \qquad q \to e^{i\alpha_A \gamma^5} q. \tag{1.4}$$

Here α_x is the charge under the global symmetry group and $\tau^a = \sigma^a \otimes I$ with σ^a the $SU(2)$ generators. The usual story of spontaneous chiral symmetry breaking involves quark condensates $\langle \bar{q} q \rangle \neq 0$ which break the $SU(2)_L \times SU(2)_R$ to its diagonal isospin subgroup resulting in the pions as the Nambu-Goldstone bosons. Being more careful

we remember that the global $SU(2)_L \times SU(2)_R$ is a symmetry only in the massless limit and is explicitly broken when quarks get a mass. Since this mass, for the light quark generations, is small, the symmetry is still approximate and the pions get a small mass.

The appearance of quark condensates also spontaneously breaks the axial $U(1)_A$ but no corresponding light Nambu-Goldstone exists in the SM. Weinberg named this the "$U(1)$-Problem" [12]. A hint to the solution of this puzzle lies in the careful phrasing that *classically*, the QCD Lagrangian (1.1) is symmetric under the global $U(1)_A$. We have concluded this based on the notion that the Lagrangian is invariant. In a quantum theory observables are calculated via path integrals and the invariance of the Lagrangian is not sufficient to conclude the invariance of the observable. In general, the Jacobian $\mathcal{J}$ of the transformation has to be taken into account

$$\int [dqd\bar{q}]\, e^{i\mathcal{S}[q,\bar{q},\ldots]} \to \int [dq'd\bar{q}']\, e^{i\mathcal{S}[q',\bar{q}',\ldots]} \mathcal{J}(q',\bar{q}',A). \tag{1.5}$$

It is a well-known fact that the $U(1)_A$ is anomalous [13, 14], the Jacobian is non-trivial [15]

$$\mathcal{J}(q',\bar{q}',A) = e^{i\int \alpha_A C \frac{g^2}{32\pi^2} G^a_{\mu\nu}\tilde{G}^{a,\mu\nu} d^4x} \tag{1.6}$$

with anomaly coefficient $C = 2$ here. Hence, it was never an actual symmetry of the quantum theory.

This by itself, however, does not solve the $U(1)$-Problem. A closer investigation reveals that, despite not being invariant, the transformation of the path integral measure can be written as a total derivative. Thus, once again, we are inclined to conclude that the Jacobian is trivial and the symmetry is preserved. In 1976 't Hooft realised that the vacuum structure of QCD is much more interesting than previously appreciated [7, 16] as the theory allows for multiple vacua. While it remains true that a total derivative in the Lagrangian does not enter at any order in perturbation

theory non-perturbative effects can be important.

Requiring our theory to have finite energy restricts the gauge fields to pure gauge in the limit $r \to \infty$ such that the field strength tensor vanishes. Formally this condition is

$$\lim_{r\to\infty} A_\mu = \Omega\partial_\mu\Omega^{-1} \tag{1.7}$$

with $\Omega \in SU(3)$. Though it might be tempting to put the stronger constraint $A_\mu \to 0$, however we must remember that this choice is not gauge invariant and hence any gauge transformation of this choice will also be a valid vacuum state

$$\frac{1}{2}A^i_\mu\lambda^i \equiv A_\mu \to \Omega A_\mu\Omega^{-1} + \frac{i}{g}\Omega\partial_\mu\Omega^{-1}. \tag{1.8}$$

Here, λ^i are the generators of $SU(3)$. For convenience we will work in the $A_0 = 0$ gauge such that only spatial gauge fields remain [17]. If we take definitive boundary conditions like $\Omega \to 1$ as $r \to \infty$, we realise that each field configuration (1.7) defines a map from the large sphere S^3 at infinity to the gauge group $SU(3)$. Such maps are topologically distinct and differ in the path Ω follows when approaching unity; $\Omega \to \exp(2\pi i n)$ with n the winding number of the map. This is a topological quantity classifying the homotopy groups of the maps and given by

$$n = \int \frac{1}{32\pi^2} G^a_{\mu\nu}\tilde{G}^{a,\mu\nu} d^4x. \tag{1.9}$$

Indeed, we find that our naive choice $A_\mu \to 0$ corresponds to $n = 0$, but other, nontrivial solutions exist [18] with winding numbers $n = 0, \pm1, \pm2, ...$

Any two field configurations with winding numbers n, m with $n \neq m$ cannot be trivially transformed into one other without leaving pure gauge. In fact, considering the transition from our naive $n = 0$ vacuum $A_\mu = 0$ to the $n = 1$ soliton of [18], we find a typical tunnelling amplitude $\propto \exp(-8\pi^2/g^2)$. Hence, any perturbation theory

calculation will miss this effect precisely because small, smooth perturbations of the $A_\mu = 0$ state never reach the higher winding number states. What is then the true vacuum state of the theory? By calculating the eigenstates of the Hamiltonian, we find the true vacuum state as a superposition of the tower of winding number states

$$|\theta\rangle \equiv \sum_n e^{in\theta} |n\rangle \,. \tag{1.10}$$

Note that any two physical theories with $\theta \neq \theta$‘ are orthogonal to each other. Thus, it is sufficient to pick one $\theta \in [0, 2\pi)$ to fully define the theory.

In the language of Lagrangian path integrals, this choice of vacuum states corresponds to the addition of the θ term in the Lagrangian (1.1). Therefore, we see that the term which we introduced merely because it is not forbidden by any symmetry of the theory is actually forced upon us by the vacuum structure of $SU(3)$ gauge theories. Further, we see that this term cannot be ignored despite being a total derivative. Yet the question persists: why can't we simply choose the CP conserving vacuum $\theta = 0$ and move on?

To answer this, we ought to include the weak interactions in the form of the quark masses into our theory. In general, the quark mass matrix is complex, as the Weak interactions explicitly violate CP [19, 20]. Without loss of generality we can go to a basis in which the matrix is diagonal $\mathcal{M} = \text{diag}(m_u, m_d e^{i \arg\det(\mathcal{M})})$. To go to a physical basis with real quark masses, we perform a $U(1)_A$ rotation of the d quarks. As discussed before, this introduces the anomaly (1.6), effectively shifting the CP violating parameter

$$\bar{\theta} \equiv \theta - \arg(\det \mathcal{M}). \tag{1.11}$$

Here we see clearly that the problem is no longer that of fine tuning $\theta \sim 0$ but rather getting two distinct contributions from two separate sectors of physics to cancel better than 10^{-10}. For excellent reviews see [21, 6, 22, 23].

1.2 Peccei-Quinn solution

One particularly elegant solution to the strong CP problem was proposed by Peccei and Quinn (PQ) in 1977 [24, 25]. Here, one effectively introduces a global, chiral, spontaneously broken $U(1)_{\mathrm{PQ}}$ to the SM, which relates the different θ vacua.

Below $\Lambda_{\mathrm{QCD}} \sim \mathcal{O}(\mathrm{GeV})$, QCD undergoes a phase transition and confines. Quark condensates spontaneously break the global $SU(2)_L \times SU(2)_R$ to its diagonal $SU(2)_I$ and the pions appear as the pseudo-Nambu Goldstone bosons. They generate a $\bar{\theta}$-dependence of the vacuum energy of QCD of the form

$$V_\pi = -m_\pi^2 f_\pi^2 \sqrt{1 - \frac{4 m_u m_d}{(m_u + m_d)^2} \sin^2\left(\frac{\bar{\theta}}{2}\right)} \tag{1.12}$$

with m_π the pion mass, f_π the pion decay constant and $m_{u,(d)}$ the up- (down-)quark mass. It is trivial to see that this potential has a vacuum state at the CP conserving angle $\bar{\theta} = 0$. We must remember, however, that $\bar{\theta}$ is not dynamical and thus does not run down the potential. Conceptually, it is precisely this fact which the PQ solution addresses; it makes $\bar{\theta}$ dynamic and lets QCD solve the rest for us.

To understand the dynamics of this solution, let us remind ourselves of the relevant aspects of the theory of pions. As argued above, the QCD Lagrangian (1.1) for the lightest two quark flavours u and d, in the limit of vanishing mass, has a global $SU(2)_I \times SU(2)_P$ symmetry group. Quark condensates $\langle \bar{q} q \rangle = v \neq 0$ are not invariant under the global $SU(2)_P$, which spontaneously breaks $SU(2)_I \times SU(2)_P \to SU(2)_I$. So far, we have only repeated what was already mentioned before. To understand the dynamics, we can construct an effective Lagrangian for the axial modes of the fluctuations around the order parameter $\langle \bar{q} q \rangle = v$

$$\Sigma(x) = -vU(x) = -v \exp\left(\frac{2}{f_\pi} i \pi^a(x) \sigma^a\right). \tag{1.13}$$

Here we introduced the pion decay constant $f_\pi = 93\,\mathrm{MeV}$. We have ignored the radial field as it does not transform under the remaining symmetries of the theory and is hence irrelevant for the following argument. The effective Lagrangian then consists of any term invariant under the global symmetry. It is sufficient to look at the leading order term

$$\mathcal{L}_\pi \supset \frac{f_\pi^2}{4} \operatorname{Tr}\left(\partial_\mu \Sigma\right)\left(\partial^\mu \Sigma^\dagger\right) = \frac{1}{2}\left(\partial_\mu \pi^a\right)\left(\partial^\mu \pi^a\right) + \mathcal{O}\left(\frac{\pi^2}{f_\pi^2}\left(\partial_\mu \pi^a\right)^2\right). \tag{1.14}$$

The other invariant combination is $\Sigma\Sigma^\dagger$, however, due to our neglect of the radial mode, such terms are trivial and do not appear. As a consequence, all higher order operators consist of derivatives of pion fields. In particular, no pion mass term is possible. This is hardly surprising, as in the massless quark limit the global symmetry is exact, thus leading to massless Nambu-Goldstone bosons.

The latter is no longer true when the quark masses are included, in which case the global $SU(2)_I \times SU(2)_P$ is only an approximate symmetry to begin with. Nevertheless, it restricts the dynamics of the pion fields. To find the leading order effect in the effective Lagrangian, we replace the $\bar{q}q$ in the mass term by its vacuum expectation value leaving

$$\mathcal{L}_\pi \supset \frac{v}{2} \operatorname{Tr}\left(\mathcal{M}_q U + \mathcal{M}_q^\dagger U^\dagger\right) = v\left(m_u + m_d \cos\left(\theta_q\right)\right)\left(1 - \frac{\pi^a \pi^a}{2 f_\pi^2}\right) + \mathcal{O}\left(\frac{\pi^3}{f_\pi^3}\right) \tag{1.15}$$

with $\theta_q = \arg\det \mathcal{M}_q$ the complex phase of the quark mass matrix. As a result of the small explicit breaking of $SU(2)_I \times SU(2)_P$ the pions get a small mass

$$m_\pi^2 = \frac{v}{f_\pi^2}\left(m_u + m_d \cos\left(\theta_q\right)\right). \tag{1.16}$$

The potential (1.12) is found from a minimisation of the mass term (1.15) after a $U(1)_A$ field redefinition which shifts the CP violating parameter θ into the quark

mass matrix phase via the anomaly. This shifting happens because of the anomaly in the $U(1)_A$ global symmetry.

It is illuminating to notice that one solution to the strong CP problem would be an exactly massless quark. If the u quark were massless, then the vacuum energy (1.12), which is proportional to the mass, would vanish. Hence a $U(1)_A$ redefinition of the massless quark field shifts the CP violating parameter θ without changing the vanishing vacuum energy. As a result all θ vacuua would be equivalent without observational consequences. Unfortunately such a solution is excluded by QCD lattice simulations [26].

To make the $\bar{\theta}$ field dynamical, Peccei and Quinn added a chiral $U(1)_{\mathrm{PQ}}$ global symmetry to the SM. It suffers from the same anomaly as the $U(1)_A$. We further demand it spontaneously breaks at a scale f_a introducing a pseudo Nambu-Goldstone boson a, the axion, which couples through the anomaly as

$$\mathcal{L} \subset -\frac{a}{f_a}\frac{g^2}{32\pi^2}G^a_{\mu\nu}\tilde{G}^{a,\mu\nu}. \tag{1.17}$$

Performing the same analysis as before, we find a potential for the axion field given by (1.12)

$$V(a) = -m_\pi^2 f_\pi^2 \sqrt{1 - \frac{4m_u m_d}{(m_u+m_d)^2}\sin^2\left(\frac{\theta + \frac{a}{f_a}}{2}\right)} \tag{1.18}$$

with the important difference, that the axion field is dynamical and will relax to the vacuum state of this potential. This vacuum state lies at $\langle\bar{\theta}\rangle = 0$ and thus the Strong CP problem is solved.

1.3 Axion Phenomenology

The first immediate consequence of the axion potential (1.18) is a mass term, which can, in principle, be extracted by a simple expansion around the vacuum state. A

more involved analysis up to next to leading order results in [27, 28]

$$m_a = 5.7\,\mu\text{eV}\left(\frac{10^{12}\,\text{GeV}}{f_a}\right). \tag{1.19}$$

The axion's coupling to SM particles depends on the UV completion of the model and is thus model dependent. The axion effective Lagrangian

$$\mathcal{L}_a = \frac{1}{2}\left(\partial_\mu a\right)^2 + \frac{a}{f_{\text{PQ}}}\frac{g^2}{32\pi^2}G^a_{\mu\nu}\tilde{G}^{a,\mu\nu} - \left(\bar{q}_L\mathcal{M}_q q_R + h.c.\right) + \frac{\partial_\mu a}{f_{\text{PQ}}}\bar{q}c_q^{(0)}\gamma^\mu\gamma_5 q + \frac{1}{4}g^{(0)}_{a\gamma\gamma}aF_{\mu\nu}\tilde{F}^{\mu\nu} \tag{1.20}$$

may, in addition to the required QCD anomaly coupling to $G^a_{\mu\nu}\tilde{G}^{a,\mu\nu}$, have an electromagnetic anomaly coupling to the electromagentic field strength tensor $F_{\mu\nu}\tilde{F}^{\mu\nu}$ with model dependent coupling strength $g^{(0)}_{a\gamma\gamma}$ and a derivative coupling to the quark current with coupling $c_q^{(0)}$ [29, 30, 31]. Here, $\tilde{F}^{\mu\nu} = 1/2\varepsilon^{\mu\nu\rho\sigma}F_{\rho\sigma}$ is the dual field strength tensor. The only non-derivative couplings of the axion are anomaly couplings to the gauge fields of which only the $SU(3)$ gauge field coupling is required for the PQ solution, the electromagnetic coupling $g^{(0)}_{a\gamma\gamma}$ may in fact be 0. Any other axion coupling is of derivative nature because of the shift symmetry which, under the assumption of vanishing anomaly couplings, would be exact.

For simplicity we, again, limit ourselves to the lightest two quark flavours u and d. We may eliminate the $aG\tilde{G}$ term by an appropriate redefinition of the quark fields as

$$q \to e^{i\gamma_5\frac{a}{2f_{\text{PQ}}}\mathcal{Q}_a}q \tag{1.21}$$

with $\mathcal{Q}_a$ some 2×2 matrix with $\text{Tr}\,\mathcal{Q}_a = 1$. The $SU(3)$ anomaly then cancels the above term in exchange for an axion dependent quark mass operator. The resulting Lagrangian is

$$\mathcal{L}_a = \frac{1}{2}\left(\partial_\mu a\right)^2 + \frac{\partial_\mu a}{f_{\text{PQ}}}\bar{q}c_q\gamma^\mu\gamma_5 q + \frac{1}{4}g_{a\gamma\gamma}aF_{\mu\nu}\tilde{F}^{\mu\nu} - \bar{q}_L\mathcal{M}_a q_R + h.c. \tag{1.22}$$

In general the quark transformation described above has an electromagnetic anomaly which redefines the coupling

$$g_{a\gamma\gamma} = g^{(0)}_{a\gamma\gamma} - (2N_c)\frac{\alpha_{\rm em}}{2\pi f_{\rm PQ}}\,{\rm Tr}\left(\mathcal{Q}_a\mathcal{Q}^2\right) \tag{1.23}$$

where $N_c = 3$ is the number of colours, $\alpha_{\rm em}$ is the electromagnetic fine-structure constant and $\mathcal{Q} = {\rm diag}(2/3, -1/3)$ is the quark charge matrix. Additional terms are generated from the quark mass operator which now includes

$$\mathcal{M}_a = e^{i\frac{a}{2f_{\rm PQ}}\mathcal{Q}_a}\mathcal{M}_q e^{i\frac{a}{2f_{\rm PQ}}\mathcal{Q}_a} \tag{1.24}$$

and the quark kinetic term which lead to a redefinition of the axions coupling to the quark current

$$c_q = c^{(0)}_q - \mathcal{Q}_a. \tag{1.25}$$

We may match these terms to the effective chiral Lagrangian consisting of (1.14) and (1.15) to get the axion's coupling to SM particles. Because of the inclusion of $U(1)_{\rm EM}$, we replace the derivatives with the appropriate gauge covariant derivatives D_μ and add the newly introduced electromagnetic and quark coupling. Since we will mostly make use of the axion's coupling to photons we simply evaluate (1.23) taking, as is customary, $\mathcal{Q}_a = \mathcal{M}_q^{-1}/Tr\mathcal{M}_q^{-1}$ [27]

$$g_{a\gamma\gamma} = g^{(0)}_{a\gamma\gamma} - \frac{\alpha_{\rm em}}{2\pi f_{\rm PQ}}\left(\frac{2}{3}\frac{4m_d + m_u}{m_u + m_d}\right) = \frac{\alpha_{\rm em}}{2\pi f_{\rm PQ}}\left(\frac{E}{N} - 1.92\right) \tag{1.26}$$

where E is the electromagnetic and N the colour anomaly coefficient. Depending on the UV completion of the axion model, the ratio E/N can take different values, the two most popular models are Kim-Shifman-Vainshtein-Zakharov (KSVZ) [32, 33] and Dine-Fischler-Srednicki-Zhitnitsky (DSFZ) [34, 35] for which the ratios are $E/N = 0$ and $E/N = 8/3$, respectively. A CP conserving axion thus couples to the $U(1)_{\rm EM}$

electromagnetic field strength tensor $F_{\mu\nu}$ via an effective dimension 5 operator

$$\mathcal{L} \subset \frac{g_{a\gamma\gamma}}{4} a F_{\mu\nu} \tilde{F}^{\mu\nu} = -g_{a\gamma\gamma} a \mathbf{E} \cdot \mathbf{B}. \tag{1.27}$$

As a direct result of the effective $a \to \gamma\gamma$ three point vertex (1.27) the axion has a finite lifetime which is easily calculated to be

$$\Gamma^{-1}_{a\to\gamma\gamma} = \frac{64\pi}{g^2_{a\gamma\gamma} m_a^3}. \tag{1.28}$$

A CP conserving QCD axion hence has a lifetime exceeding the age of the universe for $m_a \lesssim 20\,\mathrm{eV}$. As we will be mostly interested in low mass axions with $m_a \lesssim 1\,\mathrm{eV}$ we may treat the axion as a stable asymptotic state.

A second consequence of the coupling (1.27) is axion-photon mixing in electromagnetic background fields. Mixing in constant, static magnetic fields $\mathbf{B}_0$ is a well understood phenomenon [36, 37]. The presence of a background field breaks spatial invariance therefore enabling the mixing between the massless photon and the massive axion with a probability

$$P_{a\to\gamma} = \frac{g^2_{a\gamma\gamma} B_0^2 L^2}{\beta_a} \left(\frac{\sin qL/2}{qL} \right)^2. \tag{1.29}$$

The axion's velocity is β_a, the magnetic field length L and $q = \omega_a - \sqrt{\omega_a^2 - m_a^2}$ the momentum transfer necessary to mix between the massless and massive state. The functional form of the probability is intuitive, a constant magnetic field $\mathbf{B}_0$ of length L has Fourier components given by the sinc function in (1.29) which define the momentum present in the field. An infinitely long field would carry no momentum and indeed photon splitting would be forbidden in this setting [38]. However, the finite spatial extend introduces some momentum. If the momentum transfer $q < L^{-1}$ the sinc function could be approximated and the resulting probability would become

independent of q. This is one way of saying that, in this case, the mixing is coherent over the entire length L. As indicated by the sinc function, the magnetic field mainly carries low momentum modes, making the transition efficient. The opposite limit, $q > L^{-1}$ requires slightly more care. Here the probability (1.29) oscillates quickly and many times over the distance L. We must therefore understand the probability as an average over those oscillations and find a suppression by q^{-2}, again in agreement with the observation that there is only very little momentum in the large momentum modes for a constant field.

Axions may also couple to fermions through the interaction Lagrangian

$$\mathcal{L}_{aff} \supset \frac{C_f}{2f_{\mathrm{PQ}}} \bar{\Psi}_f \gamma^\mu \gamma_5 \Psi_f \partial_\mu a \tag{1.30}$$

where Ψ_f are the fermion fields. In the following we will only be interested in the electron coupling and the coefficient is [31]

$$C_e = c_e^{(0)} + \frac{3\alpha_{\mathrm{em}}^2}{4\pi^2}\left(g_{a\gamma\gamma}^{(0)} \log\left(\frac{f_{\mathrm{PQ}}}{m_e}\right) - \frac{2}{3}\frac{4m_d + m_u}{m_d + m_u}\log\left(\frac{\Lambda_{\mathrm{QCD}}}{m_e}\right)\right) \tag{1.31}$$

where $c_e^{(0)}$ is an eventual, model dependent tree level coupling of the electron to the axion. We see that the coupling to photons and pions generates loop level coupling to electrons even if the tree-level coupling is absent.

1.4 Ultraviolet completion

The axion theory as set out in this chapter is an effective theory and must thus arise from an ultraviolet (UV) complete theory at high scales. We already mentioned two such models, the KSVZ and DFSZ axion, which we will take as popular examples to review, while also stressing that they are not the only two possibilities [31]. Generally UV completion of the axion theory requires the addition of new fields which in turn

affect the axion's coupling to the SM as will be explained below.

1.4.1 The hadronic axion

The generic hadronic axion model features new heavy quarks charged under $U(1)_{\mathrm{PQ}}$ and leaves the SM quarks without tree-level coupling to the axion. The KSVZ axion [32, 33] extends the SM by a single heavy quark Q with charges

$$q_c = 3, \qquad q_L = 1, \qquad q_H = 0 \tag{1.32}$$

under colour $SU(3)_c$, $SU(2)_L$ and hypercharge, respectively. It also adds a scalar Φ with

$$q_c = 1, \qquad q_L = 1, \qquad q_H = 0. \tag{1.33}$$

The Lagrangian

$$\mathcal{L}_{\mathrm{KSVZ}} \supset (\partial_\mu \Phi)(\partial_\mu \Phi)^\dagger + \bar{Q} i \not{D} Q - (Y_Q \bar{Q}_L Q_R \Phi + h.c.) - \lambda_\Phi \left(|\Phi|^2 - \frac{v_a^2}{2} \right)^2 \tag{1.34}$$

then features a PQ symmetry

$$\Phi \to e^{i\alpha}\Phi, \qquad Q_L \to e^{i\frac{\alpha}{2}} Q_L, \qquad Q_R \to e^{i\frac{\alpha}{2}} Q_R \tag{1.35}$$

which is spontaneously broken by the potential term for Φ. In the broken phase, both the quark Q and the radial mode of the complex scalar Φ acquire large masses proportional to v_a and the axial mode of Φ is the axion. An anomalous field redefinition

$$Q \to e^{-i\gamma_5 \frac{a}{2v_a}} Q \tag{1.36}$$

then generates the topological gluon coupling (1.17) after identification $v_a = f_a$. This specific realisation does not feature tree-level couplings to photons such that the

electromagnetic anomaly coefficient is $E = 0$.

1.4.2 The DFSZ axion

The DSFZ axion [34, 35] requires two Higgs doublets H_u and H_d with PQ charges $-1/2$ and $1/2$, respectively. The complex PQ scalar field Φ has charge 1. The general potential assuming vanishing bare mass of the Higgs doublets is then

$$\begin{aligned} V(H_u, H_d, \Phi) =& \frac{\lambda_u}{2}(H_u^\dagger H_u^2 + \frac{\lambda_d}{2}(H_d^\dagger H_d)^2 + \lambda_1(H_u^\dagger H_u)(H_d^\dagger H_d) + \lambda_2(H_u^\dagger H_d)(H_d^\dagger H_u) \\ &+ |\Phi|^2 \left(\kappa_u(H_u^\dagger H_u) + \kappa_d(H_d^\dagger H_d)\right) - \left(\kappa\Phi^2 H_d^\dagger H_u + h.c.\right) \\ &+ \lambda_\Phi \left(|\Phi|^2 - v_\Phi^2\right)^2 \end{aligned} \tag{1.37}$$

giving the fields vevs we parametrize as

$$\Phi = v_\Phi e^{i\frac{a_\Phi}{v_\Phi}}, \qquad H_u = v_u e^{i\frac{a_u}{v_u}}, \qquad H_d = v_d e^{i\frac{a_d}{v_d}}. \tag{1.38}$$

We require $v_\Phi \gg v_{u,d}$ and then make the assumption $\kappa \ll 1$ such that the electroweak scale for the Higgs is preserved. In DSFZ type axion models the SM quarks and leptons carry $U(1)_{\rm PQ}$ charges $-1/2$, $-1/2$ and $-1/2$ for up-type quarks u, down-type quarks d and charged leptons E respectively. This then leads to a PQ invariant Yukawa Lagrangian

$$\mathcal{L}_{\rm Y} \supset -iY_u\bar{Q}\sigma_2 H_u^* u - Y_d\bar{Q}H_d d - Y_E\bar{L}H_d E + h.c. \tag{1.39}$$

with Y_i the Yukawa couplings. The physical axion is a linear combination of the phases in (1.38)

$$a = \frac{1}{v_a}\left(v_\Phi a_\Phi - \frac{1}{2}(v_u a_u - v_d a_d)\right), \qquad v_a^2 \sim v_\Phi^2 \tag{1.40}$$

which we may invert to find the axion's couplings to the SM fields. Under the anomalous field redefinition

$$u \to e^{i\gamma_5 \frac{a}{4v_a}} u, \qquad d \to e^{i\gamma_5 \frac{a}{4v_a}} d, \qquad E \to e^{i\gamma_5 \frac{a}{4v_a}} E \tag{1.41}$$

the axion field is removed from the mass-terms introducing

$$\delta\mathcal{L} = \frac{\alpha_s}{8\pi} \frac{a}{f_{\rm PQ}} G^a_{\mu\nu} \tilde{G}^{a,\mu\nu} + \frac{\alpha_{\rm em}}{8\pi} \frac{E}{N} \frac{a}{f_{\rm PQ}} F_{\mu\nu} \tilde{F}^{\mu\nu} \tag{1.42}$$

where $E = 8$ is the electroamgentic anomaly coefficient, $N = 3$ is the colour anomaly coefficient and $f_{\rm PQ} = v_a/2N$ was chosen. Interestingly we see that the axion field lives on the interval $[0, 2\pi v_a)$ while the QCD induced potential from the topological gluon coupling is $2\pi f_{\rm PQ}$ periodic. Hence, in general we find $N_{\rm DW} = 2N$ degenerate vacuum states. We call $N_{\rm DW}$ the domain wall number which will play a role in cosmology as discussed in section 5.4.

1.5 Axion Searches

Significant experimental and observational effort is undertaken to look for axions. It is worth noting that the techniques described in this section apply to any pseudoscalar particle coupling to electromagentism via the effective dimension 5 operator (1.27). Such particles generically arise in BSM theories like String Theory where axions are a result of low energy compactification and generically populate the low energy spectrum [39, 40]. From now, we will use the term axion to label both the CP conserving QCD axion and any other pseudoscalar which couples to electrodynamics via the $a\mathbf{E}\cdot\mathbf{B}$ coupling except for in chapters 5 and 6.

The axion-electrodynamics coupling implies a range of well-studied phenomena. Pierre Sikivie quickly realised that this can be exploited to search for axions despite

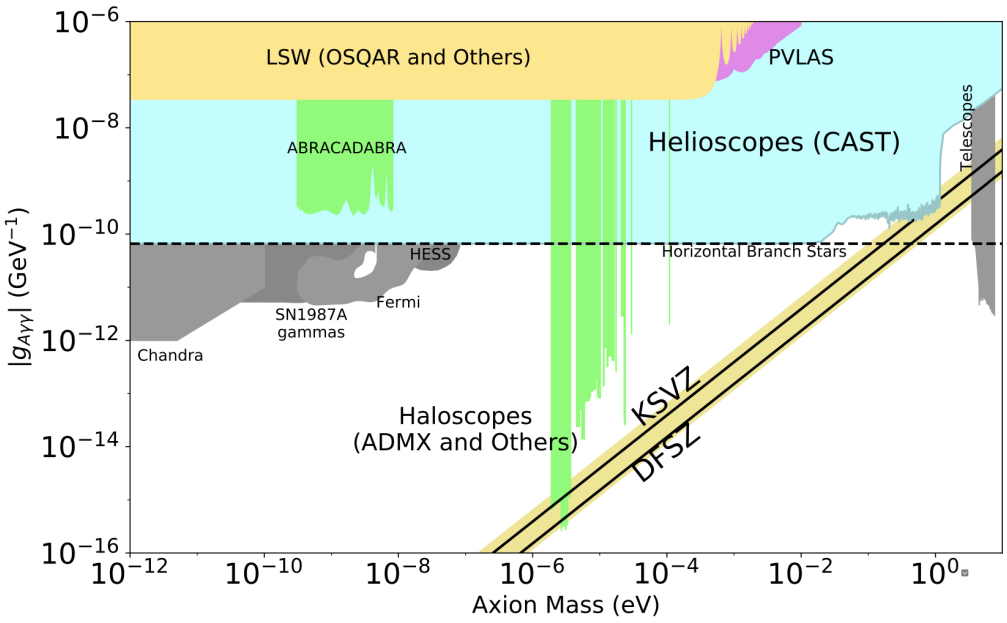

Figure 1.1: An exclusion plot showing the light axion parameter space with the current best bounds. The plot was taken from the review of particles physics [42]. For an explanation of the different bounds on the plot read section 1.5.

making them "*invisible*", meaning weakly coupled [36, 41]. Many current and ongoing searches are based on Sikivie-style detectors. The results of previous axion searches are documented on an exclusion plot, figure 1.1, which lists the free parameters of the theory, the axion mass m_a and the photon coupling $g_{a\gamma\gamma}$, and colours all parameter space in which no axion was found. It also shows the theoretical prediction for the CP conserving QCD axion for which the two parameters $g_{a\gamma\gamma}$ and m_a are no longer independent. The yellow band running from the upper right to the lower centre on the exclusion plot shows the parameter space and the width indicates a range of possible UV completions of the effective axion theories. The KSVZ and DFSZ axion are shown as reference.

We shall classify searches into three categories based on the underlying assumptions required for their interpretation: cosmological searches, astrophysical searches, and laboratory searches. An excellent review of axion search techniques by Sikivie

can be found here [43].

1.5.1 Cosmological Searches

Usually, those searches probing up to the smallest couplings are of cosmological type. Here the assumption is that axions make up the entire dark matter content of the universe (or a fraction of it in which case the bounds generally become weaker). This creates the possibility to build a detector aiming to measure the flux of dark matter here on earth. ADMX is one such search exploiting the axion-photon mixing [44, 45, 46, 47]. The detector is a microwave cavity with a very sharply defined frequency and a low loss rate. A dark matter axion with mass matching the cavities frequency may convert into an electromagnetic excitation of said cavity thereby depositing energy in the cavity and supplying a detectable signal [41, 48, 49]. There are several other cavities operating like RBF and UF [50, 51, 52], HAYSTAC [53] and ORGAN [54]. Their results are shown in green on the exclusion plot fig. 1.1. Range in mass is generally limited due to the cavity size, but the excellent quality factor enables the measurement of very weakly coupled axions at the appropriate masses.

DM axions also produce an alternative signal which detectors like the Cosmic Axion Spin Precession Experiment (CASPEr) [55, 56] are looking to exploit, that is, an oscillating nucleon EDM. A closer look at the dynamical PQ solution of the Strong CP problem reveals that the neutron EDM only vanishes in an averaged sense $\langle d_n(\bar{\theta})\rangle \propto \langle\bar{\theta}\rangle = 0$. The coherent oscillation of the axion field induces fluctuations in the neutron EDM on the order of [57]

$$d_n(\bar{\theta}) = 9 \times 10^{-35}\,\mathrm{ecm}\cos\left(m_a t\right) \tag{1.43}$$

for a QCD axion which constitutes the dark matter. An oscillating EDM will cause spin precession in nucleon spin polarized samples within an electric field. Such precess-

ing spins are generally measured with nuclear magnetic resonance (NMR) detectors which are very sensitive to low oscillation frequencies. Therefore $m_a \leq \mu$eV axion masses can be probed.

A similar approach is taken by the A Broadband/Resonant Approach to Cosmic Axion Detection with an Amplifying B-field Ring Apparatus (ABRACADABRA) collaboration [58, 59]. They exploit cooled LC cirquits to look for axions of slightly higher masses in the $m_a \sim \mu$eV range. A small scale prototype version, ABRACADABRA-10 cm has recently placed the first bounds depicted in green on figure 1.1.

There are many other DM detection experiments looking for general DM including axions. When looking in the light axion mass range, the above-mentioned techniques are the best performing and offer a good overview of the techniques used for axion DM detection. We would like to mention, however, the Xenon1T detector which recently reported excess scattering with low momentum transfer which might be explained by the existence of an axion [60, 61]. Xenon1T is a tank filled with liquid xenon which measures scintillation resulting from collisions of DM particles with xenon in the detector. Interpreting the signal as produced by an axion, the parameter space crosses the QCD band at around $m_a = 0.1 - 3\,\text{eV}$. However, this interpretation is in tension with astrophysical limits and subject to uncertainties in the background rate which will be addressed in a follow up experiment Xenon10T under commission.

It should be quite obvious that interpretation of experimental results is highly model dependent. Not only does it require knowledge of the fraction of DM constituted by axions, but also the local distribution of DM. The latter is actually not known very well [62]. Additionally, even a possible detection signal would only reveal information about a convolution of the axion-photon coupling strength and the local DM density. Untangling those two quantities is challenging; nonetheless, it is likely to become an important question in the near future. If axion DM exists, then the cosmological type searches are most likely to detect a signature first in which case

the aforementioned ambiguity between DM density and coupling strength must be addressed.

1.5.2 Astrophysical Searches

Typically, astrophysical searches follow a simple logic. With the inclusion of axions into the SM, we have an additional light degree of freedom, which should be produced in astrophysical objects. Production happens either via photon axion mixing as described in section 1.3 or in the field of nuclei via Primakoff production [63, 64]. Because of the weak coupling they should escape and produce a flux of axions from astrophysical objects. There are now two usual lines of argumentation, either we point a detector at such object and detect the flux, or we take the effect of the additional energy flux leaving the object on known physical properties and constrain the coupling strength in this way [65, 66].

Pointing a detector at the nearest and probably best understood object is the approach chosen by the CERN Axion Solar Telescope (CAST) collaboration. Their detector is a helioscope consisting of a supercooled magnetic field which converts solar axions into photons via the previously discussed interaction with probability (1.29). The axion flux from the sun is dominated by Primakoff production and peaked at $E = 3\,\mathrm{keV}$ with average energy $\langle E \rangle = 4.2\,\mathrm{keV}$ [67]. The total solar flux of axions is [68]

$$\Phi_a = 3.75 \times 10^{-9}\,\mathrm{cm}^{-2}\mathrm{s}^{-1} \left(\frac{g_{a\gamma\gamma}}{\mathrm{GeV}^{-1}}\right)^2 \tag{1.44}$$

after integration over the solar model. The detector is pointed at the sun and follows its motion over the sky measuring the flux of reconverted photons. Coherent conversion over the field covers the mass range up to $m_a < 0.02\,\mathrm{eV}$ above which the bounds drop. CAST limits the coupling strength to $g_{a\gamma\gamma} < 6.6 \times 10^{-11}\,\mathrm{GeV}^{-1}$ in this mass range. The limitation to low masses because of the momentum mismatch between

axions and photons can be overcome by filling the magnet with gas, thereby giving the photon a plasma mass. The CAST collaboration used Helium to probe masses up to $m_a \leq 1.17\,\text{eV}$ [69, 70, 71, 72]. The CAST exclusion region is shown in light blue in figure 1.1.

The sun is capable of producing axions up to masses of a few keV. To measure a flux of such high mass axions, converting into x-ray photons, a crystal is used to enhance the flux by Bragg scattering. Similar to regular Bragg scattering, massive axions mixing into photons also fulfil a Bragg condition, leading to an enhancement of flux at the appropriate angle, which can then be measured with a photon detector. Such a search was undertaken by [73]; the bounds are not indicated on the exclusion plot 1.1, but exclude couplings above $g_{a\gamma\gamma} \geq 1.7 \times 10^{-9}\,\text{GeV}^{-1}$.

The second line of argument can be applied to a variety of astrophysical objects. In terms of stars, the best bounds come from Horizontal Branch (HB) stars. These have masses similar to the sun's and their cores are burning He. This stage in the stellar evolution follows immediately after the Red Giant (RG) phase, during which the star is still burning H. The ratio of HB to RG stars, the R parameter, is sensitive to the lifetime of these stages. The inclusion of a light axion degree of freedom into the SM does significantly affect the HB stars while leaving RGs virtually unchanged [74]. Analysis of 39 Galactic Globular Clusters leads to the exclusion of axion couplings $g_{a\gamma\gamma} \geq 0.66 \times 10^{-10}\,\text{GeV}^{-1}$, indicated by a horizontal dashed line in figure 1.1.

Primakoff production of axions also takes place in core collapse supernovae and multiple observational signatures in Supernova SN1987A therefore place bounds on the available axion parameter space. Weakly-coupled axion stream out of the supernova and mix into gamma rays in the galactic magnetic field of the Milky Way. The absence of a gamma ray burst at the same time as the neutrino flash from the supernova can hence be interpreted as bounds [75]. Neutrino escape is the main source of cooling of the core collapse supernova and the resulting neutrino flash is observable on

earth. According to standard core collapse supernova models, the collapse of a massive star results in the generation of a proto neutron star. Typically, such an object is of solar mass, but has the density of nuclei and temperatures of tens of MeV [76, 77]. In these extreme conditions even neutrinos are trapped and their escape happens on timescales set by the diffusive transport resulting in a burst lasting for tens of s in agreement with observation. The inclusion of light and weakly coupled axions not trapped in the proto neutron star enhances the cooling rate thereby shortening the neutrino burst [78]. The bounds derived from observations of SN1987A are depicted in grey on the exclusion plot in figure 1.1.

For small masses the magnetic field in galaxy clusters becomes efficient at inducing axion-photon mixing in the x-ray energies. Measuring the spectra of luminous x-ray sources interposed by galaxy clusters therefore puts bounds on the coupling strength. These bounds, as most astrophysical bounds mentioned in this section, highly depend on the model assumptions used for the magnetic field within the interposing galaxy cluster. The spectra are measured by Chandra telescope and the resulting bounds are indicated in grey on the exclusion plot [79]. Also indicated in grey are bounds from the Fermi LAT collaboration using six years of spectral data to scan for irregularities stemming from axion-photon conversion in the spectrum of the radio galaxy NGC 1275 [80].

The high surface temperature of a young neutron star supernova remnant in HESS J1731-347 with rather weak magnetic field implies constraints on the coupling strength of axions such that axion bremstrahlung not be too effective [81]. The weak magnetic field allows for the assumption that neutrinos, and possibly axions, dominate the thermal evolution rather than the strong magnetic field, as is the case in young magnetars. This specimen, being the youngest and hottest neutron star with weak magnetic field discovered, therefore puts bounds which are indicated in grey on the exclusion plot 1.1.

All the above searches and associated bounds in the mass-coupling parameter space rely on a set of key assumptions which significantly weaken the reliability of the interpretation. For example, all of them require very good knowledge of the physics inside the particular astrophysical object under investigation. Supernovae in particular are computationally challenging as well as observationally sparse. For this reason, precision observations might be questionable. Even a well-studied object like the sun, however, poses some challenges and different models are not always in agreement with each other [82]. An additional source of uncertainty lies in the axion production environment. Within such hot objects the non-zero plasma frequency and high temperature conditions may affect the effective axion-photon coupling and consequentially alter the inferred limits [83].

1.5.3 Laboratory Searches

Laboratory searches trade the distinct advantage of model independence against generically weaker limits compared with the above searches. The reason for unfavourable performance can be found in the bounds dependence on the interaction strength $g^4_{a\gamma\gamma}$. A possible axion must be produced, thereby interacting once and then reconverted into a detectable signal, generally requiring two vertex interactions instead of a single one when measuring a background flux. Arguably the same is true for stellar bounds. However astrophysical objects have the natural advantage of large size and extreme conditions. Full control over both the production and reconversion stage also allows for individual tests of the axion-photon coupling and coupling to other particles, thus eliminating a further source of uncertainty in the data interpretation.

Laboratory experiments searching for the axion-photon coupling usually exploit a Sikivie-style detector exploiting the axion-photon mixing explained in the previous section [36]. Light shining through wall searches (LSW) fire a laser into a strong, constant magnetic field thereby facilitating axion production [84]. An interposing wall

then blocks the laser light from entering the detector which consists of yet another identical magnetic field in front of a photon detector. Axions which were produced within the first field traverse the wall because of their weak interaction which makes the wall transparent to such particles. Any axion propagating into the second magnetic field may then be reconverted into a photon which is subsequently measured by the detector. A positive signal therefore looks like light which passed through the wall, hence the name LSW. There are several LSW searches operating, like the Any Light Particle Search (ALPS) [85, 86] and the Optical Search for QED Vacuum Birefringence, Axions, and Photon Regeneration (OSQAR) experiment [87], which produced the current best bounds as indicated in yellow on fig. 1.1. The shape of the exclusion region is easily obtainable from the transition probability (1.29) which is constant for low axion masses and drops like q^{-2} once the transition is no longer coherent. LSW detectors are conceptually very similar to helioscopes, in fact they exploit the same physics simply replacing the solar source by a laser shining into a magnetic field.

An alternative detection technique relies on the polarization-dependent axion-photon coupling and on the axion having mass. A polarised beam of photons traversing a magnetic field suffers from Birefringence and Dichroism [88]. Dichroism is a small rotation of the polarisation plane of the beam, which is due to a depletion of photons with polarisation in the direction of the magnetic field, while photons polarised in the orthogonal plane propagate unaffected. Birefringence in contrast leads to elipticity in the polarisation when the appropriately polarised photons mix with massive axions, thereby acquiring a phase factor relative to the unaffected orthogonal mode. Both effects were measured by the Polarizzazione del Vuoto con LASer (PVLAS) collaboration [89] and their non-observation placed bounds indicated in pink on fig. 1.1.

Not shown on the exclusion plot are higher axion masses which are investigated

using different techniques. At very low masses, the axion mediates long range forces and fifth force bounds apply. The present thesis is primarily interested in axion masses around eV and below, and therefore will not review these techniques here.

Chapter 2

Stimulated Light Shining Through Wall Search For Axion Detection

Traditional light shining through wall type searches, as described in 1.5.3, utilise comparatively low power continuous lasers to seed the axion field, accumulating data over a long time-span. This is possible because the axion photon transition is facilitated by an external, strong and constant magnetic field **B** through which the continuous laser can propagate for extended periods of time. Also, the detection region, which we will refer to as the detector in the following unless otherwise specified, consists of an identical magnetic field guaranteeing conversion at all times. The transition probability was given in (1.29)

$$P_{a\to\gamma} = \frac{g_{a\gamma\gamma}^2 B^2 L^2}{\beta_a} \left(\frac{\sin qL/2}{qL}\right)^2 \tag{2.1}$$

with q the momentum transfer, β_a the axion's velocity, B the magnetic field strength and L the magnetic field's length. The number of axions produced in the conversion stage, and similarly the number of signal photons, depends on the flux of photons from the seed pulse. As a reference we will use the seed pulse utilised for the ALPs experiment [90, 85], a laser producing 800 mW after frequency doubling to $\omega = 2.4\,\mathrm{eV}$,

resulting in a flux of $\Phi_{\rm ALPs} \simeq 10^{18}\,{\rm s}^{-1}$ photons. With this information we may trivially find the axion flux onto the detector $\Phi_a = \Phi_{\rm ALPs} P_{a\to\gamma}$. For the signal photons entering the photon detector we simply repeat to find $\Phi_s = \Phi_{\rm ALPs} P^2_{a\to\gamma}$. From here we conclude that the signal in such a setup grows linearly in exposure time and initial seed flux. It is the latter that we aim to improve upon by utilising two high power laser pulses with large photon flux.

Additionally, traditional LSW searches generally perform well for low mass axions but quickly lose sensitivity when the axion mass increases and the momentum transfer required for an axion-photon transition becomes too large, $qL/2 > 1$. This can be seen in the transition probability (2.1) whose momentum transfer dependence arises from a spatial Fourier transform of the magnetic background field and is indicative of the momentum which is present in the background. A laser beam consists of coherent real photons of frequency ω_j and momentum $\mathbf{k}_j$, we will say the field carries momentum $\mathbf{k}_j$ in the following. In contrast the static, constant magnetic field $\mathbf{B}$ only carries limited momentum due to its finite size. Axions with small mass require little momentum transfer $q = \omega_a - \sqrt{\omega_a^2 - m_a^2}$ and their transition is coherent over the full length of the magnetic field. Large momentum modes are suppressed and so is any transition probability for large momentum transfer. In this limit, the $\sin^2 qL/2$ oscillates very rapidly and many times over the magnetic field length. It can hence be replaced by its average and the probability decays like q^{-2} [91].

Replacing the static magnetic background field by a second laser beam, carrying momentum, we aim to improve the bounds placed on axions in the $m_a \sim$ eV mass range by both, overcoming the momentum transfer suppression and a favourable scaling in the photon number, N^2 [3]. It is worth pointing out that the Xenon1T collaboration has recently reported an excess scattering in their low momentum bin [60] which, if real and interpreted as axions, would hint at a coupling strength crossing the QCD axion band at eV masses [61] (see the green band in fig. 2.2 It is necessary to

mention however that the statistical significance is not sufficient for strong claims and the axion interpretation of the signal is in strong tension with astrophysics. A follow-up experiment Xenon10T is under construction and will be capable of investigating the excess.

The set-up under investigation follows the same principle as other LSW searches; It is divided into three main components, the generation region, the wall and the detector. The generation region is on the left hand side and consists of two colliding high power laser beams which lead to axion production. We investigate this stage in section 2.1. In the centre an interposing wall blocks the seed pulses from entering the detector. We will assume that the wall's thickness, which can be chosen appropriately, grants perfect absorption, and the weak axion coupling will ensure its transparency to axions for the parameters under consideration here. We also mention that a 10 cm distance between the generation region and the detector is assumed later on, which will provide a sizeable spatial offset between the reconverted photons and the seed beams additional to the temporal delay due to the massive axion's propagation speed. For detection we consider a traditional constant magnetic field detector in [3] and detection through a stimulating laser beam in [5]. Perhaps unsurprisingly, the latter performs favourably due to overcoming the momentum transfer suppression and the favourable scaling with photon number N^3. Hence, we concentrate on stimulated detection in section 2.2. Using stimulation to detect dark matter axions was investigated in [92, 93].

If we assume for now that all three beams are identical in frequency and photon number, then the range of couplings $g_{a\gamma\gamma}$ testable in the aforementioned scheme scales like $N^{-3/4}$ as a result of the three incoming laser beams and the two interaction vertices. The geometry of the colliding plane waves results in a dependence on the collision angle $\propto \sin(\alpha/2)^{-1}$ because of the effective coupling $\mathbf{E} \cdot \mathbf{B}$. Utilising the kinematics at the three point vertices of axion production and reconversion, we may

recast this as a mass dependence $\propto (m_a/\omega_a)^{-2}$. The bounds we achieve after calculation of the process indeed scale like expected, compare (2.35), with the additional factors arising from the volume integrations, as explained in the following.

It is worth noting that one could devise schemes in which the reconverted measurable signal are other SM particles, like electron-positron pairs [2] which we investigate in chapter 4. For now we choose to limit ourselves to the reconversion into photons insofar as, this way, the final signal only depends upon a single coupling of the axion, the axion-photon coupling $g_{a\gamma\gamma}$ and interpretation is simple.

The equations of motion of this system consisting of photons and axions are Maxwell's equations modified by the axion coupling (1.27). They are known in the literature as axion-electrodynamics and arise from the Lagrangian [36]

$$\mathcal{L} = -\frac{1}{4}F_{\mu\nu}F^{\mu\nu} + \frac{g_{a\gamma\gamma}}{4}aF_{\mu\nu}\tilde{F}^{\mu\nu} + \frac{1}{2}\left(\partial_\mu a\right)\left(\partial^\mu a\right) + \frac{1}{2}m_a^2 a^2. \tag{2.2}$$

The Gauss law for magnetism is unchanged

$$\nabla \cdot \mathbf{B} = 0, \tag{2.3}$$

and so is the Maxwell-Faraday law of induction

$$\nabla \times \mathbf{E} = -\partial_t \mathbf{B}. \tag{2.4}$$

The electric Gauss's law however gets a source from the axion field

$$\nabla \cdot \mathbf{E} = g_{a\gamma\gamma}\left(\nabla a\right) \cdot \mathbf{B} \tag{2.5}$$

and Ampère's law includes an axion current

$$\nabla \times \mathbf{B} = \partial_t \mathbf{E} + g_{a\gamma\gamma}\left(\mathbf{E} \times \nabla a - \mathbf{B}\partial_t a\right). \tag{2.6}$$

The axion field itself is described by a Klein-Gordon type equation

$$\left(\partial_t^2 - \nabla^2 + m_a^2\right) a = -g_{a\gamma\gamma}\mathbf{E}\cdot\mathbf{B}. \tag{2.7}$$

From the modified Maxwell's equations we may derive the wave equations for the electric and magnetic fields and find

$$\left(\partial_t^2 - \nabla^2\right)\mathbf{E} = -g_{a\gamma\gamma}\left(\partial_t\left(\mathbf{E}\times\nabla a - \mathbf{B}\partial_t a\right) + \nabla\left((\nabla a)\cdot\mathbf{B}\right)\right) \tag{2.8}$$

for the electric and

$$\left(\partial_t^2 - \nabla^2\right)\mathbf{B} = g_{a\gamma\gamma}\nabla\times\left(\mathbf{E}\times\nabla a - \mathbf{B}\partial_t a\right) \tag{2.9}$$

for the magnetic field.

2.1 Axion Field Production

The set-up under investigation is shown in figure 2.1 where, as anticipated, we have replaced the constant magnetic field in the detector with a third, stimulating laser beam. As we will argue below, this substantially increases the sensitivity, exploiting the large energies which current day lasers can deliver onto target. As a direct consequence of the large energy per laser pulse, and the corresponding very high photon occupation number of the laser mode, the electromagnetic fields are well described as being classical and effectively external. The latter aspect precludes the treatment of any back-reaction which is justified by the smallness of the coupling $g_{a\gamma\gamma}$. We are interested in the lowest order effect in a perturbation series in $g_{a\gamma\gamma}$ or, to put it differently, we are only interested in the tree-level amplitude and need not concern ourselves with higher order effects. Therefore, we take the incoming beams to be

plane waves of the form

$$\mathbf{E}_j = \frac{1}{2}\left(\boldsymbol{\mathcal{E}}_j e^{i\omega_j t - i\mathbf{k}_j\cdot\mathbf{x}} + c.c.\right), \qquad \mathbf{B}_j = \frac{1}{2}\left(\boldsymbol{\mathcal{B}}_j e^{i\omega_j t - i\mathbf{k}_j\cdot\mathbf{x}} + c.c.\right). \tag{2.10}$$

We justify this assumption by noting that the pulselength and spatial extend of the lasers we consider later on are large when compared with their wavelength, $\tau\omega_j \gg 1$. Let us further make the simplifying assumption that the two colliding laser beams are identical, except for the polarisation and propagation direction. This introduces a symmetry into the collision system and leads to a simple form of the geometry factors. We will drop this assumption and quote the resulting more complicated equations in Appendix A. The two colliding lasers define a plane of collision which we take without loss of generality to be the x_1, x_3 plane and we work in coordinates centred on the production region. Using the last freedom to fix the final axion momentum $\mathbf{k}_a = \mathbf{k}_1 + \mathbf{k}_2$ along x_3 we may write

$$\frac{\mathbf{k}_1}{\omega_1} = \begin{pmatrix} -\sin\frac{\alpha}{2} \\ 0 \\ \cos\frac{\alpha}{2} \end{pmatrix}, \quad \frac{\boldsymbol{\mathcal{E}}_1}{|\boldsymbol{\mathcal{E}}_1|} = \begin{pmatrix} 0 \\ 1 \\ 0 \end{pmatrix}, \quad \frac{\boldsymbol{\mathcal{B}}_1}{|\boldsymbol{\mathcal{B}}_1|} = -\begin{pmatrix} \cos\frac{\alpha}{2} \\ 0 \\ \sin\frac{\alpha}{2} \end{pmatrix} \tag{2.11}$$

and for the second beam

$$\frac{\mathbf{k}_2}{\omega_2} = \begin{pmatrix} \sin\frac{\alpha}{2} \\ 0 \\ \cos\frac{\alpha}{2} \end{pmatrix}, \quad \frac{\boldsymbol{\mathcal{E}}_2}{|\boldsymbol{\mathcal{E}}_2|} = \begin{pmatrix} \cos\frac{\alpha}{2} \\ 0 \\ -\sin\frac{\alpha}{2} \end{pmatrix}, \quad \frac{\boldsymbol{\mathcal{B}}_2}{|\boldsymbol{\mathcal{B}}_2|} = \begin{pmatrix} 0 \\ 1 \\ 0 \end{pmatrix}. \tag{2.12}$$

The angle at which the two beams collide is α.

Having concluded that the laser beams are indeed classical, we find that the axion field, sourced by a classical source, is also classical and we assume it to be of the form

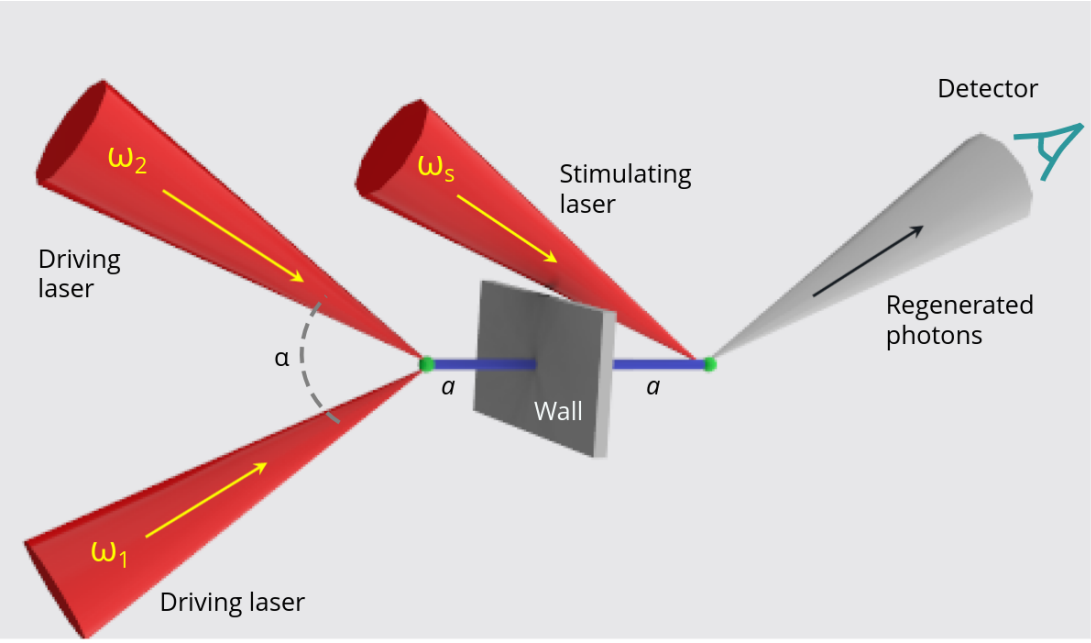

Figure 2.1: A diagram of the experimental setup. The collision of two lasers results in the production of any hypothetical axions. Such weakly coupled particles pass through a central wall blocking the laser photons from entering the detector region. An appropriately timed third laser facilitates the reconversion into photons behind the wall. Those reconverted photons are measured with a detector.

$$a = \frac{1}{2}\left(\tilde{a}(\mathbf{x})e^{i\omega_a t} + c.c.\right). \tag{2.13}$$

Once again, it must be noted that we assume that $\tau\omega_a \gg 1$. However, we may not make the same assumption about the spatial dependence. The axion is a massive particle and thus its momentum k_a may, for all we know, be small compared to the energy. To find the axion field we must solve equation (2.7) with the initial beams (2.10)

$$\left(-\omega_a^2 - \nabla^2 + m_a^2\right)\tilde{a}(\mathbf{x})e^{i\omega_a t} = -g_{a\gamma\gamma}|\boldsymbol{\mathcal{E}}_1||\boldsymbol{\mathcal{E}}_2|\sin^2\frac{\alpha}{2}e^{i(\omega_1+\omega_2)t - i(\mathbf{k}_1+\mathbf{k}_2)\cdot\mathbf{x}}. \tag{2.14}$$

In writing down equation (2.14) we have dropped terms with phases $i(\pm\omega_1 \mp \omega_2)t$

as we are only interested in the scattering process resulting in the sum frequency $\omega_a = \omega_1 + \omega_2$. To solve for the axion field, we find the fundamental solution

$$G(\mathbf{x}) = \int \frac{d^3k}{(2\pi)^3} \frac{e^{i\mathbf{k}\cdot\mathbf{x}}}{-\omega_a^2 + \mathbf{k}^2 + m_a^2} = \frac{e^{-i\sqrt{\omega_a^2 - m_a^2}|\mathbf{x}|}}{4\pi|\mathbf{x}|} \tag{2.15}$$

where we neglected the advanced solution and only keep the retarded one. The axion field is then obtained via an integration over the beam overlap V

$$\tilde{a}(\mathbf{x})e^{i\omega_a t} = -\frac{g_{a\gamma\gamma}}{4\pi}|\boldsymbol{\mathcal{E}}_1||\boldsymbol{\mathcal{E}}_2| \sin^2\frac{\alpha}{2} e^{i\omega_a t} \int_V d^3y e^{-i\mathbf{k}_a\cdot\mathbf{y}} \frac{e^{-i\sqrt{\omega_a^2 - m_a^2}|\mathbf{x}-\mathbf{y}|}}{|\mathbf{x}-\mathbf{y}|}. \tag{2.16}$$

We want to evaluate the axion field at the reconversion region which is separated from the origin by a macroscopic distance d. In particular $d \gg \ell$ where ℓ is the side-length of the beam overlap which, for simplicity, we assume to be a cube. Hence, we may approximate

$$\int_V d^3y e^{-i\mathbf{k}_a\cdot\mathbf{y}} \frac{e^{-i\sqrt{\omega_a^2 - m_a^2}|\mathbf{x}-\mathbf{y}|}}{|\mathbf{x}-\mathbf{y}|} \sim \frac{e^{-ik_a d}}{d} \int_V d^3y e^{ik_a\left(\hat{x} - \hat{k}_a - \frac{\mathbf{y}}{2d} + \frac{\hat{x}\cdot\mathbf{y}}{2d}\hat{x} + \mathcal{O}\left(\frac{|\mathbf{y}|}{d}\right)^2\right)\cdot\mathbf{y}} \tag{2.17}$$

where $\hat{x} = \mathbf{x}/|\mathbf{x}|$ denotes the direction in which we are evaluating the field and we limit $d \gg |\mathbf{y}|$, $\sqrt{k_a|\mathbf{y}|^3}$. We also took $k_a = \sqrt{\omega_a^2 - m_a^2}$ as appropriate for an on-shell axion. Limiting ourselves to an observation direction along the axion momentum, $\hat{x} - \hat{k}_a \sim 0$, we may readily evaluate the resulting integral

$$\frac{1}{V}\int_V d^3y e^{-ik_a\left(\frac{\mathbf{y}}{2|\mathbf{x}|} - \frac{\hat{x}\cdot\mathbf{y}}{2|\mathbf{x}|}\hat{x}\right)\cdot\mathbf{y}} = \left(\frac{\sqrt{\pi}(1-i)}{\sqrt{\frac{k_a\ell^2}{|\mathbf{x}|}}} \mathrm{Erf}\left[\frac{(1+i)}{4}\sqrt{\frac{k_a\ell^2}{|\mathbf{x}|}}\right]\right)^2. \tag{2.18}$$

As we increase the spotsize of the two incoming lasers, therefore increasing l and the interaction volume, the axion field amplitude grows linear in volume as long as $l^2 \leq d/k_a$. Further increase of the spotsize will only result in a growth of the axion field amplitude proportional to ℓ. The scaling above is of course only true if we assume

the laser fields $|\boldsymbol{\mathcal{E}}_j|$ to be constant. In a real laser, rather than the field's amplitude, its energy per pulse is fixed and the amplitude therefore drops like $|\boldsymbol{\mathcal{E}}_j| \propto \ell^{-2}$ resulting in a larger axion field amplitude up to $\ell^2 \sim d/k_a$ above which the decrease in the field amplitudes starts beating the increase from the volume overlap. We therefore conclude that $\ell^2 \sim d/k_a$ is the ideal size for the interaction region and in the following we make the assumption that the beam overlap is small enough such that the integral (2.18) trivialises. Thence the axion field at large distances from the beam overlap is

$$\tilde{a}(\mathbf{x}) = -\frac{g_{a\gamma\gamma}}{4\pi} V |\boldsymbol{\mathcal{E}}_1||\boldsymbol{\mathcal{E}}_2| \sin^2 \frac{\alpha}{2} \frac{e^{-ik_a|\mathbf{x}|}}{|\mathbf{x}|}. \tag{2.19}$$

Note that the apparent spherical symmetry is merely an artefact of our assumptions which break when looking far enough from $\hat{x} - \hat{k}_a \sim 0$. In this case the volume integral is highly oscillatory and effectively vanishes leaving an axion field which is highly peaked around $\hat{k}_a$. Our assumptions hold for a cone around this direction and amount to taking the axion field amplitude constant over this cone. Because the axion field divergence is small, the reconversion region will have size of the same order as the beam overlap V. Thus, we only need the field within a narrow cone around $\hat{k}_a$.

For later use we calculate the time derivative which is trivial

$$\partial_t \tilde{a}(\mathbf{x}) e^{i\omega_a t} = i\omega_a \tilde{a}(\mathbf{x}) e^{i\omega_a t} \tag{2.20}$$

and the gradient at a distance d from the beam overlap V

$$\nabla \tilde{a}(\mathbf{x}) = -\mathbf{k}_a \frac{1 + ik_a d}{k_a d} \tilde{a}(\mathbf{x}) \tag{2.21}$$

which is also oriented along $\hat{k}_a$.

2.2 Axion Field Detection

To detect the axion field (2.19), we collide a third laser beam with the axion flux sourcing an electromagnetic field via the right hand side of (2.8) and (2.9). Again, we write the laser beam like in (2.10) with label "s" for stimulating beam. The electric field which is sourced by the axion field is defined as

$$\mathbf{E} = \frac{1}{2}\left(\tilde{\mathbf{E}}(\mathbf{x})e^{i\omega t} + c.c.\right) \qquad \mathbf{B} = \frac{1}{2}\left(\tilde{\mathbf{B}}(\mathbf{x})e^{i\omega t} + c.c.\right). \tag{2.22}$$

A simple perturbation series in $g_{a\gamma\gamma}$ reveals that the relevant equations are

$$\left(-\omega^2 - \nabla^2\right)\tilde{\mathbf{E}}(\mathbf{x})e^{i\omega t - i\mathbf{k}\cdot\mathbf{x}} = -\frac{g_{a\gamma\gamma}}{2}e^{i(\omega_a-\omega_s)t} \tag{2.23}$$

$$\left[i(\omega_a-\omega_s)\left(\boldsymbol{\mathcal{E}}_s^* \times \nabla\tilde{a} - i\omega_a\boldsymbol{\mathcal{B}}_s^*\tilde{a}\right)e^{i\mathbf{k}_s\cdot\mathbf{x}} + \nabla\left((\nabla\tilde{a})\cdot\boldsymbol{\mathcal{B}}_s^* e^{i\mathbf{k}_s\cdot\mathbf{x}}\right)\right] \tag{2.24}$$

for the electric field, while the magnetic field satisfies

$$\left(-\omega^2 - \nabla^2\right)\tilde{\mathbf{B}}(\mathbf{x})e^{i\omega t} = \frac{g_{a\gamma\gamma}}{2}\nabla\times\left(\boldsymbol{\mathcal{E}}_s^* e^{i\mathbf{k}_s\cdot\mathbf{x}}\times\nabla\tilde{a} - i\omega\boldsymbol{\mathcal{B}}_s^* e^{i\mathbf{k}_s\cdot\mathbf{x}}\tilde{a}\right)e^{i(\omega_a-\omega_s)t}. \tag{2.25}$$

This time, in contrast to the generation process, we are interested in the stimulated decay which corresponds to $\omega = \omega_a - \omega_s$ and drop all other terms. In fact there is a rather straightforward argument why only the stimulated decay of axions will contribute when turning to the vacuum energy momentum conservation of the process. At the three point vertex of axion production, we had effectively three degrees of freedom, we can change the energy of either laser beam ω_j and the collision angle α. The choice of laser frequency fixes the resulting axion energy $\omega_a = \omega_1 + \omega_2$ and the angle fixes its momentum $\mathbf{k}_a = \mathbf{k}_1 + \mathbf{k}_2$. Only on-shell axions propagate the macroscopic distance to the reconversion region, therefore only axions of mass

$$m_a^2 = 4\omega_1\omega_2\sin^2\frac{\alpha}{2} \tag{2.26}$$

may be produced. Ignoring the final axion momentum direction, the choice of laser energies and collision angle determines the axion parameters. Now, assume the signal photons is produced via scattering such that $\omega = \omega_a + \omega_s$ and $\mathbf{k} = \mathbf{k}_a + \mathbf{k}_s$. Both photons involved in the process are on-shell and thus their momenta satisfy $|\mathbf{k}_2| = \omega_2$ and $|\mathbf{k}| = \omega$. The massive axion has $|\mathbf{k}_a| = (\omega_a^2 - m_a^2)^{1/2} < \omega_a$. Energy and momentum cannot be conserved at the same time because $|\mathbf{k}_a + \mathbf{k}_s| \leq |\mathbf{k}_a| + |\mathbf{k}_s| < |\mathbf{k}|$.

The stimulated decay of the axion may only happen into specific combinations of photon energies and collision angle. This is most easily seen when going to the rest-frame of the axion. The decay to two photons in this frame may only happen into two photons with equal but opposite momentum. Boosting to the laboratory frame may change the energies of the two photons and their angle, however the parameters are not independent. Thus, the simplest possible decay channel is via stimulated decay through a copy of either beam 1 or 2. Note that in principle we could change the polarisation of the stimulating beam, resulting in a signal photon with rotated polarisation relative to whichever beam we did not choose for stimulation. We take this as further justification for single photon counting to be possible as this allows us to discriminate between background and signal photons. In the following we choose to use as stimulating beam a copy of beam 2, the reason being that for this beam $\mathbf{k}_a \cdot \boldsymbol{\mathcal{B}}_s = 0$ and the electric field source simplifies. As it turns out, the bounds are unaffected by this choice.

The source on the right hand side of (2.23), after substitution of the axion field (2.19), can be written as

$$\mathbf{j}(\mathbf{x}) = -g_{a\gamma\gamma}\mathbf{j}_0\tilde{a}(\mathbf{x})e^{i\mathbf{k}_s\cdot(\mathbf{x})}e^{i\omega t} \tag{2.27}$$

where

$$\mathbf{j}_0 = \omega\left((\boldsymbol{\mathcal{E}}_s^* \times \mathbf{k}_a)\,\frac{i-k_a d}{k_a d} + \omega_a \boldsymbol{\mathcal{B}}_s^*\right) + \left(\mathbf{k}_a\left(\frac{1+ik_a d}{k_a d}\right)^2 - \mathbf{k}_s\frac{i-k_a d}{k_a d}\right)(\boldsymbol{\mathcal{B}}_s^* \cdot \mathbf{k}_a)\,. \tag{2.28}$$

With the specific choice of stimulating beam we made, $(\boldsymbol{\mathcal{B}}_s^* \cdot \mathbf{k}_a) = 0$ and the second term in $\mathbf{j}_0$ vanishes. The fundamental solution of the wave equation is identical to (2.15) in the limit $m_a \to 0$ and the axion sourced electric field is thence

$$\tilde{\mathbf{E}}(\mathbf{x}) \simeq -g_{a\gamma\gamma}\int_{V'} d^3y \frac{e^{-i\omega|\mathbf{x}-\mathbf{y}|}}{8\pi|\mathbf{x}-\mathbf{y}|}\mathbf{j}_0\tilde{a}(\mathbf{y})e^{-i\mathbf{k}\cdot\mathbf{y}}. \tag{2.29}$$

Once again we approximate the overlap of axion flux and stimulating laser beam as a cube of sidelength ℓ because of the minimal axion field divergence. Increasing the volume of the stimulating beam further will not lead to any enhancement as all axions are contained within $V' \sim V$. We further assume the envelope of the axion field constant over the volume V', as $d \gg \ell$. Detection of the electric field will happen at a photon detector placed at a distance D away from V'. Once again assuming $D \gg k\ell^2$ we may make the simplification

$$\tilde{\mathbf{E}}(\mathbf{x}) \simeq -g_{a\gamma\gamma}\frac{e^{-i\omega|\mathbf{x}|}}{8\pi|\mathbf{x}|}\mathbf{j}_0\tilde{a}(d)\int_{V'} d^3y e^{-i\omega(\hat{k}-\hat{x})\cdot\mathbf{y}}. \tag{2.30}$$

The volume integral is equivalent to the Fourier transformation of a constant function with compact support over V and readily evaluated to be

$$\frac{1}{V'}\int_{V'} d^3y e^{-i\omega(\hat{k}-\hat{x})\cdot\mathbf{y}} = \mathrm{sinc}\left(\frac{\ell'\omega}{2}(1-\hat{x}\cdot\hat{y}_1)\right)\mathrm{sinc}\left(\frac{\ell'\omega}{2}\hat{x}\cdot\hat{y}_2\right)\mathrm{sinc}\left(\frac{\ell'\omega}{2}\hat{x}\cdot\hat{y}_3\right). \tag{2.31}$$

In the evaluation of the integral above we chose the alignment of the cube approximating the interaction region such that $\hat{k}$ is a unit vector pointing to the face of the cube. As expected, we find the maximum of this function when $\hat{x} = \hat{y}_1$, precisely

when looking in the direction of signal photon momentum. Contrary to before, however, we are interested in maximising the solid angle over which we detect photons as there is no penalty in increasing the detector size. Therefore, we may not limit ourselves to $\hat{k} - \hat{x} \sim 0$. Any other orientation of the cube V' should not change the result appreciably.

To estimate the signal strength and subsequently project the bounds an experiment following this set up might produce, we find the electric fields power

$$\mathcal{P} = \int d\vartheta d\varphi \sin(\vartheta) D^2 \left| \tilde{\mathbf{E}}(D, \vartheta, \varphi)_\perp \right|^2 \cos^2(\omega t) \,. \tag{2.32}$$

The $\cos^2(\omega t)$ dependence arises from the *c.c.* terms in (2.22). As we are integrating over a sphere of radius D to find the power, the spatial phase does not enter. In general an electromagnetic wave sourced by an axion field is no longer well described by only the vector potential and the electric field may have components along the momentum $\mathbf{k}$. This is a result of the modified Maxwell's equations and Poisson's equation being non-trivial $\nabla^2\Phi = -g_{a\gamma\gamma}(\nabla a)\cdot\mathbf{B}$ with Φ the scalar potential. In the presence of an axion field there is no residual gauge freedom to set $\Phi = 0$. For our choice of stimulating beam, at least to lowest order in $g_{a\gamma\gamma}$ we do retain this gauge freedom as $(\nabla a)\cdot\mathbf{B} = 0$, however in general we must project the electric field onto an orthogonal coordinate plane relative to the photon momentum $\mathbf{k}$ as any parallel component may not propagate in vacuum and does not reach the detector.

Because of the strongly peaked distribution, we may extend the solid angle integral to an integral over the entire sphere and evaluate the resulting integral to leading order in $(\ell'\omega)^{-1}$

$$\begin{aligned} &\int \operatorname{sinc}^2\left(\frac{\ell'\omega}{2}(1 - \sin(\vartheta)\cos(\varphi))\right) \operatorname{sinc}^2\left(\frac{\ell'\omega}{2}\sin(\vartheta)\sin(\varphi)\right) \operatorname{sinc}^2\left(\frac{\ell'\omega}{2}\cos(\vartheta)\right) d^2\Omega \\ &\simeq \frac{4\pi^2}{(\ell'\omega)^2}. \end{aligned} \tag{2.33}$$

We thus find the energy in the electromagnetic field

$$E = \frac{g_{a\gamma\gamma}^4}{64\pi^2}\frac{\ell^2}{d^2}\omega_a^2 E_1 E_2^2 \sin^4\frac{\alpha}{2}\left(1-\frac{k_a}{\omega_a}\cos\frac{\alpha}{2}\right)^2 \tag{2.34}$$

where we assumed the incoming beams focused such that the beams are cubes of sidelength ℓ and hence the laser energy contained in the matching interaction volume $E_j = \int \mathcal{P}_j d\tau = |\mathcal{E}_j|^2\ell^3/2$ is simply the laser energy per pulse. Inverting the expression to find the testable parameter space is now trivial and it extends up to

$$g_{a\gamma\gamma} \geq \left(32\pi^2 d\frac{\sqrt{1-\left(\frac{m_a}{\omega_a}\right)^2}}{\left(\frac{m_a^2}{4\omega^2}\right)^4}E^{-3}\right)^{\frac{1}{4}} \tag{2.35}$$

as long as both beams are identical and we assume the interaction volume to have optimal sidelength $\ell^2 = d/k_a$.

2.3 Projected Bounds

To assess the performance of the proposal above, we evaluate the projected bounds utilising the specifications of the Aton 4 laser at ELI beam lines. This laser system operates at optical frequencies $\omega = 1.55\,\mathrm{eV}$ with $E = 1.5\,\mathrm{kJ}$ energy per pulse and has pulselengths of $\tau = 150\,\mathrm{fs}$ up to $\tau = \mathrm{ns}$. The optimal beam overlap V was found earlier and thus we choose to focus the beam to a cube with matching pulselength $\tau = \sqrt{d/k_a}$. The number of signal photons incident onto the photon detector is then approximated as $N_\gamma \sim E/\omega$. The Aton 4 laser has a repetition rate of $1\,\mathrm{min}^{-1}$ resulting in 1440 shots per day. Under the assumption that single photon counting is possible, the projected bounds for square interaction volume $\ell = \ell' = \tau$ and maximal

testable $m_a \sim 3.08\,\mathrm{eV}$ are found

$$g_{a\gamma\gamma} \geq 1.5 \times 10^{-7}\,\mathrm{GeV}^{-1} \left(\frac{E}{1.5\,\mathrm{kJ}}\right)^{-\frac{3}{4}} \left(\frac{d}{10\,\mathrm{cm}}\right)^{\frac{1}{4}} \tag{2.36}$$

and are shown as red region in the exclusion plot 2.2. The maximal mass arises from the requirement that the two colliding lasers be at least 1° off perfect counter-propagation, which is necessary to avoid damaging an actual laser.

As was discussed in (2.26) the laser frequencies and the collision angle sets the mass of the axion we probe. To exclude the whole region shown in the exclusion plot 2.2 we consider a realistic laser field with spectral width modelled as a Gaussian around the central frequency ω_j with width $\Delta\omega_j$. As long as $\Delta\omega_j/\omega_j \ll 1$ our earlier calculation still applies but the axion mass under investigation will no longer be single valued but have a Gaussian distribution around the mass corresponding to the central frequencies. Indeed we find

$$\frac{\delta m_a}{m_a} \simeq \frac{\Delta\omega_1}{\omega_1} + \frac{\Delta\omega_1}{\omega_1} \tag{2.37}$$

to be the mass interval over which the bounds vary by less than $\sqrt{2}$. We may thus probe the depicted mass region continuously by scanning through appropriately spaced collision angles with angle increments given by

$$\delta\alpha = 2\frac{\delta m_a}{m_a}\left(\csc\alpha - \cot\alpha\right). \tag{2.38}$$

The angular step size and mass interval are shown in figure 2.3. Putting a limit of 1° from parallel and anti-parallel propagation of the two lasers for practical reasons, we conclude that the mass region indicated in the exclusion plot may be covered in ~ 30 steps. In principle we may extend the region down to lower masses by exploiting the collision of two photons in a converging laser beam at arbitrarily small angles similar

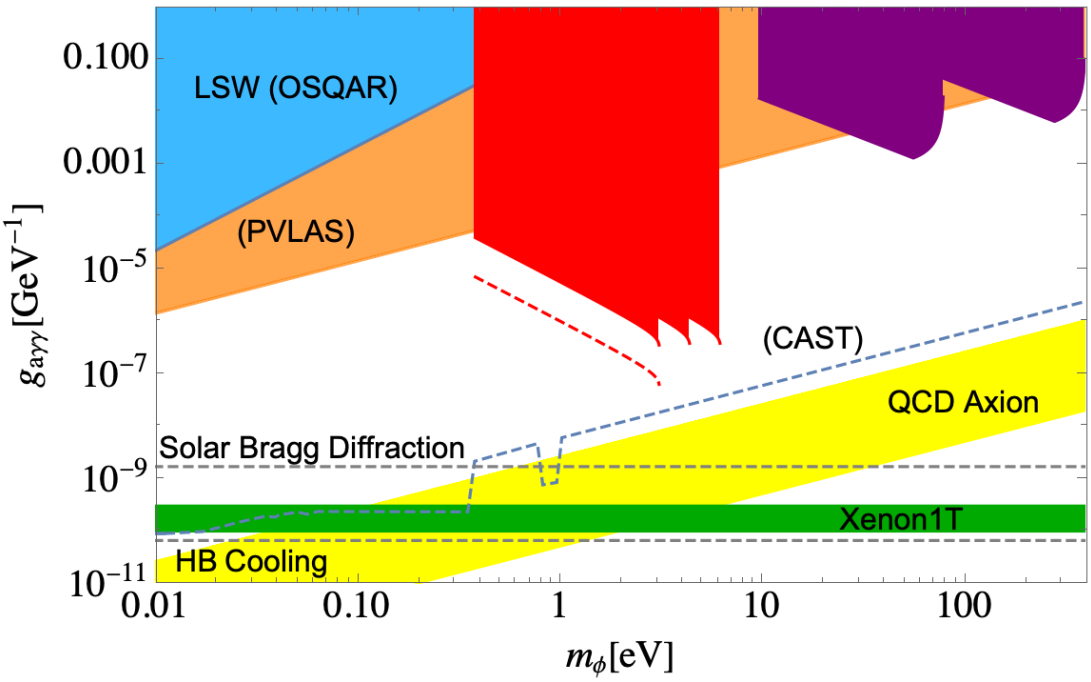

Figure 2.2: Exclusion plot for axion parameter space. The light blue region shows existing bounds from the OSQAR experiment [87]; the orange region is excluded by PVLAS [89]; the dashed blue line depicts CAST constraints [94]; the lower horizontal dashed line comes form stellar cooling lifetimes [95] and the upper from solar Bragg diffraction experiments [73]. The green region shows the Xenon1T anomaly interpreted as QCD axion signal [60, 61]. The red region on the left indicates the reach of the set-up described in the main text using three optical lasers. This region is extended in mass by combinations of frequency doubled beams, also indicated by the additional peaks in red. The dashed red line indicates the improvement for a 15 kJ laser. The purple region on the right shows the projected bounds for the collision of an optical 1.5 kJ laser and an X-ray laser like the European X-FEL. The frequency is tunable between $\omega = 1-25$ keV allowing us to probe anything between the two purple extremes. The QCD axion region, shown in yellow, indicates particular theoretical predictions for where the axion might be, if it constitutes the dark matter [96].

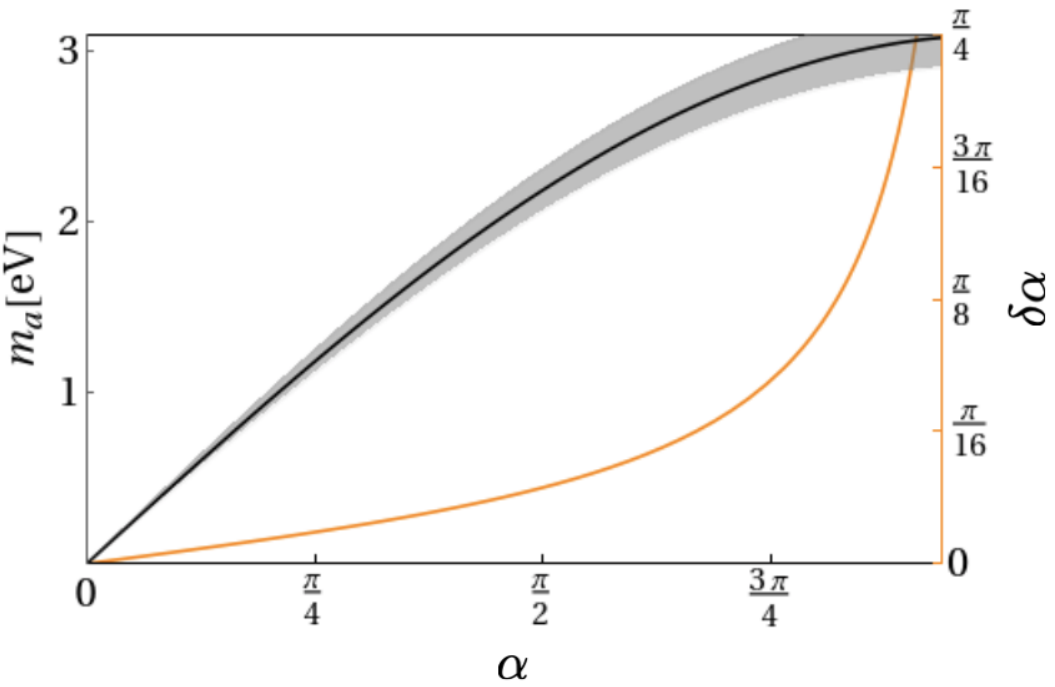

Figure 2.3: The orange curve plots the angular step size $\delta\alpha$ against the chosen angle α for each shot. On the left axis, the black curve indicates the central mass probed for a given α and $\omega_1^0 = \omega_2^0 = 1.55\,\text{eV}$, the shaded region indicates the width $\pm\delta m_a$. Assuming a minimum possible step-size $\delta\alpha \gtrsim 1°$, the full mass range can be scanned in ~ 30 shots. This step size imposes a lower bound on $\alpha \gtrsim 0.4\,\text{rad}$ corresponding to $m_a \gtrsim 0.6\,\text{eV}$.

to [97], however the bounds fall below the PVLAS bounds and do not probe new parameter space.

By exploiting frequency doubled beams we can extend the mass interval to larger masses. The red region directly to the right of the red projected bound in figure 2.2 is a projection for a frequency doubled beam under the assumption of 10% energy loss in the conversion. While just an estimate, techniques are efficient enough, that the bounds do not deviate significantly from the indicated ones.

To extend the mass interval to still higher masses we may exchange one optical generation laser with an x-ray beam. In general, substituting both beams would fur-

ther extend the mass interval, however the substantially smaller energies per pulse of x-ray sources render this approach sub-optimal. The European X-FEL operates at $\omega = \text{keV}$ with a pulse length $\tau = 228\,\text{eV}^{-1}$ and energy per pulse of $E = 0.5\,\text{mJ}$. The shorter pulselength limits the interaction region to a cube of sidelength τ and the resulting bounds are shown in purple in figure 2.2. Note that due to the asymmetric beams the simple expressions from before no longer apply, we quote the appropriate expressions in Appendix A. Note, also that the shape of the exclusion region varies because of the altered geometry. For a pair of symmetric beams the maximal bounds are found for $\mathbf{k}_a \to 0$, when the two beams collide head on. In this case, the electric and magnetic field of both beams perfectly align and $|\mathbf{E}_i \cdot \mathbf{B}_j|$ is maximal. For asymmetric beams the situation becomes more difficult and the maximum may no longer simply lie at the smallest $\mathbf{k}_a$.

Having obtained the results for asymmetric beams, we may now fill out part of the parameter space in between by combinations of frequency multiplied beams. The same is true for the collision of an optical and a x-ray beam because the latter is tunable up to 25 keV. The achievable region is indicated in fig 2.2 by the purple region.

Chapter 3

Parametric co-linear Axion photon instability

Parametric instabilities are common in laser plasma interactions resulting in the exponential growth of a coupled secondary wave at the expense of a strong pump pulse. We aim to investigate the coupling of axions to a strong pump laser, identifying a similar parametric instability, which we then aim to derive a measurable signal from to complement other laboratory axion searches.

The physical process leading to an instability is a positive feedback loop which transfers energy from a seed into the unstable mode. The latter will already be populated, either from a probe beam or the instability grows from noise. In the case of Raman instability, which is very reminiscent to the process described in the remainder of this section, a laser beam incident on a plasma excites plasma waves which become unstable [98]. Microscopically what happens is that the incident wave p_i^μ decays into a plasma wave p_l^μ and a secondary photon, the sideband, p_s^μ satisfying

$$p_i^\mu = p_l^\mu + p_s^\mu. \tag{3.1}$$

The initial laser beam displaces electrons in the plasma, leading to a plasma wave.

The moving plasma electrons emit radiation, the scattered sideband mode. This sideband mode in turn increases the ponderomotive force on the electrons expelling them further resulting in a positive feedback loop under which the plasma wave grows exponentially for early times [99]. A similar situation appears for an axion-photon system with the axion-photon coupling (1.27) taking the role of the ponderomotive force. An electromagnetic seed beam decays into a scattered sideband and an exponentially growing axion mode. The results described in this chapter were published in [4] and the arguments closely follow the arguments therein.

We envisage a set-up involving a strong laser beam, the pump, propagating in a vacuum. In the following the terms pump and seed are used interchangeably. We also consider the case in which the beam propagates in a plasma but it turns out that for our purposes limiting ourselves to the vacuum case is superior. By having a probe beam propagating parallel to the pump we start the parametric decay instability and feed energy from the pump into the probe and an axion mode. To achieve coupling between the beams, the probe pulse is polarised orthogonal compared to the pump and therefore the transfer in energy is accompanied by a change in polarisation of the combined electromagnetic field of pump and probe. We aim to measure this change in polarisation. As such the set-up shows similarities to [100] and the PVLAS search [89] but uses a different mechanism. The set-up is shown in figure 3.1 with pump and probe co-propagating from the left and a polarisation detector on the right.

Previous considerations of the axion-photon coupling were mostly limited to static, constant fields as in [37, 91] which break the spatial invariance of the background and therefore allow photon axion mixing. This is the starting point of LSW type experiments or searches like CAST. Previous work on axion photon coupling in electromagnetic waves focused on the scattering processes as in [100, 3] but did not account for parametric instabilities. The situation in plasmae is less well researched, however some work was done assuming electromagnetic duality symmetry [101, 102], a sym-

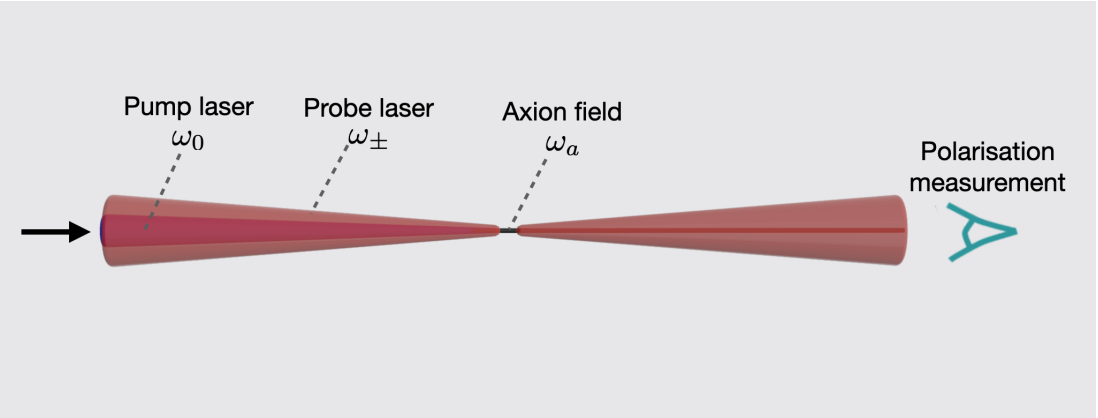

Figure 3.1: A cartoon of the set-up described in the text. A strong pump pulse co-propagates with a weaker probe of orthogonal polarisation. They couple via the parametric instability found in this chapter and energy is transferred from the pump into the probe and an axion mode. Because of the orthogonal polarisation, there is a change in polarisation of the combined electromagnetic wave which can be measured.

metry low energy electromagnetism does not posses. Parametric decay instabilities in axion photon systems was investigated in [103] where the authors consider dispersion relations close to the vacuum ones and simplify their system to first order differential equations. This effectively assumes that the growth rate $\Gamma \ll \omega$ the energy of the axion, an assumption which does not hold in our analysis.

3.1 Instability growth rate

The system of axions and photons is again described by Axion electrodynamics as in the previous chapter. We now also include electric charges but ignore the axion's coupling to fermions. Including electromagnetic charges, the Gauss law for magnetism

$$\nabla \cdot \mathbf{B} = 0 \tag{3.2}$$

and the Maxwell-Faraday law of induction

$$\nabla \times \mathbf{E} = -\partial_t \mathbf{B} \tag{3.3}$$

are unchanged, however, Gauss's law gets an additional source from the axion field

$$\nabla \cdot \mathbf{E} = 4\pi\rho + g_{a\gamma\gamma} (\nabla a) \cdot \mathbf{B} \tag{3.4}$$

and Ampère's law includes an additional current

$$\nabla \times \mathbf{B} = 4\pi\mathbf{J} + \partial_t \mathbf{E} + g_{a\gamma\gamma} (\mathbf{E} \times \nabla a - \mathbf{B}\partial_t a) . \tag{3.5}$$

Here, ρ is the electromagnetic charge density and $\mathbf{J}$ the electromagnetic charge current. The observable fields are defined by the gauge fields $A^\mu = (\Phi, \mathbf{A})$

$$\mathbf{E} = -\partial_t \mathbf{A} - \nabla\Phi \tag{3.6}$$

and

$$\mathbf{B} = \nabla \times \mathbf{A}. \tag{3.7}$$

To close the description of our system we take the plasma to be a simple fluid, an assumption which should generally be acceptable given that our axions do not couple to the charged fermions directly but only through the electromagnetic fields. Therefore the charge conservation equation is unaltered after we gauge fix $\nabla \cdot \mathbf{A} = 0$

$$\partial_t \rho + \nabla \cdot \mathbf{J} = 0. \tag{3.8}$$

The fluid motion follows a Vlasov equation

$$\partial_t \mathbf{u} + (\mathbf{u} \cdot \nabla)\, \mathbf{u} = -\frac{e}{m_e} (\mathbf{E} + \mathbf{u} \times \mathbf{B}) - \frac{\nabla P}{n_e m_e} \tag{3.9}$$

with P the pressure.

Newton's law is simple to apply after two simplifying assumptions. We first assume that any density fluctuations are orthogonal to $\mathbf{A}$, an assumption which amounts to ignoring pressure effects. The density fluctuations stem from the seed beams electric field expelling electrons from regions of high field to regions of lower field. The result is a pressure wave which runs along the seed pulse wave. As long as we ignore edge effects this assumption is justified. The second assumption concerns the electron motion. We will assume non-relativistic motion to neglect the influence of the magnetic field. Note that in the end the electron motion plays a small role in deriving the limits under consideration here, which makes this assumption relatively unimportant. Under these assumptions

$$\partial_t \mathbf{u}_t = -\frac{e}{m_e} \partial_t \mathbf{A} \tag{3.10}$$

with $\mathbf{u}_t$ the transverse electron velocity and m_e the electron mass. Thence the transverse current

$$\mathbf{J}_t \equiv -e n_e \mathbf{u}_t = -\frac{e^2 n_e}{m_e} \mathbf{A} \tag{3.11}$$

where n_e is the electron density. The ions are considered stationary.

From Gauss's law (3.4) we find Poisson's equation

$$\nabla^2 \Phi = -4\pi\rho - g_{a\gamma\gamma}\, (\nabla a) \cdot (\nabla \times \mathbf{A})\,. \tag{3.12}$$

Assuming appropriate boundary conditions of vanishing currents at spatial infinity,

Poisson's equation and charge conservation fix the longitudinal part of the current

$$\mathbf{J}_l = \partial_t \nabla\Phi - g_{a\gamma\gamma}\partial_t \left(a\nabla \times \mathbf{A}\right) = 0. \tag{3.13}$$

We are then ready to find the wave equation governing the gauge field evolution from Ampère's law and the above assumptions. We find

$$\left(\partial_t^2 - \nabla^2 + \omega_{\rm pl}^2\right)\mathbf{A} = g_{a\gamma\gamma}\left(\nabla \times (a\partial_t \mathbf{A}) + (\nabla a) \times (\nabla\Phi)\right). \tag{3.14}$$

Here we defined the plasma frequency $\omega_{\rm pl}^2 = 4\pi e^2 n_e/m_e$, the natural oscillation frequency of a plasma.

The axion field is described by a Klein-Gordon equation

$$\left(\partial_t^2 - \nabla^2 + m_a^2\right) a = -g_{a\gamma\gamma}\mathbf{E}\cdot\mathbf{B}. \tag{3.15}$$

We proceed by performing a linear stability analysis of the coupled equations for the plasma response (3.9), the gauge potentials (3.12), (3.14) and the axion field (3.15). We will assume the presence of a strong pump pulse, the seed and linearise the system around such pump. We define for this purpose a set of background fields and fluctuation fields evolving in those backgrounds. Take

$$\mathbf{A} \equiv \mathbf{A}_0 + \delta\mathbf{A}, \qquad n_e \equiv n_0 + \delta n, \qquad \Phi \equiv 0 + \delta\Phi, \qquad a \equiv 0 + \delta a \tag{3.16}$$

and make the assumption that $\delta\mathbf{A}, \delta\Phi, \delta a, \delta n \ll \mathbf{A}_0, n_0$, all fluctuation fields are small. Note that here we are assuming that the initial seed beam is still well described by only the vector potential, an assumption which only holds for early times. Nonetheless, this should be enough, insofar as we are mainly interested in the early stages of the instability and due to the weak coupling $g_{a\gamma\gamma}$ the growth rate will be too slow

for back-reaction onto the seed to become significant. We will also find that the high degree of accuracy in polarisation measurements allows for the detection of this instability well before this assumption breaks down. Therefore, we linearise the equations by dropping higher order terms in the fluctuation fields. In the following we are concerned with situations in which equilibrium is not reached and the above assumption continues to be true throughout the duration of the experiment.

We find a set of linearised equations

$$\left(\partial_t^2 + \omega_{\rm pl}^2 - 3v_e^2\nabla^2\right)\delta n = \frac{e^2 n_0}{m_e^2}\nabla^2\left(\mathbf{A}_0\cdot\delta\mathbf{A}\right) + g_{a\gamma\gamma}\frac{e n_0}{m_e}\left(\nabla\delta a\right)\cdot\left(\nabla\times\mathbf{A}_0\right) \tag{3.17}$$

with v_e the electrons thermal velocity entering through the pressure term,

$$\nabla^2\delta\Phi = 4\pi e\delta n - g_{a\gamma\gamma}\left(\nabla\delta a\right)\cdot\left(\nabla\times\mathbf{A}_0\right) \tag{3.18}$$

and

$$\left(\partial_t^2 + \omega_{\rm pl}^2 - \nabla^2\right)\delta\mathbf{A} = -\frac{4\pi e^2}{m_e}\delta n\mathbf{A}_0 + g_{a\gamma\gamma}\nabla\times\left((\partial_t\mathbf{A}_0)\delta a\right) \tag{3.19}$$

for the Gauge fields and

$$\left(\partial_t^2 - \nabla^2 + m_a^2\right)\delta a = g_{a\gamma\gamma}\left[\left(\partial_t\delta\mathbf{A} + \nabla\delta\Phi\right)\cdot\left(\nabla\times\mathbf{A}_0\right) + \left(\nabla\times\delta\mathbf{A}\right)\cdot\partial_t\mathbf{A}_0\right] \tag{3.20}$$

for the axion field. To solve these coupled equations we perform a spatial Fourier analysis

$$f\left(\mathbf{k},t\right) \equiv \int f\left(\mathbf{x},t\right)e^{-i\mathbf{k}\cdot\mathbf{x}}\frac{d^3\mathbf{x}}{\left(2\pi\right)^{3/2}}. \tag{3.21}$$

Taking the seed background field to be $\mathbf{A}_0 \equiv \mathbf{A}_0\cos\left(k_0.x\right)$ we are then left with

$$\begin{aligned}\left(-\partial_t^2 - \mathbf{k}^2 - \omega_{\rm pl}^2\right)\delta\mathbf{A}(\mathbf{k},t) = \frac{\omega_{\rm pl}^2}{2}\left(\frac{\delta n_+}{n_0}e^{i\omega_0 t} + \frac{\delta n_-}{n_0}e^{-i\omega_0 t}\right)\mathbf{A}_0 \\ - g_{a\gamma\gamma}\frac{\omega_0}{2}\left(\mathbf{k}\times\mathbf{A}_0\right)\left(\delta a_- e^{-i\omega_0 t} - \delta a_+ e^{i\omega_0 t}\right),\end{aligned} \tag{3.22}$$

$$\mathbf{k}^2\delta\Phi(\mathbf{k},t) = -4\pi e\delta n + \frac{g_{a\gamma\gamma}}{2}\mathbf{k}\cdot(\mathbf{k}_0\times\mathbf{A}_0)\left(\delta a_- e^{-i\omega_0 t} - \delta a_+ e^{i\omega_0 t}\right), \tag{3.23}$$

$$\left(-\partial_t^2 - \omega_{\rm ek}^2\right)\frac{\delta n(\mathbf{k},t)}{n_0} = \frac{\mathbf{k^2}e^2}{2m_e^2}\mathbf{A}_0\cdot\left(\delta\mathbf{A}_- e^{-i\omega_0 t} + \delta\mathbf{A}_+ e^{i\omega_0 t}\right) \tag{3.24}$$
$$- \frac{g_{a\gamma\gamma}}{2}\frac{e}{m_e}\mathbf{k}\cdot(\mathbf{k}_0\times\mathbf{A}_0)\left(\delta a_- e^{-i\omega_0 t} - \delta a_+ e^{i\omega_0 t}\right)$$

and

$$\left(-\partial_t^2 - \mathbf{k}^2 - m_a^2\right)\delta a(\mathbf{k},t) = \frac{g_{a\gamma\gamma}}{2}\Bigg[\mathbf{k}\cdot(\mathbf{k}_0\times\mathbf{A}_0)\left(\delta\Phi_- e^{-i\omega_0 t} - \delta\Phi_+ e^{i\omega_0 t}\right) \tag{3.25}$$
$$+\mathbf{A}_0\cdot\left(e^{i\omega_0 t}\left(\omega_0\mathbf{k}_+ - i\mathbf{k}_0\partial_t\right)\times\delta\mathbf{A}_+ - e^{-i\omega_0 t}\left(\omega_0\mathbf{k}_- - i\mathbf{k}_0\partial_t\right)\times\delta\mathbf{A}_-\right)\Bigg].$$

We have used shorthand notation $f_\pm$ to mean $f(\mathbf{k}\pm\mathbf{k}_0)$. Looking at the coupled equations we can see that only such fields couple whose momenta satisfy the mode matching condition

$$\mathbf{k}_0 = \mathbf{k}_a + \mathbf{k}_\gamma. \tag{3.26}$$

Because there is both, $\pm\mathbf{k}_0$ in the seed pulse, both the sum and difference sideband modes contribute.

To proceed, we now make another simplifying assumption, we will work in the co-linear limit where all waves propagate in parallel. Hence, $\mathbf{k}\propto\mathbf{k}_0$ for all modes, which simplifies the situation substantially. Dividing the gauge field $\delta\mathbf{A}$ into two components, one parallel and one orthogonal to the seed field $\delta\mathbf{A}_{||}$ and $\delta\mathbf{A}_\perp$, we find that only the orthogonal piece couples to the axion field. Remembering that the axion-photon coupling is polarisation dependent and vanishes for parallel polarised fields, this is to be expected. We can also see this in the equations where now $\mathbf{k}\cdot(\mathbf{k}_0\times\mathbf{A}_0)\equiv 0$ and $\mathbf{A}_0\cdot\left(\mathbf{k}\times\delta\mathbf{A}_{||}\right) = 0$. In fact the whole system splits into two separate subsystems, the parallel gauge field couples to the density waves through

the following system of equations

$$\left(-\partial_t^2 - \mathbf{k}^2 - \omega_{\mathrm{pl}}^2\right) \delta\mathbf{A}^{\parallel}(\mathbf{k},t) = \frac{\omega_{\mathrm{pl}}^2}{2}\left(\frac{\delta n_+}{n_0}e^{i\omega_0 t} + \frac{\delta n_-}{n_0}e^{-i\omega_0 t}\right)\mathbf{A}_0, \tag{3.27}$$

$$\mathbf{k}^2\delta\Phi(\mathbf{k},t) = -4\pi e\delta n \tag{3.28}$$

and

$$\left(-\partial_t^2 - \omega_{\mathrm{ek}}^2\right)\frac{\delta n(\mathbf{k},t)}{n_0} = \frac{\mathbf{k}^2 e^2}{2m_e^2}\mathbf{A}_0 \cdot \left(\delta\mathbf{A}_-^{\parallel}e^{-i\omega_0 t} + \delta\mathbf{A}_+^{\parallel}e^{i\omega_0 t}\right). \tag{3.29}$$

This system is identical to that describing the Raman instability, which was mentioned at the beginning of this chapter. For this reason, and because it is decoupled from the axion field, we will not go into further detail.

The interesting bit is the remaining coupled system describing the perpendicular field

$$\left(-\partial_t^2 - \mathbf{k}^2 - \omega_{\mathrm{pl}}^2\right)\delta\mathbf{A}^{\perp}(\mathbf{k},t) = -g_{a\gamma\gamma}\frac{\omega_0}{2}\left(\mathbf{k}\times\mathbf{A}_0\right)\left(\delta a_- e^{-i\omega_0 t} - \delta a_+ e^{i\omega_0 t}\right) \tag{3.30}$$

closed with

$$\left(-\partial_t^2 - \mathbf{k}^2 - m_a^2\right)\delta a(\mathbf{k},t) = \frac{g_{a\gamma\gamma}}{2}\mathbf{A}_0 \cdot \Big(e^{i\omega_0 t}\left(\omega_0\mathbf{k}_+ - i\mathbf{k}_0\partial_t\right)\times\delta\mathbf{A}_+^{\perp} - e^{-i\omega_0 t}\left(\omega_0\mathbf{k}_- - i\mathbf{k}_0\partial_t\right)\times\delta\mathbf{A}_-^{\perp}\Big). \tag{3.31}$$

As we are specifically interested in the perpendicular fluctuation field we will from now on suppress the label $\perp$ when referring to this field. We then proceed to solve the equations by making an ansatz for the time dependence

$$f(\mathbf{k},t) = f(\mathbf{k})e^{-i\omega(\mathbf{k})t} \tag{3.32}$$

reducing the set of coupled differential equations to a set of algebraic equations in $\omega(\mathbf{k})$. We attempt to solve the equations by substitution of (3.30) into (3.31) to eliminate the fields $\delta\mathbf{A}$. In principle we are left with an infinite tower of coupled axion fields $a(\mathbf{k} \pm j\mathbf{k}_0)$, $j \in \mathcal{Z}$ which arises from (3.26). An axion with momentum $\mathbf{k}$ propagating in the seed pulse couples to a photon with momentum $\mathbf{k} \pm \mathbf{k}_0$. Such a photon then interacts with a seed photon to form axions of momentum $\mathbf{k} \pm \mathbf{k}_0 + \mathbf{k}_0$. Each of those axions then starts the same process again, hence a whole cascade of axions modes is produced. In reality, however, the production of all higher harmonic modes is heavily suppressed. Such terms can generally arise in two distinct ways, by cascading as described before or from the spectral width of the seed pulse. In the former case their appearance is generally higher order in the coupling $g_{a\gamma\gamma}$ as is apparent from the fact that $a(\mathbf{k} \pm (j+1)\mathbf{k}_0)$ only appears after $a(\mathbf{k} \pm j\mathbf{k}_0)$ is already present and decayed. In the second case, a photon away from the central momentum of the beam with $j\mathbf{k}_0$ seeds the instability and immediately generates an axion with $a(\mathbf{k} \pm j\mathbf{k}_0)$. Modelling the beam as Gaussian with a very narrow spectral width we can also ignore this effect based on the suppression of photons in the tails of the distribution. We will thus proceed by dropping all fields of momentum $\mathbf{k} \pm 2\mathbf{k}_0$ and higher.

The system of algebraic equations is then solved for axion fields $a(\mathbf{k})$ and photon fields $\delta\mathbf{A}_\pm$ with frequencies $\omega(k)$ satisfying the dispersion relation

$$D^a\left(\omega(k), k\right) = \frac{g_{a\gamma\gamma}^2 A_0^2}{4}\left(\omega_0 k - \omega(k) k_0\right)\left(\frac{\omega_0(k-k_0)}{D^\gamma\left(\omega(k)-\omega_0, k-k_0\right)} + \frac{\omega_0(k+k_0)}{D^\gamma\left(\omega(k)+\omega_0, k+k_0\right)}\right). \tag{3.33}$$

For notational convenience we have defined the bare dispersions in the decoupling limit $g_{a\gamma\gamma} \to 0$

$$D^a\left(\omega(k), k\right) = \omega(k)^2 - k^2 - m_a^2 \tag{3.34}$$

and

$$D^{\gamma}\left(\omega(k)\pm\omega_0, k\pm k_0\right) \equiv \left(\omega(k)\pm\omega_0\right)^2 - \left(k\pm k_0\right)^2 - \omega_{\mathrm{pl}}^2. \tag{3.35}$$

Note that despite the decoupling of the plasmons from the axions in the chosen co-linear limit, the plasma changes the photon's dispersion relation and gives it an effective mass ω_{pl}. As we will see, this mass plays an interesting role in the axion-photon instability we find.

To solve the dispersion relation we first proceed numerically to get an idea of the hierarchies involved. The numerical solution of the dispersion relation (3.33) is straight forward: it is a polynomial of 6th order, which, as such has 6 solutions. We are interested in any complex solution. If such a solution exists, we will conclude that the system is unstable and grows exponentially with time, as can be seen from (3.32)

$$e^{-i\omega(k)t} = e^{-i\Re(\omega(k))t+\Im(\omega(k))t}. \tag{3.36}$$

This exponential growth will only be present as long as the assumptions we made above hold, especially the hierarchy between seed field and sideband mode only holds in the early stages and eventually stops the exponential growth. Figure 3.2 shows the numerical solution to the dispersion relation (3.33) exhibiting an instability. The dotted green curve shows the bare axion dispersion (3.34) for comparison. In blue we see the axion's energy, the real part of the frequency $\omega(k)$ and the dashed yellow line indicates the imaginary part, the growth rate. Some interesting behaviour emerges, which should be explained in the following.

The first observation we make is that the growth rate is essentially constant in axion momentum when the momentum is low and sharply drops off at a cut-off value above which no instability is found. We also find that the axion's energy $\Re(\omega(k))$ is orders of magnitude smaller than the seed pulse frequency. It is in fact much smaller than the growth rate which will later complicate the analytic calculation. The fact

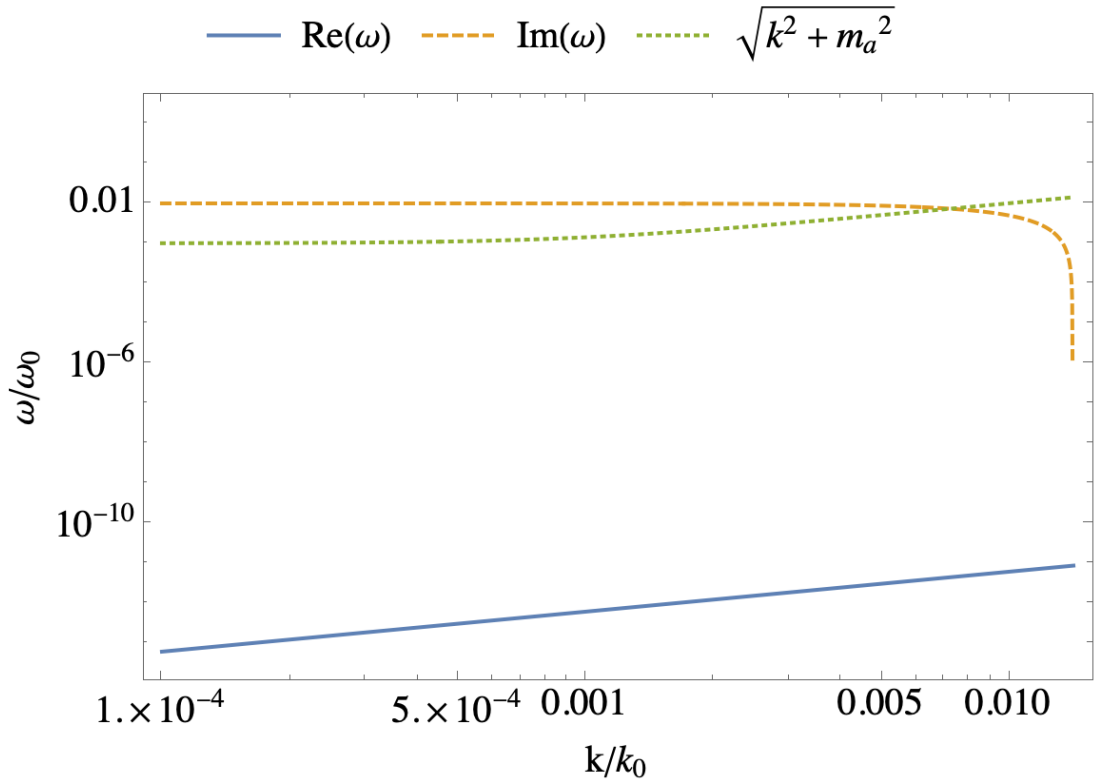

Figure 3.2: The plot shows the growing solution to the dispersion relation (3.33). The blue solid curve shows the real part $w(k)$ corresponding to the modes' frequency while the dashed yellow curve depicts the growth rate Γ. Note that here we included the $\mathcal{O}(k^2)$ contributions to show the cutoff. As a reference we include the vacuum dispersion relation for an axion with the same mass in dotted green. For illustration purposes, we have chosen $m_a/\omega_0 = 10^{-2}$ and $g_{a\gamma\gamma}A_0 = 10^{-3}$. We see that even for such large values, the axion frequency is negligibly small. The plasma frequency $\omega_{\rm pl} = 0$ here, see the main text for discussion on the effect of the plasma.

that it is much smaller than the bare dispersion in vacuum makes the mode evanescent [104]. In essence this means that the propagating axion mode cannot propagate out into vacuum as it does not have enough energy to support its mass. This is fully analogous to a light wave incident on a supercritical plasma, a plasma with density such that $\omega_\gamma < \omega_{\rm pl}$. The electromagnetic wave cannot propagate into the plasma and is reflected. Note that not every unstable axion mode we find is necessarily evanescent,

but for sufficiently large axion mass they are. Generally a mode is evanescent if its energy is below its vacuum mass.

We can make two further observations when scanning the plasma density and axion mass. We find that there is a cutoff mass above which we can no longer find an instability. This is to be expected, as in the co-linear limit, only very light axions with negligible mass fulfil energy-momentum conservation at the three point vertex between axion and two photons. It should be noted that in the vacuum limit, the decay of a massless particle to a massive one is forbidden, however in our case the background is a strong electromagnetic field. The energy momentum conservation condition is modified due to the presence of the strong laser fields and plasma density. A toy example was investigated in [105] where a similar observation was made; while a perturbative calculation around the vacuum state suggests the decay of a massless to a massive particle is forbidden, non-perturbative analysis reveals that the process can take place in sufficiently strong fields for small enough masses $m_a/\omega_0 \ll 1$. We will find the precise condition later on in this section. Further, we may notice that changing the plasma frequency affects the growth rate only marginally but changes the axion's energy significantly. It is changed so significantly that the unstable axion mode travels backwards for sufficiently dense plasmas and forward in the vacuum limit. A backwards propagating mode is characterised by a relative sign between frequency $\omega(k)$ and momentum k.

In the following we will use the above observations to solve the dispersion relation (3.33) analytically. We will then use this solution to make the above statements concerning cutoffs and relative sizes precise. For simplicity we begin by considering the vacuum limit $\omega_{\mathrm{pl}} \to 0$. The dispersion relation is a 6^{th}-order polynomial in $\omega(k)$. As they are stable, the two real roots $\omega(k) = k$ can be discarded. If there exists an instability in the system, eventually the unstable mode, growing exponentially, will dominate, hence we are justified in dropping the other modes. We proceed by working

with the remaining 4^{th}-order polynomial and splitting $\omega(k)$ into its real and imaginary parts $\omega(k) = w(k) + i\Gamma(k)$ for $w(k), \Gamma(k) \in \mathcal{R}$. The resulting real and imaginary equations are linearly independent and therefore must be satisfied individually.

The remaining imaginary equation is a cubic polynomial in the growth rate $\Gamma(k)$ with one trivial solution $\Gamma(k) = 0$ and two non-trivial ones

$$\Gamma = \pm\sqrt{\frac{3kw^2 + 2w^3 - 4w\omega_0^2 - k^3 - m_a^2(w+k) + \frac{g_{a\gamma\gamma}^2 A_0^2}{4} k\omega_0^2}{k - 2w}}. \tag{3.37}$$

We know that, with the ansatz (3.32), only a positive $\Gamma(k)$ corresponds to growth, hence we focus on the positive root only. After substituting $\Gamma(k)$ into the real part of the equation, we are then left with a single algebraic equation for $w(k)$. Figure 3.2 shows that in our case, the frequency $w(k)$ is very small, thus motivating an expansion in $w(k)$, which we find to be

$$w(k) = k\frac{(g_{a\gamma\gamma}A_0)^2}{64}\left(\left(\frac{g_{a\gamma\gamma}A_0}{2}\right)^2 - \left(\frac{m_a}{\omega_0}\right)^2\right). \tag{3.38}$$

Here we dropped terms of order 6 in $(g_{a\gamma\gamma}A_0)$, (m_a/ω_0) and k as being small. The growth rate can then be expressed as

$$\Gamma(k) = \omega_0\sqrt{\left(\frac{g_{a\gamma\gamma}A_0}{2}\right)^2 - \left(\frac{m_a}{\omega_0}\right)^2 - \left(\frac{k}{k_0}\right)^2}, \tag{3.39}$$

where we have again dropped higher order terms in $(g_{a\gamma\gamma}A_0)$, (m_a/ω_0) and (k/k_0).

Upon a closer look at (3.39), the qualitative behaviour of the numerical solution depicted in fig 3.2 is recovered. We find growth below a cutoff in k, which is defined by

$$k_{\text{cutoff}} = k_0\sqrt{\left(\frac{g_{a\gamma\gamma}A_0}{2}\right)^2 - \left(\frac{m_a}{\omega_0}\right)^2}. \tag{3.40}$$

For larger k, $\Gamma(k)$ becomes imaginary and our solution, which intimately relies upon

the linear independence of the equations for the imaginary and real part we split earlier, breaks down. We had already found before that the growth rate is essentially constant in $k < k_{\text{cutoff}}$, a behaviour which is obvious here and allows us to suppress the dependence of Γ in the following. (3.39) also reveals a second cutoff for $m_a/\omega_0 > g_{a\gamma\gamma}A_0$ above which no instability is found.

From (3.38) we can calculate the phase velocity of the unstable modes

$$v_a = \frac{\partial w(k)}{\partial k} = \frac{(g_{a\gamma\gamma}A_0)^2}{64}\left(\left(\frac{g_{a\gamma\gamma}A_0}{2}\right)^2 - \left(\frac{m_a}{\omega_0}\right)^2\right), \tag{3.41}$$

which can be much slower than the speed of light even for massless $m_a = 0$ axions. Surprisingly, the axions' velocity appears to vanish in the decoupling limit $g_{a\gamma\gamma} \to 0$. Upon closer inspection we realise that in fact our method of solution breaks down in this limit. The growth rate (3.39) becomes imaginary in this case and the two equations we got by splitting $\omega(k)$ into a real and an imaginary part are no longer linearly independent. In fact, we can see that, in the decoupling limit, the bare dispersion is recovered already from the dispersion relation (3.33).

The inclusion of a plasma in our set up does not alter our method for solving the equation. In this case, however, the solution becomes less tractable. Reproducing the full result leaves only little insight. On the other hand, finding the lowest order correction stemming from the plasma frequency will reveal interesting behaviour. The frequency of the axion field to lowest order in this circumstance is

$$w_{\text{pl}}(k) = -\frac{1}{2}\frac{\omega_{\text{pl}}^2}{\omega_0^2}\frac{\left(\frac{g_{a\gamma\gamma}A_0}{2}\right)^2}{\left(\frac{g_{a\gamma\gamma}A_0}{2}\right)^2 - \frac{m_a^2}{\omega_0^2}}k + \mathcal{O}(\omega_{\text{pl}}^4) \tag{3.42}$$

with special attention to the sign of the solution. The presence of a plasma changes the relative sign between $w(k)$ and k, the wave propagates in the opposite direction. While the axion wave was co-propagating with the seed beam before, it is now back-

scattered. Compared to the frequency in (3.38) it is also revealed that the frequency is significantly larger in a background plasma alongside the axion velocity

$$v_a^{\rm pl} = \frac{\partial w_{\rm pl}(k)}{\partial k} = -\frac{1}{2}\frac{\omega_{\rm pl}^2}{\omega_0^2}\frac{\left(\frac{g_{a\gamma\gamma}A_0}{2}\right)^2}{\left(\frac{g_{a\gamma\gamma}A_0}{2}\right)^2 - \frac{m_a^2}{\omega_0^2}}. \tag{3.43}$$

This makes the inclusion of a plasma inferior to the vacuum case. In a plasma, the effective time for which the instability grows is set by the crossing time of the axions because they can no longer be assumed stationary as was clearly possible in the vacuum case (3.38). As was already suggested by the numerical solution, the growth rate does not change significantly

$$\Gamma_{\rm pl}(k) = \Gamma(k)\left(1 - \frac{1}{2}\frac{\omega_{\rm pl}^2}{\omega_0^2}\frac{\left(\frac{g_{a\gamma\gamma}A_0}{2}\right)^2}{\left(\frac{g_{a\gamma\gamma}A_0}{2}\right)^2 - \frac{m_a^2}{\omega_0^2}}\right). \tag{3.44}$$

In addition to that, the cut-off momentum (3.40) does not change substantially. When considering a real experiment, the addition of a plasma also adds to the background signal and complicates the analysis. To this end, we conclude that the optimal set-up is in vacuum, $\omega_{\rm pl} \to 0$ and adopt this limit in the following.

3.2 Experimental signal and projected bounds

There is a plethora of possible signatures to measure the existence of axions by means of the instability discussed above. Unfortunately, the smallness of the axion frequencies $w(k)$ which become unstable renders most of them unobservable. Physically, the seed pulse breaks into an axion and a sideband photon, hence depleting the energy of the pump. This, however, is not detectable for two reasons: first, our calculation makes the assumption that the seed beam is a background field and does not significantly change. This is ensured by the hierarchy between the seed field and the

fluctuation fields. Further, the axion's frequency is so small, $w(k) \ll \omega_0$, that any sideband mode will be within the spectral width of any realistic seed laser. Therefore, the laser beam only loses the energy going into axion radiation, which is negligible for the same reason: the frequency is small.

Upon closer inspection, it becomes apparent that while the frequency of the sideband modes is essentially indistinguishable from the seed laser frequency, the polarisation is different. The coupling (1.27) ensures that the two photons are orthogonally polarized; thus, while the energy of the seed beam decreases like $w(k)N_a$, the polarisation changes much faster.

The set-up we have in mind consists of a pump pulse polarised in $\hat{x}$ and a weaker probe with polarisation in $\hat{y}$. We require the presence of the probe such that the instability can commence. The first axions are created via stimulated decay of a laser photon at ω_0 into a photon of the probe laser and an axion. Once present the axion field grows through the $\mathbf{E} \cdot \mathbf{B}$ source term, which takes the role of the ponderomotive force in the Raman instability. The large hierarchy between the pump pulse and the other modes ensures that together with the axion field, the probe beam field also grows while the pump is depleted [99, 106]. Because of the slow growth rate at hand we need not concern ourselves with the termination of the growth once the fluctuation fields become comparable to the pump pulse.

We define the initial polarisation of the combined seed and probe wave as

$$\mathcal{P}(0) = \frac{\mathbf{A} \cdot \hat{x} - \delta\mathbf{A} \cdot \hat{y}}{A_0} \equiv 1 - \varepsilon. \tag{3.45}$$

Here, $\varepsilon \equiv \delta A/A_0 < 1$. For early times, the pump pulse is unaffected and only the probe grows alongside the axion mode through the

$$\frac{g_{a\gamma\gamma}A_0}{2}\delta a e^{-i\omega_0 t + \gamma t} \tag{3.46}$$

source term on the right hand side of (3.30) where we ignore the small shift in frequency as $w(k) \ll \omega_0$. Since the growth rate does not depend on k, the Fourier transform is trivial. Thus, the polarisation has a time dependence given by

$$\mathcal{P}(t) = 1 - \varepsilon - (g_{a\gamma\gamma} A_0)\xi e^{\Gamma t}. \tag{3.47}$$

We need not know ξ very well as it will eventually only enter the sensitivity in a log and not play a significant role. Change in the polarisation of lasers can be measured to astonishing accuracy as was demonstrated by e.g. the PVLAS collaboration [89]. It should definitely be possible to measure polarisation changes on the order of $\Delta\mathcal{P} \sim 0.001$ and probably better. Taking this as a reference value we are ready to project the reach of an experiment utilising the above instability to search for axions.

Straightway, we appreciate that the most important part in the signal calculation is the exponential. The timescale of growth t will be set by the laser pulse length τ. The growth rate (3.39) depends on the laser parameters

$$\Gamma = 9.4 \times 10^{-5}\,\mathrm{s}^{-1} \left(\frac{g_{a\gamma\gamma}}{10^{-8}\,\mathrm{GeV}^{-1}}\right) \left(\frac{\mathcal{I}}{\mathrm{W/cm}^2}\right)^{\frac{1}{2}}. \tag{3.48}$$

Here we calculate the laser intensity from the energy per pulse $\mathcal{E}_0$, the pulse length τ and the focal spot size ℓ

$$\mathcal{I} \equiv \frac{\mathcal{E}_0}{\tau \ell^2} = \frac{A_0^2}{\omega_0 \tau \ell^2}. \tag{3.49}$$

The very small axion momentum requires the focus to be maintained for long distances $> k^{-1}$. This has a simple explanation: when calculating the dispersion relation, we have effectively assumed infinite extent of the modes involved. For this assumption to hold, the axion wavelength must be shorter than the laser pulse spatial size. Once this assumption breaks down, the axion no longer fits into the pulse and such long wavelength modes are not present in the spectrum. This is equivalent to

quantising the system in a box whose spatial extend sets an upper bound on the wavelength of any mode inside. We thus find a lower bound on the axion wavelength $\lambda_a \geq k_{\text{cutoff}}^{-1}$ and estimate that distance

$$\lambda_a \geq 3.2 \times 10^{12}\,\text{m} \left(\frac{g_{a\gamma\gamma}}{10^{-8}\,\text{GeV}^{-1}}\right)^{-1} \left(\frac{\mathcal{I}}{\text{W/cm}^2}\right)^{-\frac{1}{2}}. \tag{3.50}$$

At this point, two problems become apparent. First, the wavelength is very long and the lower bound is intensity dependent and therefore depends on the focal spotsize through (3.49). We hence need to minimise the focal spot size such that the intensity is maximised while at the same time keeping the focus over macroscopic distances.

The highest laser intensity currently operating systems can generate is around $\mathcal{I} = 10^{23}\,\text{W/cm}^2$ and this lasts for $\tau \sim 10\,\text{fs}$ [107]; for a review of current laser technology see [108]. Such intensities would correspond to a wavelength of $\lambda_a = 9\,\text{m}$. Generating and maintaining long laser focuses might be possible with a variety of approaches in the future. For example, the latest plasma-waveguides are capable of maintaining a laser focus over 10 m scales [109, 110]. It is also worth pointing out that the required focus length decreases mildly with laser power, hence the problem will become marginally simpler in the future. Nonetheless, the scaling is not sufficient to expect a solution to the problem simply from improving laser technology. In fact, the Schwinger limit, sometimes called the critical field strength of QED, corresponds to intensities $\mathcal{I}_{\text{crit}} \sim 10^{29}\,\text{W/cm}^2$. At higher intensities, pair production becomes efficient. Schwinger limit fields would correspond to axion wavelengths $\lambda_a > 1\,\text{cm}$ still much larger than optical wavelengths of the seed beam and therefore continues to pose a challenge for the length of the focus. We conclude that an increase in laser intensity does help to bring the axion wavelength down to sizes which fit into the target vacuum chambers of high power laser systems, but is not sufficient to reach couplings as low as the current best bounds of alternative searches like LSW. Note

that the situation worsens when trying to go beyond those bounds, as can be seen in (3.50).

Another challenge is the generally slow growth rate requiring long pulses in time. The e-folding time is readily found from (3.48) and must be compared to the pulse-length of a $\mathcal{I} = 10^{23}\,\mathrm{W/cm^2}$ pulse which lasts for $\tau \sim 10\,\mathrm{ps}$. This restricts the couplings we can probe. Assuming we are capable of measuring a polarisation change $\Delta\mathcal{P}$, by inverting (3.47) we find

$$g_{a\gamma\gamma} \geq 3.4 \times 10^{-2}\,\mathrm{GeV}^{-1} \left(\frac{\mathcal{I}}{10^{23}\,\mathrm{W/cm^2}}\right)^{-\frac{1}{2}} \left(\frac{\tau}{10\,\mathrm{fs}}\right)^{-1} \ln\left[\frac{\Delta\mathcal{P}}{(g_{a\gamma\gamma}A_0)\xi}\right]. \tag{3.51}$$

The log gives a small contribution, it is not inconceivable to measure $\Delta\mathcal{P} \lesssim 0.01$. For the laser parameters quoted here, $g_{a\gamma\gamma}A_0 \sim 8$.

As we can see, currently operating laser systems are only capable to probe couplings well below the current best laboratory limits set by LSW type searches. It is conceivable to perform the search we envisaged above, since for couplings that small, the axion wavelength lower limit is only $\lambda_a > 3\,\mu\mathrm{m}$ which is close to the wavelength of the optical seed laser. Maintaining a focus over such length-scales is indeed possible.

Above, we have taken the timescale of the experiment to be equal to the laser's pulselength τ. This warrants closer investigation, as there is a second timescale in the problem, that is the time required by the axions to leave the focal region. Fortunately, the phase velocity (3.41) is negligible and we may thus take the axions to be effectively stationary over the course of the interaction. This, however, changes significantly when a plasma is included.

The instability cuts off at large masses, hence our bounds only extend to

$$m_a \leq 6.8 \times 10^{-2}\,\mathrm{eV} \left(\frac{g_{a\gamma\gamma}}{3.4 \times 10^{-2}\,\mathrm{GeV}^{-1}}\right) \left(\frac{\mathcal{I}}{10^{23}\,\mathrm{W/cm^2}}\right)^{\frac{1}{2}} \tag{3.52}$$

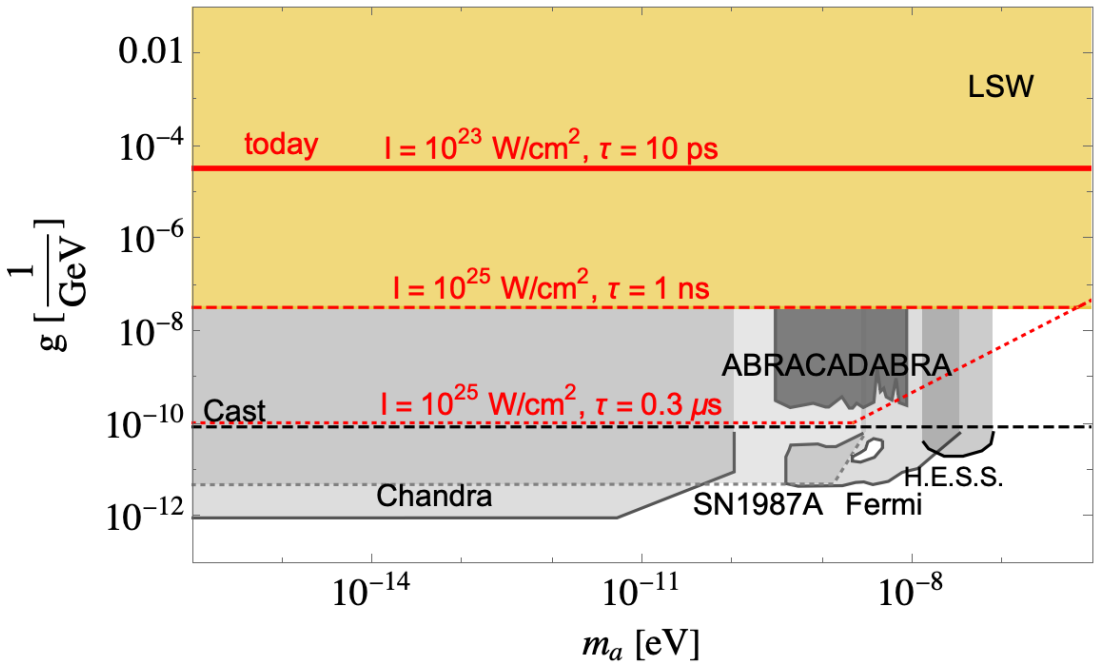

Figure 3.3: Axion exclusion plot indicating past experiments and the current work. The coloured regions correspond to purely laboratory-based experiments, while in grey-scale we indicate astrophysical and dark matter bounds. Results from light-shining through wall experiments are shown in yellow [85, 87]. The dark grey region is excluded by the ABRACADABRA collaboration [58] looking for dark matter axions. The dashed black line indicates CAST constraints [94]. The lighter grey regions are excluded by the Chandra telescope [79], observations made on the SN1987A supernova [75], the Fermi LAT collaboration [80] and considerations of a Hot Neutron Star in HESS J1731-347 [81]. The solid red line indicates the reach of an experiment as described in the main text with laser intensities of $\mathcal{I} = 10^{23}\,\mathrm{W/cm^2}$ with pulselength $\tau = 10\,\mathrm{ps}$. The dashed and dotted red lines indicate the laser requirements to reach bounds similar to LSW and CAST respectively.

and drop off above that. The drop off is calculated according to

$$g_{a\gamma\gamma} = 3.4 \times 10^{-2}\,\mathrm{GeV}^{-1} \left(\frac{m_a}{6.8 \times 10^{-2}\,\mathrm{eV}} \right). \tag{3.53}$$

We thus find that the above discussed approach can probe couplings as indicated by the solid red line in fig. 3.3. For reference, the plot also shows laser parameters necessary to reach the current best laboratory bounds and CAST limits. In general better sensitivity can be obtained by both, increasing intensity or longer pulses. While the scaling of (3.51) with pulselength τ is favourable over the scaling with intensity $\mathcal{I}$, we have to point out that only increasing the pulse length is not enough. The problem of focal length must also be addressed.

It is worth mentioning that this approach can, unfortunately, not be used to probe the QCD axion. Here, the coupling and mass are no longer independent but rather $g_{a\gamma\gamma} \propto m_a$. To reach this, we would need $A_0 \geq 10^{18}\,\mathrm{eV}$, which is above the Schwinger critical field limit.

There are two canonical routes to extend upon the results in this chapter. We can move away from the laboratory setting and aim to apply this instability in astrophysical settings in which the long axion wavelength is less of a problem. The challenge remains to find suitable conditions in which we have intense beams of radiation with well defined polarisation in this case.

Another possibility which we aim to investigate in the future lies in the assumptions we made to simplify the calculation. Dropping the co-linear limit is one obvious improvement, but perhaps more interesting would be to allow for a phase mismatch in (3.26). The idea is the following: By allowing a small phase mismatch Δk such that $k_0 = k_a + k_\gamma + \Delta k$ we may get to a situation in which k_a, the momentum of the axion mode no longer needs to be as negligible as in the perfect phase matching case above. Effectively because we can trade the smallness of k_a to a cancellation between k_a and Δk. The detailed behaviour of this system will have to be analysed in a future investigation to ascertain whether such a system still exhibits instabilities and whether the postulated increase in axion momentum holds.

We conclude that in its current state, the here proposed set-up is inferior to

alternative searches like [3], however, further interesting avenues are to be explored.

Chapter 4

Axion-like-particle decay in strong electromagnetic backgrounds

With the discovery of the laser and the steady increase in peak power [111] electromagnetic fields approach getting strong enough to observe electron-positron pair production [112, 113, 114]. The decay of photons in a laser background has already been seen in [115, 116]. At fields above the critical field of quantum electrodynamics (QED)

$$F_{\mathrm{QED}} = \frac{m_e^2}{|e|} = 1.3 \times 10^{18}\,\mathrm{V/m}, \tag{4.1}$$

in the literature also known as the Schwinger critical field, the decay of an electromagnetic field quantum into an electron-positron pair is no longer exponentially suppressed. The work done on an electron (positron) per Compton length corresponds to more than the electron's (positron's) rest-mass. Hence, real, on-shell pairs may be created.

Pair creation is a non-linear process and typically involves the interaction of many electromagnetic field quanta to transfer sufficient energy. The parameter governing the importance of multi-photon interactions is the classical non-linearity or intensity

parameter

$$\xi = \frac{eA}{m_e} \tag{4.2}$$

with A the amplitude of the electromagnetic wave potential. If $\xi \geq 1$ an electron becomes relativistic from rest within one laser cycle by absorbing many photons. Multi-photon processes are suppressed and perturbation theory can be performed for $\xi \ll 1$ but cannot be ignored once $\xi \geq 1$. Note that (4.2) is not Lorentz invariant, however an invariant formulation was found in [117]

$$\xi^2 = \frac{\langle k_\mu T^{\mu\nu}(\phi) k_\nu \rangle_\phi}{m_e^2 (\kappa.k)^2} = \frac{\left\langle k_\mu \left((F^2)^{\mu\nu} - \frac{1}{4}\eta^{\mu\nu} \operatorname{Tr} F^2 \right) k_\nu \right\rangle_\phi}{m_e^2 (\kappa.k)^2} \tag{4.3}$$

where k_μ and κ_μ are the massive seed-particles and background fields four-momenta, $T^{\mu\nu}$ is the stress-energy tensor, $F^{\mu\nu}$ the electromagnetic field strength tensor and $\langle . \rangle_\phi$ is a cycle-average over the phase.

A third governing invariant can be defined as

$$\chi = \sqrt{\frac{|(F^{\mu\nu} p_\nu)^2|}{m_e F_{\mathrm{QED}} (\kappa.p)^2}} \tag{4.4}$$

commonly known as the quantum non-linearity parameter [118]. It indicates the strength of quantum effects an electron with momentum p_ν experience in a field with amplitude $F^{\mu\nu}$.

As mentioned, pair production from seed-photons has been widely studied in the literature [119, 120, 118]. The axion's coupling to fermions (1.30) allows for axion seeded pair production, which can be used as a complimentary axion search to the di-photon regeneration experiments, probing a different SM coupling g_{ae}. Axion seeded pair production differs from the corresponding photon seeded process because of the pseudoscalar nature of the axion and the finite axion mass. The latter reduces the energy gap between the initial axion state and the final electron positron pair, thereby

lowering the strength requirement of the electromagnetic field for unsuppressed pair production. By having the axion have an appreciable Lorentz boost, the field in the rest-frame can be further enhanced. The decay of an axion into a pair in a plane wave background was investigated in [121], while axion production in the interaction of electrons and high intensity laser beams was studied previously in [121, 122, 123, 124]. We will review the standard strong field QED techniques (see [125, 126, 127, 128, 129]) in section 4.1 and then calculate the axion seeded pair production rate in 4.2. We then aim to investigate the detection capabilities of a LSW type set-up where the axions are produced via bremsstrahlung steming from the interaction of an energetic electron beam with a solid target. The resulting axions then propagate into a detection region, shielded from any SM background produced in the collision and enter a strong magnetic field in which they decay into electron positron pairs. The magnetic field lowers the axion masses for which unsuppressed decay is possible to below $m_a = 2m_e$. With the above set-up the signal depends solely on the axion's coupling to electrons g_{ae} and is hence truly complimentary to the traditional di-photon LSW searches. Relatively heavy axions $m_a > 1\,\mathrm{MeV}$ are constrained by beam dump experiments [130, 131], however going below $m_a \lesssim 1\,\mathrm{MeV}$, laboratory searches are needed.

4.1 Furry Picture

The wavefunction of an electron in an electromagnetic field satisfies the Dirac equation

$$\left(\gamma^\mu \left(i\partial_\mu - eA_\mu\right) - m_e\right)\Psi = 0 \tag{4.5}$$

with e the $U(1)_{\mathrm{em}}$ charge and m_e the mass of the electron. A_μ is the $U(1)_{\mathrm{em}}$ gauge field. Restricting ourselves to plane wave fields, the Dirac equation can be solved

exactly [132]

$$\Psi_p = \frac{\left(1 + e\frac{\not{\kappa}\not{A}(\phi)}{2\kappa.p}\right)}{\sqrt{2p^0 V}} \exp\left(ip.x + i\int_0^\phi \frac{2ep.A(\tilde{\phi}) - e^2A^2(\tilde{\phi})}{2\kappa.p} d\tilde{\phi}\right) u_p \tag{4.6}$$

with $\phi = \kappa.x$ the phase, $A(\phi)$ the background field potential (only dependent on ϕ for a plane wave) and u_p the electron spinor. The slash stands for contraction with a Dirac matrix $\not{\kappa} = \gamma^\mu \kappa_\mu$ and '.' is the Minkowski connection $\kappa.p = \kappa^\mu p_\mu$. For photons $\kappa^2 \equiv 0$ and the electron momentum is on-shell $p^2 \equiv m^2$. This wave-function describes a *dressed* electron on which one can perform perturbation theory in the small radiation field given by the emission of photons or axions. Acting with the kinetic four momentum operator $\Pi_m u = i\partial_\mu - eA_\mu$ we may find the kinetic momentum of the Wolkow state (4.6)

$$\Psi_p^* \Pi_\mu \Psi_q = p_\mu - eA_\mu + \kappa_\mu \left(\frac{2ep.A - e^2A^2}{2\kappa.p}\right) - \kappa_\mu \frac{e\not{\kappa}\not{A}}{2\kappa.p}. \tag{4.7}$$

After time averaging eliminates the linear terms in the gauge field A_μ we find the time averaged kinetic momentum

$$\bar{p}_\mu \equiv p_\mu - \frac{e^2\bar{A}^2}{2\kappa.p}\kappa_\mu. \tag{4.8}$$

From here it is natural to assign an effective mass to the state

$$m_*^2 = \bar{p}^2 = m_e^2\left(1 - \frac{e^2\bar{A}^2}{m_e^2}\right). \tag{4.9}$$

This mass is known in the literature as the dressed mass of an electron in a plane wave field. As long as the photon field is weak $eA \ll m_e$ the electron's dressed mass is equal the rest-mass. In this limit we may calculate perturbatively in eA because the dominant process will be the one involving least photons. Each additional

photon interaction comes with a factor eA/m_e making it progressively less likely. This is the standard perturbation expansion into Feynman diagrams. If, however, the field becomes strong, $eA \geq m_e$, such a perturbative expansion breaks down, as additional photon interactions are no longer suppressed. The electron is now no longer well described by the vacuum wave-function and the Wolkow states are used. The electron's mass is re-normalised by many photon interactions and in this sense is *dressed* by the photon field. Describing the electron ground state in a background plane wave field then allows us to do perturbation theory on the radiation field which is once again small [118]. Formally we split the photon field into a background field A_μ and a perturbation field, the radiation field, $\tilde{A}_\mu$. The background field is absorbed into the free field Lagrangian of the electron and the radiation field may be treated perturbatively

$$\mathcal{L} = \bar{\Psi}\left(i\partial\!\!\!/ - m_e\right)\Psi - e\bar{\Psi}\gamma_\mu\Psi\left(A_\mu + \tilde{A}_\mu\right) = \bar{\Psi}\left(i\partial\!\!\!/ - eA\!\!\!/ - m_e\right)\Psi - e\bar{\Psi}\gamma_\mu\Psi\tilde{A}_\mu. \quad (4.10)$$

The free electron wavefunction then satisfies (4.5) and has the form of the Wolkow states (4.6) which form an orthonormal basis [133]. This is known as the Furry picture [134].

4.2 Pair creation probability

The coupling of axions to fermions takes the form

$$\mathcal{L}_{ae} \supset g_{ae} a \bar{\Psi}_p \gamma_5 \Psi_q^+ \quad (4.11)$$

where the free field electron states are now full Wolkow states (4.6). Because of the smallness of g_{ae} we are free to perform a perturbative expansion in the axion electron

coupling and terminate the Dyson series at tree-level. The S-matrix element is then

$$\mathcal{S} = ig_{ae} \int d^4x a \bar{\Psi}_p \gamma_5 \Psi_q^+. \tag{4.12}$$

We take the axion field to be a plane wave with momentum k

$$a(x) = \frac{1}{\sqrt{2k^0 V}} e^{-ik.x} \tag{4.13}$$

which results in

$$\mathcal{S} = \frac{ig_{ae}}{\sqrt{8k^0 p^0 q^0 V^3}} \int \Xi e^{i(p+q-k).x + i\int_0^\phi \left(\frac{2ep.A(\tilde{\phi}) - e^2A^2(\tilde{\phi})}{2\kappa.p} + \frac{2eq.A(\tilde{\phi}) + e^2A^2(\tilde{\phi})}{2\kappa.q} \right) d\tilde{\phi}} d^4x \tag{4.14}$$

where

$$\Xi = \bar{u}_p \left(1 + \frac{e\not{A}(p)\not{\kappa}}{2\kappa.p} \right) \gamma_5 \left(1 + \frac{e\not{\kappa}\not{A}(q)}{2\kappa.q} \right) v_q. \tag{4.15}$$

We may simplify the analysis by changing to light-front coordinates in which [135]

$$\mathbf{x}^\pm \equiv x^0 \pm x^3, \qquad \mathbf{x}^\perp = (0, x^1, x^2, 0). \tag{4.16}$$

By choosing $\kappa = \kappa^+/2(1,0,0,1)$, the plane wave phases are now $\phi = \kappa^0 x^-$, independent of the other coordinates. We may thus perform most of the integrals in (4.12) by decomposing

$$d^4x = \frac{1}{2} dx^+ dx^- d^2x^\perp = \frac{dx^+ d^2x^\perp d\phi}{2\kappa^0} \tag{4.17}$$

which leaves the only dependence on x^+ and $x^\perp$ in the phase and results in

$$\mathcal{S} = \frac{ig_{ae}(2\pi)^3}{\sqrt{8k^0 p^0 q^0 V^3 \kappa^0}} \delta^{-,\perp}(p+q-k) \int \Xi e^{ir\phi + i\int_0^\phi \left(\frac{2ep.A(\tilde{\phi}) - e^2A^2(\tilde{\phi})}{2\kappa.p} + \frac{2eq.A(\tilde{\phi}) + e^2A^2(\tilde{\phi})}{2\kappa.q} \right) d\tilde{\phi}} d\phi. \tag{4.18}$$

where $r = \frac{p^+ + q^+ - k^+}{2\kappa^0}$. For convenience we have transformed all co-vectors to vectors by the relations

$$x_\pm = \frac{1}{2}x^\mp, \qquad x_\perp = -x^\perp. \tag{4.19}$$

From the S-matrix element we get the transition probability as

$$P_{a\to e^+e^-} = V^2 \int \sum_{\text{spin}} \text{Tr}\,|\mathcal{S}|^2 \,\frac{d^3p d^3q}{(2\pi)^6} \tag{4.20}$$

The trace and spin sum are simply evaluated to be

$$\begin{aligned} \frac{T}{4} &\equiv \frac{1}{4}\sum_{\text{spin}} \text{Tr}\,|\Xi|^2 \\ &= m_e^2 + p.q + e\frac{[A(\phi)+A(\phi')]}{2}.\left(p\frac{\kappa.k}{\kappa.p} - q\frac{\kappa.k}{\kappa.q}\right) - e^2\frac{A(\phi).A(\phi')}{2}\frac{(\kappa.k)^2}{\kappa.p\kappa.q} \end{aligned} \tag{4.21}$$

where we used the on-shell condition $q^2 = m_e^2$. The integral is again expanded in light-front coordinates

$$\frac{d^3p}{2p^0} = \frac{dp^- d^2p^\perp}{2p^-}\theta\left(p^-\right)\Big|_{p^+p^- = m_a^2 + (p^\perp)^2} \tag{4.22}$$

and we may perform the d^3p integral because of the momentum conserving delta functions. We readily find

$$P_{a\to e^+e^-} = \frac{g_{ae}^2}{8(\kappa^0)^2 k^-}\int \frac{dp^- d^2p^\perp}{(2\pi)^3 p^- q^-}\theta(p^-)\theta(q^-)\int d\sigma d\theta T e^{i\int_{\sigma-\frac{\theta}{2}}^{\sigma+\frac{\theta}{2}}\left[\frac{ep.A}{\kappa.p} - \frac{eq.A}{\kappa.q} - \frac{e^2A^2}{2}\frac{\kappa.k}{\kappa.p\kappa.q}\right]d\phi + i\theta r} \tag{4.23}$$

where we have defined the average and difference phases

$$\sigma \equiv \frac{\phi+\phi'}{2}, \qquad \theta \equiv \phi - \phi'. \tag{4.24}$$

We can now use the identity

$$r = \frac{k.p}{\kappa.q} - \frac{m_a^2}{2\kappa.q} \tag{4.25}$$

and definition of the plane wave momentum

$$\Pi = p - eA + \kappa\frac{2eA.p - e^2A^2}{2\kappa.p} \tag{4.26}$$

to write

$$P_{a\to e^+e^-} = \frac{g_{ae}^2}{4(2\pi)^3(\kappa^0)^2k^-}\int\frac{d^2p^\perp dp^-}{p^-q^-}\theta(p^-)\theta(q^-)\int d\sigma d\theta T e^{i\int_{\sigma-\frac{\theta}{2}}^{\sigma+\frac{\theta}{2}}\frac{k.\Pi}{\kappa.q}d\phi - i\theta\frac{m_a^2}{2\kappa.q}}. \tag{4.27}$$

Let us remove the dependence on q by noting that the momentum absorbed from the background field is

$$p + q - k = \lambda\kappa \qquad \Leftrightarrow \qquad \lambda = \frac{2k.p - m_a^2}{2\kappa.q}. \tag{4.28}$$

To find λ we used the on-shell conditions $p^2 = q^2 = m_e^2$ and $\kappa^2 = 0$. This results in the identity

$$m_e^2 + p.q = k.p\frac{\kappa.k}{\kappa.q} - \frac{m_a^2}{2}\frac{\kappa.p}{\kappa.q} \tag{4.29}$$

which we use to rewrite the trace (4.21)

$$\frac{T}{4} = k.p\frac{\kappa.k}{\kappa.q} - \frac{m_a^2}{2}\frac{\kappa.p}{\kappa.q} + \frac{e\left[A(\phi) + A(\phi')\right]}{2}.\left(p\frac{\kappa.k}{\kappa.p} - q\frac{\kappa.k}{\kappa.q}\right) - \frac{e^2A(\phi).A(\phi')}{2}\frac{(\kappa.k)^2}{\kappa.p\kappa.q}. \tag{4.30}$$

The exponent is

$$e^{i\theta\left(\frac{k.p}{\kappa.q} - \frac{m_a^2}{2\kappa.q}\right) + i\int_{\sigma-\frac{\theta}{2}}^{\sigma+\frac{\theta}{2}}\left(\frac{\kappa.k}{2\kappa.p\kappa.q}(2eA.p - e^2A^2) - \frac{ek.A}{\kappa.q}\right)d\phi} \tag{4.31}$$

which resembles parts of the expression for the trace. Indeed we may make the

substitution

$$\kappa.p\frac{\kappa.k}{\kappa.q} \to -i\kappa.k\partial_\theta + \frac{m_a^2}{2}\frac{\kappa.k}{\kappa.q} + \frac{\kappa.k}{\kappa.q}\frac{ek.(A(\phi)+A(\phi'))}{2} + \frac{(\kappa.k)^2}{2\kappa.q\kappa.p}\left(\frac{e^2A^2(\phi)+e^2A^2(\phi')}{2} - ep.(A(\phi)-A(\phi'))\right) \tag{4.32}$$

resulting in

$$\frac{T}{4}e^{i(\ldots)} = \left(\frac{m_a^2}{2} + \frac{(\kappa.k)^2}{\kappa.q\kappa.p}\frac{e^2(a(\phi)-a(\phi'))^2}{4} - i\kappa.k\partial_\theta\right)e^{i\int_{\sigma-\frac{\theta}{2}}^{\sigma+\frac{\theta}{2}}\frac{k.\Pi}{\kappa.q}d\phi - i\theta\frac{m_a^2}{2\kappa.q}}. \tag{4.33}$$

The integral over the derivative term results in contributions from the boundary at the infinite past/future. Demanding that the probability not depend on the boundary term, we may drop the term. We can now perform the $d^2p^\perp$ integral trivially because the only dependence is in the exponent. We can see that noting the identity

$$k.p = \frac{m_e^2+(p^\perp)^2}{2}\frac{\kappa.k}{\kappa.p} - p^\perp k^\perp + \frac{m_a^2+(k^\perp)^2}{2}\frac{\kappa.p}{\kappa.k} \tag{4.34}$$

to write the exponent as

$$e^{-i\theta\frac{\kappa.k}{2\kappa.p\kappa.q}\left\langle e^2A^2\right\rangle - i\theta\frac{m_a^2}{2\kappa.k} + \frac{i\theta}{\kappa.q}\left(\frac{m_e^2}{2}\frac{\kappa.k}{\kappa.p} + \frac{(k^\perp)^2}{2}\frac{\kappa.p}{\kappa.k} - \langle ek.A\rangle\right)}\int d^2p^\perp e^{\frac{i\theta}{\kappa.q}\left(\frac{(p^\perp)^2}{2}\frac{\kappa.k}{\kappa.p} - p^\perp\left(k^\perp - \frac{\kappa.k}{\kappa.p}e\langle A\rangle\right)\right)}. \tag{4.35}$$

The Gaussian integral results in

$$\int d^2p^\perp e^{\frac{i\theta}{\kappa.q}\left(\frac{(p^\perp)^2}{2}\frac{\kappa.k}{\kappa.p} - p^\perp\left(k^\perp - \frac{\kappa.k}{\kappa.p}eA\right)\right)} = \frac{2\pi i}{\theta}\frac{\kappa.p\kappa.q}{\kappa.k}e^{-i\theta\frac{\kappa.p}{2\kappa.q\kappa.k}\left(k^\perp - \frac{\kappa.k}{\kappa.p}e\langle A\rangle\right)^2} \tag{4.36}$$

which leaves the probability

$$P_{a\to e^+e^-} = i\frac{g_{ae}^2}{16\pi^2\eta_k}\int d\sigma dt\frac{d\theta}{\theta}\left(\delta^2 + \frac{e^2(A(\phi)-A(\phi'))^2}{2t(1-t)}\right)e^{i\frac{\theta}{2\eta_k}\left(\frac{\mu(\theta)}{t(1-t)} - \delta^2\right)}. \tag{4.37}$$

We have defined the mass fraction $\delta^2 = m_a^2/m_e^2$, the lightfront momentum fraction $t = p^-/k^-$ and the energy parameter $\eta_k = \kappa.k/m_e^2$. The Kibble mass factor is [136]

$$\mu(\theta) = 1 + \left\langle \frac{eA}{m_e} \right\rangle^2 - \left\langle \left(\frac{eA}{m_e} \right)^2 \right\rangle \tag{4.38}$$

with the minus coming from $A^2 = -(A^\perp)^2$ and we have used the identity

$$\frac{(\kappa.k)^2}{\kappa.p\kappa.q} = \frac{1}{t(1-t)}. \tag{4.39}$$

We may perform the t integral analytically [137, 138]

$$P_{a\to e^+e^-} = \frac{g_{ae}^2}{32\pi^2\eta_k} \int d\sigma \frac{d\theta}{\theta} \Bigg(h(\theta)\delta^2 \mathrm{K}_1(h(\theta)) + \left(h(\theta)\delta^2 + ie^2(A(\phi) - A(\phi'))^2 \right) \mathrm{K}_0\left(ih(\theta)\right) \Bigg) e^{-ih(\theta) - i\theta\frac{\delta^2}{2\eta_k}} \tag{4.40}$$

where $\mathrm{K}_n(x)$ is the modified Bessel function of second kind.

4.2.1 Local constant field approximation

If the intensity parameter of the background field $\xi \gg 1$ motion is generally ultra-relativistic and the plane wave field is approximately that of a constant crossed field in the electrons rest-frame [118, 139]. A constant crossed field has $\mathbf{E} \cdot \mathbf{B} = 0$. In this regime we can approximate the field as locally constant, which amounts to representing the probability in an arbitrary plane wave by an integral over the laser phase of the probabilities at the local field values [140, 141, 142]. To extract the local constant

field approximation (LCFA), we expand the probability to $\mathcal{O}(\theta^3)$

$$\theta\mu = \theta + \frac{1}{\theta}\left(\int_{\sigma-\frac{\theta}{2}}^{\sigma+\frac{\theta}{2}} \frac{eA}{m_e} d\phi\right)^2 - \int_{\sigma-\frac{\theta}{2}}^{\sigma+\frac{\theta}{2}} \left(\frac{eA}{m_e}\right)^2 d\phi \tag{4.41}$$

$$\simeq \theta + \frac{1}{\theta}\left(\frac{e}{m_e}\int_{\sigma-\frac{\theta}{2}}^{\sigma+\frac{\theta}{2}} \left(A_0 + \frac{dA}{d\phi}\phi\right) d\phi\right)^2 - \frac{e^2}{m_e^2}\int_{\sigma-\frac{\theta}{2}}^{\sigma+\frac{\theta}{2}} \left(A_0 + \frac{dA}{d\phi}\phi\right)^2 d\phi. \tag{4.42}$$

Making use of the fact that the field is approximately constant, $dA/d\phi \simeq$ const., we find

$$\theta\mu = \theta + \frac{1}{12}\frac{e^2}{m_e^2}\left(\frac{dA}{d\sigma}\right)^2 \theta^3 \tag{4.43}$$

where the + arises from $A.A = -(A^\perp)^2 \equiv -A^2$. Analogously we find

$$(A(\phi) - A(\phi'))^2 = -\theta^2 \frac{e^2}{m_e^2}\left(\frac{dA}{d\sigma}\right)^2. \tag{4.44}$$

Using the standard integrals

$$\int_{-\infty}^{\infty} \frac{d\theta}{\theta + i\varepsilon} e^{i(r\theta + c_3\theta^3)} = -2\pi i \mathrm{Ai}_1\left(\frac{r}{(3c_3)^{\frac{1}{3}}}\right) \tag{4.45}$$

and

$$\int_{-\infty}^{\infty} d\theta\theta e^{i(r\theta + c_3\theta^3)} = -\frac{2\pi i}{(3c_3)^{\frac{2}{3}}}\mathrm{Ai}'\left(\frac{r}{(3c_3)^{\frac{1}{3}}}\right) \tag{4.46}$$

we may write the LCFA probability

$$P^{\mathrm{LCFA}}_{a\to e^+e^-} = \frac{g_{ae}^2}{4\pi\eta_k}\int d\sigma dt \left[\frac{\delta^2}{2}\mathrm{Ai}_1(z) - \chi_k(\sigma)\sqrt{z_0}\mathrm{Ai}'(z)\right] \tag{4.47}$$

with

$$z_0 = \left(\frac{\chi_k(\sigma)}{\chi_p(\sigma)\chi_q(\sigma)}\right)^{\frac{2}{3}}; \qquad z = z_0 - \frac{\delta^2}{\chi_k(\sigma)\sqrt{z_0}}. \tag{4.48}$$

Here $\chi_k = \eta_k(-\varepsilon.a')/m$ where ε is the laser polarisation 4 vector $\varepsilon^\mu = (0, \varepsilon^\perp, 0)$.

Assuming a constant crossed field, we can write the exponent of (4.37) as

$$i\frac{\theta}{2\eta_k}\left(\frac{\mu(\theta)}{t(1-t)}-\delta^2\right)=\frac{i\vartheta}{\chi_k t(1-t)}\left(1+\frac{\vartheta^2}{3}-\delta^2 t(1-t)\right) \tag{4.49}$$

where we defined $\vartheta=\chi_k\theta/2$. In the centre of mass frame the maximal momentum fraction $t=p^-/k^-=1/2$ and we identify a threshold value $\delta^2=4$.

4.2.2 Below threshold

If $\delta^2<4$ then $1-\delta^2 t(1-t)>0$ and we call the situation below threshold if also $\chi_k\ll 1$. We can then evaluate

$$P^{\mathrm{LCFA},\delta^2<4}_{a\to e^+e^-}\sim\frac{g_{ae}^2}{4\pi}\frac{m_e}{k^-}\frac{L}{\lambda_C}\chi_k\frac{\sqrt{3}}{4\sqrt{2}}\left(1+\frac{\delta^2}{8}\right)^{-\frac{1}{2}}\left(1+\frac{\chi_k}{2}\frac{\delta^2}{4-\delta^2}\right)e^{-\frac{8}{3\chi_k}\left(1-\frac{\delta^2}{4}\right)^{\frac{3}{2}}}. \tag{4.50}$$

Intuitively the form of the exponent can be understood by energy momentum conservation [143], the energy of the produced electron is

$$E_p(\tau)=\sqrt{\mathbf{p}^2+e^2\mathbf{E}^2\tau^2+m_e^2} \tag{4.51}$$

where τ is the time. The energy difference between the states is

$$\Delta E(\tau)=E_p(\tau)+E_{k-p}(\tau)-E_k(\tau)\simeq\frac{2m_e^2}{k}\left[\left(1+\frac{(e\mathbf{E}\tau)^2}{m_e^2}\right)\frac{\mathbf{k}^2}{4\mathbf{p}\cdot(\mathbf{k}-\mathbf{p})}-\frac{\delta^2}{4}\right] \tag{4.52}$$

which for weak fields $\chi_k\ll 1$ approximates to

$$\Delta E(\tau)=\frac{2m_e^2}{k}\left(1-\frac{\delta^2}{4}\right)>1 \tag{4.53}$$

below threshold. Making use of the WKB method we find the form of the exponent

$$P_{a\to e^+e^-}\propto e^{i\int_0^\tau\Delta E(\tau')d\tau'}=e^{-\frac{8}{3\chi_k}\left(1-\frac{\delta^2}{4}\right)^{\frac{3}{2}}} \tag{4.54}$$

where we made use of the saddle-point method to evaluate the integral to the smallest τ_* for which $\Delta E(i\tau_*) = 0$. This time is

$$\tau_* = \frac{m_e}{e|\mathbf{E}|}\sqrt{1 - \frac{\delta^2}{4}}. \tag{4.55}$$

The production probability (4.50) has the usual exponential suppression expected for a tunnelling amplitude. The field here is too weak to bridge the gap between the threshold pair creation energy of $2m_e$ despite the fact that the axion has a small mass which lowers this gap. Below threshold, the latter effect is too weak and quantum tunnelling is the only option.

4.2.3 Above threshold

If $\delta^2 > 4$ then at least some region of the t integral will fall into the $1 - \delta^2 t(1-t) < 0$ regime. This leads to a modified structure of the integral which we evaluate to find

$$P^{\mathrm{LCFA},\delta^2>4}_{a\to e^+e^-} \sim \frac{g_{ae}^2}{4\pi}\frac{m_e}{k^-}\frac{L}{\lambda_C}\left(\frac{1}{2}\sqrt{\delta^2(\delta^2-4)} - \frac{\chi_k\sqrt{3}}{8}\frac{\left(4+\frac{\delta^2}{4-\delta^2}\right)}{\left(1+\frac{\delta^2}{8}\right)^{\frac{1}{2}}}\cos\left[\frac{8}{3\chi_k}\left(\frac{\delta^2}{4}-1\right)^{\frac{3}{2}}\right]\right). \tag{4.56}$$

Here we see that despite the weak background field, pair creation is no longer exponentially suppressed because the large axion mass bridges the gap to the pair creation threshold energy. Indeed we find a non-zero probability for decay even in the $A \to 0$ limit

$$P^{\mathrm{LCFA},\delta^2>4,A=0}_{a\to e^+e^-} \sim \frac{g_{ae}^2}{4\pi}\frac{m_e\int dt}{2}\sqrt{\delta^2(\delta^2-4)}. \tag{4.57}$$

4.2.4 Strong field

The last remaining part of parameter space to explore is when the fields becomes strong, $\chi_k \gg 1$. In this case the simplest way to get the probability is to realise that

the arguments of the Airy functions in (4.47)

$$|z| = \frac{1}{\chi_k^{\frac{2}{3}}} \left(\frac{1}{t(1-t)} \right)^{\frac{2}{3}} \left| 1 - \delta^2 t(1-t) \right| \ll 1. \tag{4.58}$$

To keep the expansion consistent we must also demand $\delta^2 \ll \chi_k^{\frac{2}{3}}$. Integration then results in

$$P^{\text{LCFA}}_{a \to e^+e^-} \sim \frac{g_{ae}^2}{4\pi} \frac{m_e}{k^-} \frac{L}{\lambda_C} \frac{2^{\frac{4}{3}} \pi \chi_k^{\frac{2}{3}}}{3^{\frac{1}{3}} \Gamma\left(\frac{1}{6}\right) \Gamma\left(\frac{7}{6}\right)}. \tag{4.59}$$

To cross-check the functional dependence we once again turn to the intuitive picture based on momentum conservation [143]. In the strong field limit (4.52) approximates to

$$\Delta E(\tau) = \frac{2e^2 \mathbf{E}^2}{k} \tau^2 \tag{4.60}$$

and we find the relevant timescale of the process via $\tau_q = \Delta E^{-1}$ from the uncertainty relation. Then, the rate is proportional to g_{ae}^2/τ_q, the classical timescale of motion does not play any role here, as the field is strong enough to provide the electrons with enough energy over the quantum time to allow for pair production without exponential suppression. The quantum time is found

$$\tau_q = \frac{1}{\Delta E(\tau_q)} \qquad \Leftrightarrow \qquad \tau_q \simeq \left(\frac{k}{e^2 \mathbf{E}^2} \right)^{\frac{1}{3}} \tag{4.61}$$

resulting in $P^{\text{LCFA}}_{a \to e^+e^-} \propto \chi_k^{\frac{2}{3}}$ as found above.

In this limit, there is no longer the concept of a threshold for the axion mass as the field is strong enough to provide the necessary energy for pair creation independent of the axion's mass.

4.3 Constant magnetic field

Most laboratory experiments implement constant magnetic fields to reconvert axions into detectable SM particles. A constant magnetic field in the lab frame may not be described as a crossed field. However, in the frame of the ultrarelativistic seed-particles $k^-/m_e \gg 1$, the field is well approximated by a constant crossed field with

$$eA^1(\phi) \to m_e \frac{k^0}{k^-}\frac{L}{\lambda_C}\frac{F_0}{F_{\rm QCD}}\phi \tag{4.62}$$

where the nominal frequency of the constant field is defined as $\kappa^0 = 2\pi/L$ where L is the spatial extend of the magnetic field. The Compton wavelength is $\lambda_C = 2\pi/m_e$ and F_0 is the amplitude of the field strength. From here we find

$$\chi_k(\sigma) \to \frac{F_0}{F_{\rm QCD}}\frac{k^-}{m_e}; \qquad \frac{1}{\eta_k}\int d\sigma \to \frac{m}{k^-}\frac{L}{\lambda_Q} \tag{4.63}$$

and we can now use the above calculated probabilities to estimate the produced pairs.

Let us envisage an experimental set-up utilising the 17.5 GeV electron beam driving the European x-fel incident on a thin foil target to produce Bremsstrahlung similar to the LUXE experiment [144]. We estimate the rate of axionic Bremsstrahlung for a thin target [145]

$$k^- \frac{dN(k^-)}{dk^-} \sim \frac{g_{ae}^2}{e^2}\frac{X}{X_0}\left(\frac{4}{3} - \frac{4}{3}\frac{k^-}{p^-} + \left(\frac{k^-}{p^-}\right)^2\right) \tag{4.64}$$

from which we may find the number of regenerated axions

$$N_\phi = N_e N_{\rm shots}\left(\frac{g_{ae}^2}{4\pi}\right)^2 \frac{X}{X_0}\frac{L}{2\gamma_e\lambda_C}\int_0^1 \frac{dx}{x^2}\left(\frac{4}{3} - \frac{4}{3}x + x^2\right)\int_0^1 dt \frac{\partial R}{\partial t}\bigg|_{\chi_k = 2\gamma_e \frac{B}{B_{\rm QED}}x} \tag{4.65}$$

Here, X/X_0 is the number of radiation lengths in the foil, γ_e is the relativistic gamma

factor of the electrons and $x = k^-/p^-$. We have also defined the rate

$$P^{\text{LCFA}}_{a\to e^+e^-} = \frac{g_{ae}^2}{4\pi}\frac{L}{\lambda_C}\frac{m_e}{k^-} \tag{4.66}$$

to make the g_{ae} dependence in (4.65) explicit. When applying the analysis to a $B = 5\,\text{T}$ magnet of length $L = 4.21\,\text{m}$ as is used in the ALPs experiment at DESY [85] we find that only a small parameter range outside of the above threshold scenario $m_a > 2m_e$ can be explored. Already for axion masses $m_a < (2 - 10^{-2})\, m_e$ the signal is exponentially suppressed, see [2]. We conclude that such LSW type set-ups are more suitable for di-photon regeneration like described in the previous chapters and significant improvement in field strength would be required to make this set-up probe significantly lower masses than $m_a = 2m_e$ where vacuum pair production from heavy axions becomes possible. Nevertheless, the reduction of the threshold mass by the field and the above calculated rate can be of interest in for example astrophysical contexts where much stronger fields can be found around compact objects.

This concludes the first part of the thesis about novel direct axion detection experiments. There are many complementary avenues to explore. We saw in chapter 2 that replacing the static magnetic fields of traditional LSW type searches with strong laser beams leads to interesting phenomena and ultimately results in an enhanced sensitivity for intermediate axion masses around $m_a \sim 1\,\mathrm{eV}$. This type of search scales favourably with laser energy due to the inclusion of a third, regenerating beam on the detection side of the interposing wall. Because the axion mass can be selected through the beam frequencies and the collision angle, this method is well suited for cross-validation of a positive signal should it fall within the mass parameter range. Chapter 3 introduced a complementary search strategy for very low mass axions which utilises the newly found axion-photon parametric decay instability to induce a rotation in the polarisation of the laser pulses. While currently operating laser systems fall short on probing new parameter space, the shortcomings might be overcome in the future. Finally, in chapter 4 the axion-photon coupling $g_{a\gamma\gamma}$ was replaced with the axion-electron coupling g_{ae} to investigate axion regeneration through pair creation in strong background fields. This approach is capable of probing a distinct SM coupling and therefore is complementary to the above two.

In the second part of the thesis the axion's role in the early universe cosmology is investigated. From here on on-wards the term "axion" refers only to the QCD axion as reviewed in chapter 1.

Chapter 5

Axion Cosmology

Multiple stages of spontaneous symmetry breaking and a low mass result in non-trivial cosmological impact of the axion. To understand the significance we set the scene by a short review of the relevant aspects of the "standard cosmology". Note that in this chapter, as well as in chapter 6, we use the term axion to mean *only the QCD axion* as described in the beginning of chapter 1.

5.1 Standard ΛCDM cosmology

The standard cosmological model starts with the cosmological principle, the postulate that the universe as a whole is homogeneous and isotropic when viewed on large enough scales. That is to say that while on small scales it undeniably is inhomogeneous, these inhomogeneities will average out on cosmological scales. One line of argument for the cosmological principle relies on the isotropy of the cosmic microwave background (CMB) [146, 147]. While recent studies put the standard cosmological model in question [148, 149], in the following, we will assume it. Invoking the cosmological principle drastically simplifies the geometry, allowing us to specify the metric of the universe in terms of two parameters only: the radius of curvature k and the dynamical scale factor $R(t)$. The latter may only depend on time because of the

assumption of isotropy and homogeneity. The metric is then of Friedman-Lemaitre-Robertson-Walker (FLRW) type

$$ds^2 = g_{\mu\nu}dx^\mu dx^\nu = dt^2 - R^2(t)\left(\frac{dr^2}{1-kr^2} + r^2 d\mathbf{\Omega}^2\right) = R^2(\eta)\left(d\eta^2 - \frac{dr^2}{1-kr^2} + r^2 d\mathbf{\Omega}^2\right) \tag{5.1}$$

with conformal time $\eta = \int_0^t dt'/R(t')$. Without loss of generality we are free to rescale the radial coordinate such that $k = \pm 1, 0$. We can see here the power of the cosmological principle, which almost entirely fixes the geometry of the universe. We are left with three distinct choices, the universe can either be closed ($k = 1$), it can be flat ($k = 0$) or open $k = -1$. Observation seems to suggest a flat universe with $k = 0$, which we adopt in the remainder of the chapter. For a review see [150, 42].

A FLRW type universe is dynamical with a single dynamical parameter, the scale factor $R(t)$ describing the expansion of space. What drives the expansion is the energy content of the universe as can be seen by the Einstein equations

$$\mathcal{R}_{\mu\nu} - \frac{1}{2}\mathcal{R}g_{\mu\nu} + \Lambda g_{\mu\nu} = 8\pi G T_{\mu\nu} \tag{5.2}$$

which link the curvature of space as parametrized by the Riemann tensor $\mathcal{R}_{\mu\nu}$ to the energy-momentum tensor $T_{\mu\nu}$. G is Newtons constant and Λ is the cosmological constant. The energy momentum tensor is highly constrained due to the symmetries we imposed onto the metric of space-time and for now we make the further assumption that it only contains perfect fluids with energy density ρ and pressure P

$$T_{\mu\nu} = -P g_{\mu\nu} + (P + \rho)u_\mu u_\nu \tag{5.3}$$

where $u_\mu = \delta_{\mu,0}$ is the fluid velocity in co-moving coordinates.

The Einstein equations (5.2) together with the FLRW metric (5.1) yield the Fried-

mann equations for the scale factor

$$\frac{1}{R(t)^2}\left(\frac{\partial R(t)}{\partial t}\right)^2 = \frac{8\pi G}{3}\rho + \frac{\Lambda}{3} \tag{5.4}$$

and

$$\frac{1}{R(t)}\frac{\partial^2 R(t)}{\partial t^2} = -\frac{4\pi G}{3}(\rho + 3P) + \frac{\Lambda}{3}. \tag{5.5}$$

The types of perfect fluids we are concerned with have an equation of state of the form $P = w\rho$ with constant w. Relativistic matter or radiation has $w = 1/3$ and non-relativistic matter $w = 0$. For these types of fluids solving the above equations when Λ is negligible is simple and results in

$$R(t) = R_0 t^{\frac{2}{3(w+1)}}. \tag{5.6}$$

By convention, we choose R_0 such that $R(t_0) = 1$ where t_0 is today. This form of the scale factor describes the universe well over long periods of its evolution and only at transition periods from domination of one form of matter to the other more care must be taken. Note that the cosmological constant Λ as measured has only recently begun to play an appreciable role and is unimportant for our discussion of early cosmology here. We will therefore not delve into the substantial body of literature and debate about it and include it only in the Einstein equations for the sake of completeness. The standard cosmological model is also called ΛCDM indicating the two types of additional energy density included on top of the SM, cold dark matter and the cosmological constant.

Defining the normalised expansion rate to describe the expansion of space

$$H(t) \equiv \frac{1}{R(t)}\frac{\partial R(t)}{\partial t}, \tag{5.7}$$

the Hubble parameter as first discovered by Hubble [151], we may recast the first

Friedman equation (5.4) as a cosmological sum rule. We first define the critical energy density of the universe, the amount required to make it flat, $\rho_{\text{crit}} = 3H^2/8aG$ and then use it to define the density parameters $\Omega_x \equiv \rho_x/\rho_{\text{crit}}$. The Friedman equation then reads

$$\frac{H(t)^2}{H(t_0)^2} = \frac{\Omega_{\text{R}}(t_0)}{R(t)^4} + \frac{\Omega_{\text{M}}(t_0)}{R(t)^3} + \Omega_\Lambda(t_0) \tag{5.8}$$

where $\Omega_{\text{R}}(t_0)$ is the energy density of radiation today, $\Omega_{\text{M}}(t_0)$ that of matter and $\Omega_\Lambda(t_0)$ the energy density of the cosmological constant. Thus, specifying a cosmological model reduces to the specification of the energy density content which then fixes the metric completely, at least as long as the cosmological principle is invoked. Note that by construction $\Omega_{\text{R}}(t_0) + \Omega_{\text{M}}(t_0) + \Omega_\Lambda(t_0) = 1$. In principle we are now ready to specify the different density parameters and retrace the evolution of the universe, however, one essential complication arises in our real universe due to particle interactions. We must therefore first give a very brief overview of Thermodynamics in FLRW universes [152, 153, 150].

We firstly classify particle species based on their equilibrium with the background plasma. A particle species typically establishes equilibrium if its interaction rate is faster than the expansion rate of the underlying spacetime $\Gamma \geq H^{-1}$. When this is fulfilled, any scattering transforming the particles in question to background constituents happens fast enough to be reversed before the expansion is noticeable therefore equilibrium may be established. In the very early universe, when temperatures were very large and, due to the steepest dependence radiation dominated the universes evolution, the expansion rate was slow; $H^{-1} \propto T^{-2}$ and all species were in equilibrium. As the temperature drops and the universe expands, particle densities drop like $n \propto R(t)^{-3}$ and eventually become so low that the scattering rate $\Gamma \propto n$ drops too low to maintain equilibrium. We say that the particle species has frozen out.

If in equilibrium at temperature T, the particles distribution will be

$$f(\mathbf{p}) = \frac{1}{e^{E(\mathbf{p})/T} \pm 1} \tag{5.9}$$

with $+1$ for fermions and -1 for bosons. The particles 3-momentum satisfies $E(\mathbf{p})^2 = m^2 + \mathbf{p^2}$. We then find the equilibrium number density [154, 155]

$$n_i = \frac{g_i}{(2\pi^3)} \int f_i(\mathbf{p}) d^3p = \begin{cases} \frac{\xi(3)}{\pi^2} g_i T^3 \cdot \begin{cases} 1 & \text{boson} \\ \frac{3}{4} & \text{fermion} \end{cases} & T \gg m_i \\ g_i \left(\frac{m_i T}{2\pi}\right)^{3/2} e^{-m_i/T} & T \ll m_i \end{cases} \tag{5.10}$$

the equilibrium energy density

$$\rho_i = \frac{g_i}{(2\pi^3)} \int E(\mathbf{p}) f_i(\mathbf{p}) d^3p = \begin{cases} \frac{\pi^2}{30} g_i T^4 \cdot \begin{cases} 1 & \text{boson} \\ \frac{7}{8} & \text{fermion} \end{cases} & T \gg m_i \\ m_i n_i & T \ll m_i \end{cases} \tag{5.11}$$

and the equilibrium pressure

$$P_i = \frac{g_i}{(2\pi^3)} \int \frac{\mathbf{p}^2}{3E(\mathbf{p})} f_i(\mathbf{p}) d^3p = \begin{cases} \frac{1}{3}\rho_i & T \gg m_i \\ n_i T & T \ll m_i \end{cases} \tag{5.12}$$

as functions of the number of spin states of species i, g_i and the temperature. $\xi(3) = 1.202$ is the Riemann Zeta function. We will call fields with $T \gg m_i$ relativistic and $T \ll m_i$ non-relativistic since the former have energy much larger than their mass and the latter mainly contribute their restmass to the energy density of the universe. A particle species which starts out relativistic, so contributes to the radiation density parameter $\Omega_{\mathrm{R}}(t_0)$ may become non-relativistic during the universe's

evolution when the temperature drops below its mass. It then contributes to the matter content $\Omega_{\mathrm{M}}(t_0)$. Note that the labels radiation and matter are in this sense equivalent to relativistic and non-relativistic, respectively. We may use these equations to determine the relation between temperature and time in the early, radiation dominated universe

$$t(T) = 2.42\,\mathrm{s}\frac{1}{\sqrt{g_*}}\left(\frac{T}{\mathrm{MeV}}\right)^{-2} \tag{5.13}$$

with g_* the effective number of relativistic spin degrees of freedom

$$g_* = \sum_{\text{boson}} g_i + \frac{7}{8}\sum_{\text{fermion}} g_i \tag{5.14}$$

which itself is temperature dependent as can easily be inferred from our discussion above. The effective degrees of freedom of the SM are calculated on the lattice [28] which is accurate to a temperature around $T \sim 100\,\mathrm{GeV}$ above which we introduce dependence onto the BSM model under investigation. Note that relation (5.13) is only accurate away from changes to g_* due to freeze out. In the following we will use the terms time and temperature interchangeably.

When a species becomes non-relativistic while in equilibrium, its abundance plummets which is expected because pair production of such particle is exponentially suppressed at low energies. The universe as of today has vanishing radiation $\Omega_{\mathrm{R}}(t_0) = 8.24 \times 10^{-5}$ and much larger matter content $\Omega_{\mathrm{M}}(t_0) = 0.27$ [156]. Due to the different scaling, however, the early universe was radiation dominated. Utilising the sum rule (5.8) we may infer the cosmological constant contribution $\Omega_\Lambda(t_0) = 0.73$, dominating the evolution of the universe today. This concludes the very basics of the standard ΛCDM model. Having specified the energy density content we are now ready to sketch the cosmic history of the universe to put the axion's role into perspective.

Let us very briefly sketch the evolution of the universe as long as accurately described by the SM below temperatures of $T \sim 100\,\mathrm{GeV}$. The temperature of

the photon bath today is $T_0 = 2.7\,\mathrm{K}$, the temperature of the CMB. Going up in temperature, or equivalently back in time, we encounter the period of recombination and photon decoupling at temperatures $T \sim 10^{-9}\,\mathrm{GeV}$. At this point the temperature is low enough that stable, neutral hydrogen atoms form and the photons no longer have enough energy to ionise them into a plasma. Their mean free path as a result increases drastically and they begin effectively free streaming leading to the formation of the CMB. Going to even higher temperatures, we find the universe to be radiation dominated above temperatures of around $T10^{-8}\,\mathrm{GeV}$. At $T \sim 10^{-3}\,\mathrm{GeV}$ Big Bang Nucleosynthesis (BBN) occurred and protons and neutrons combined into heavier nuclei setting the abundances of such heavier elements up to Lithium. As this epoch is dominated by very well understood atomic physics and good quality data is readily available, BBN is an excellent test ground for BSM theories [153]. Before the heavier elements could be formed, at temperatures around $T \sim \mathrm{GeV}$, the quark-gluon plasma hadronised and protons and neutrons formed. Going even higher we find that at temperatures $T \sim 100\,\mathrm{GeV}$ the electroweak symmetry broke marking the onset of model dependence on BSM theories.

The PQ symmetry breaking, at least for the QCD axion under current cosmological constraints, occurred at much higher energies $T = v_a \sim 10^{12}\,\mathrm{GeV}$, however the axion mass only turns on at the QCD scale around $T \sim \mathrm{GeV}$. As we will argue in section 5.4, this is the time at which dangerous topological defects form which may then be around during BBN. This may impose serious constraints on possible axion models.

5.2 Horizon Problem and Inflation

The discovery of the CMB and its remarkable isotropy not only provides a seemingly powerful argument for the cosmological principle, but also results in a rather

interesting puzzle. The CMB originates in the early universe from the temperature at which photons fell out of equilibrium with the electron-proton plasma and the universe became transparent. As a result photons suddenly started free streaming and we see an imprint of this in form of the CMB on the sky. But why is the CMB so isotropic and why should we expect the universe to be FLRW in the first place? After all, we believe the universe to be causal and hence two CMB photons arriving on the earth from opposite directions would never have been in causal contact, yet their temperature agrees up to $\delta T/T = 10^{-5}$ [157].

To make this statement more precise, we first define the particle horizon as the largest distance any signal may have travelled from the initial singularity at $t = 0$. The physical size of the horizon is given by

$$D(t) = R(t) \int_0^t \frac{dt'}{R(t')} \sim \begin{cases} 3t & \text{matter dominated} \\ 2t & \text{radiation dominated} \end{cases} . \tag{5.15}$$

At the time of recombination t_r the present universe consisted of many causal patches of size $D(t_r) \sim t_r$. Two points p and q on the spatial hypersurface at t_r are causally connected iff they lie within each other's past light-cone. In the FLRW universe we live in this should only be true for two points on the sky separated by less then $\sim 2^\circ$ on the sky. We would therefore not expect the CMB to be isotropic on larger scales, yet we observe it to be correlated over the entire sky.

One possible solution is to invoke a period of inflation, or quasi deSitter expansion. A deSitter universe is characterised by constant Hubble parameter $H(t) \equiv H_i$ and has metric

$$ds^2 = R(t)\eta_{ij}dx^i dx^j. \tag{5.16}$$

Constant expansion rate H_i implies that the scale factor $R(t) \propto e^{H_i t}$ and the universe expands exponentially fast. The two points p and q may now very well have been

in causal contact because the period of exponential expansion inflates each causal patch such that, if inflation had lasted long enough, our entire Hubble patch may have originated within a single causal patch before inflation. We therefore have an explanation for the remarkable homogeneity of the CMB. Achieving inflation in a natural way appears to be rather challenging but exact models of inflation go beyond the scope of this work. We will, in the following, simply assume that, some time after the initial singularity, the universe underwent a period of inflation. Once inflation ends the inflaton, the field driving inflation, decays and reheats the universe which got super-cooled $T \propto R(t)^{-1}$ as the universe rapidly expanded. This is what we call the big bang. Subsequently recombination happens and the CMB is formed with causal horizons much larger than naively expected [158, 159].

5.3 Axion Dark Matter

Soon after the discovery of the PQ solution to the strong CP problem, it was realised that the anomalous, spontaneously broken $U(1)_{\mathrm{PQ}}$ results in a pseudo-Nambu Goldstone, the axion. By making this light particle weakly coupled, the axion can be made "invisible" and is a natural candidate for dark matter with an interesting cosmological history.

At high scales the complex PQ field Φ has a Higgs-like Lagrangian density which for the purposes of this chapter may be parametrized as

$$\mathcal{L}_a = \frac{1}{2}\left(\partial_\mu \Phi^\dagger\right)\left(\partial^\mu \Phi\right) - \frac{\lambda_a}{4}\left(\Phi^\dagger \Phi - v_\Phi^2\right)^2 . \tag{5.17}$$

Below a temperature $T \sim v_a$ the vacuum expectation value of the field changes from $\langle \Phi \rangle = 0$ to $|\langle \Phi \rangle| = v_a$ thereby spontaneously breaking the $U(1)_{\mathrm{PQ}}$. The axion field is the Nambu Goldstone boson of this broken symmetry living on the circle of radius v_a

in field space

$$\Phi = v_a e^{i\frac{a(x)}{v_a}} \tag{5.18}$$

where we ignore radial fluctuations, justified by their large mass. Hence the complex PQ field quickly relaxes to its radial minimum while the axion field stays without potential until the QCD quark condensate forms at much lower temperature, as described in chapter 1. Hence without a potential the initial value for the radial axion field is chosen at random. Regions of the universe which are in causal contact at the moment of $U(1)_{\mathrm{PQ}}$ breaking will end up choosing the same initial value effectively breaking the universe up into causal regions with randomly chosen axion field value.

The equations of motion of the axion field in a FLRW universe can then easily be obtained

$$\left[\left(\frac{\partial}{\partial t}\right)^2 + 3H(t)\frac{\partial}{\partial t} - \frac{1}{R(t)^2}\nabla^2\right] a(x) + V'(a(x)) = 0 \tag{5.19}$$

where for later convenience we have already included a potential $V(a)$. Taking the simplest axion model this potential is $V = 0$ above the QCD scale, however the introduction of additional BSM fields may in principle lead to a non-zero potential even above that scale.

There are now two qualitatively different scenarios, the PQ symmetry can either break before the period of inflation or after.

5.3.1 Pre-inflational PQ breaking

In the former case, the axion is homogenised over vast distances and we may drop the term in (5.19) proportional to ∇^2. We will make the assumption that the universe is radiation dominated, an assumption which is backed by the relative scaling of radiation and matter discussed in the previous sections. We may then find the axion

field satisfying the equations of motion as

$$a(t) = a_0 + a_{1/2}\frac{1}{\sqrt{t}} \tag{5.20}$$

with a_0 and $a_{1/2}$ some constants. Hence, the axion field evolves towards a constant as the universe expands, the Hubble drag term $3H(t)\partial_t a(x)$ freezes the axion field.

Once the temperature drops below the QCD scale, $\langle\bar{q}q\rangle \neq 0$ and the axion acquires a potential (1.18). The Hubble drag now acts against the potential gradient which eventually will come to dominate and cause the axion field to start oscillating coherently at t_1. This happens when $3H(t_1) \sim m_a$, which defines t_1. Including the full potential (1.18) requires numerical solution of the equation of motion (5.19) however, to illustrate the physics we make the assumption that the initial axion field is small such that we may approximate $\sin(a/v_a) \sim a/v_a$ and solve the equation explicitly

$$a(t) = \alpha f_{\rm PQ}\left(\frac{t_1}{t}\right)^{\frac{3}{4}}\cos\left(\int_{t_1}^{t}\left(m_a^2 + \frac{3}{16t^2}\right)dt'\right). \tag{5.21}$$

$\alpha f_{\rm PQ}$ is the initial, randomly chosen axion field value, α is what is called the missalignment angle in the literature. The number density of axions is then

$$n_a(t) = \frac{1}{2}m_a|a(x)|^2 = \frac{1}{2}m_a(\alpha f_{\rm PQ})^2\left(\frac{R(t_1)}{R(t)}\right)^3. \tag{5.22}$$

Note that the number of axions per co-moving volume is conserved. Technically this is only true when the axion mass has reached its zero temperature value as it itself is temperature dependent, however the dependence is steep and we will therefore make the assumption that the mass switches on abruptly [27, 28].

The energy density in axions is then readily found

$$\rho_a = m_a n_a(t_1)\left(\frac{R(t_1)}{R(t)}\right)^3. \tag{5.23}$$

Two important points should be addressed. First, the collective axions do indeed scale like matter, as is required from a suitable DM candidate. Secondly, the amount of energy density depends on the initial misalignment angle and is therefore not precisely calculable. This unfortunately will not be resolved for $U(1)_{\mathrm{PQ}}$ breaking before inflation, however we may still get a reasonable estimate of the DM contribution of axions by adopting the natural assumption that $\alpha \sim \mathcal{O}(1)$. Then

$$\Omega_a \sim 0.15 \left(\frac{f_{\mathrm{PQ}}}{10^{12}\,\mathrm{GeV}^{-1}} \right)^{\frac{7}{6}} \left(\frac{0.7}{h} \right)^2 \alpha^2 \tag{5.24}$$

with h parametrizing the present day Hubble constant $H_0 = h100\,\mathrm{km/s\,Mpc}$.

5.3.2 Post-inflation PQ breaking

If inflation happens before PQ symmetry breaking, the situation changes substantially. We no longer have the axion field homogenised over large distances and therefore on top of the zero momentum mode of the section above there are higher momentum modes contributing. To give an estimate equivalent to above, we perform a Fourier analysis of the equation of motion prior to the axion field acquiring mass

$$\left(\left(\frac{\partial}{\partial t} \right)^2 + \frac{3}{2t} \frac{\partial}{\partial t} + \frac{k^2}{R(t)^2} \right) \tilde{a}(\mathbf{k}, t) = 0. \tag{5.25}$$

The wavelength of the axion modes $2\pi R(t)/k$ divides the spectrum into sub-horizon modes fitting within the causal horizon and the super-horizon modes stretching beyond. The zero momentum solution $k = 0$ is identical to above with the exception that the expansion of the universe brings more and more Hubble patches into causal contact which effectively replaces the arbitrary initial misalignment angle with an average over many Hubble volumes. Therefore, the contribution of the axion field's coherent oscillation to the energy density of the universe is fully calculable in the

post-inflation scenario. Solutions can be found for the higher momentum cases

$$a(\mathbf{k},t) = \begin{cases} a_0(\mathbf{k}) + a_{1/2}(\mathbf{k})\frac{1}{\sqrt{t}} & \text{super-horizon} \\ \alpha f_{\rm PQ}\frac{R(t_{\rm PQ})}{R(t)}\cos\left(\int \frac{k^2}{R(t')^2}dt'\right) & \text{sub-horizon} \end{cases} \tag{5.26}$$

indicating that all super-horizon modes evolve towards a momentum dependent constant, they are frozen. The sub-horizon modes have energy $\omega^2 \sim k^2/R(t)^2$ and therefore the number density of axions in higher momentum modes per co-moving volume is conserved mode by mode. Their contribution to the energy density is found to be

$$\rho_a = \frac{1}{2}m_a^2 f_{\rm PQ}^2(1+N_{\rm DW}^2)\left(\frac{R(t_1)}{R(t)}\right)^3 \tag{5.27}$$

where the first term comes from the zero momentum modes and the second term from the higher momentum ones. We also made use of the fact that the axions will be non-relativistic after t_1 to calculate the contribution today

$$\Omega_a \sim 0.15\left(1+N_{\rm DW}^2\right)\left(\frac{f_{\rm PQ}}{10^{12}\,{\rm GeV}^{-1}}\right)^{\frac{7}{6}}\left(\frac{0.7}{h}\right)^2. \tag{5.28}$$

An additional complication, however, arises in the post-inflation PQ breaking scenario. Topological defects may form (see section 5.4) and their contribution must be taken into account. There is however debate over the contribution arising from axion strings and domain walls. To estimate the contribution coming from axion strings, we must first understand the spectrum of axions radiated off such strings when they collapse. There are two basic arguments debated in the literature: the string can either oscillate many times at a frequency set by the size of the string loop L before collapsing, in which case the spectrum is concentrated around $2\pi/L$ [160, 161, 162]. Alternatively, the string collapses almost instantaneously, resulting in a spectrum $dE/dk \propto k^{-1}$ with cut-offs set by the loop size and $2\pi v_a$ [163, 164].

Recent computer simulations seem to support the former scenario [165]. Another contribution stems from axion domain walls. Again the spectrum is difficult to obtain and computer simulations are challenging because of the large separation of scales between the walls thickness m_a^{-1} and the Hubble size H^{-1} [166]. We will conclude by mentioning that the question of topological defect decay to the axion abundance remains a matter of debate [167]. By specifying a mechanism of decay, we hope to shed some light onto this question in the future.

In this most simple set-up we may now find a bound on the axion decay constant $f_{\rm PQ}$ by demanding its contribution not overclose the universe; $f_{\rm PQ} \lesssim 10^{12}\,{\rm GeV}$. There is a large body of literature which extends this axion window. We will only mention [168, 169], which aims to find an explanation for relaxing the initial misalignment angle to small values by a mechanism similar to our approach discussed in section 5.5.

5.4 Topological defects

Once $U(1)_{\rm PQ}$ breaks the universe consists of causal patches in which the PQ field ran down the wine bottle potential in a random angular direction. Because of the topology of the vacuum manifold there exist closed paths in real space which map onto a non-trivial path in field space, a path which winds around the circle n times, see figure 5.1. Such field configuration can arise whenever the vacuum manifold is connected but not simply connected. The field in real space must then have a region within the closed path where $a = 0$, thus leaving the vacuum manifold [170]. This field configuration is known as a cosmic string because the region of space in which the field is not in vacuum shrinks to a quite thin string. Its thickness is $\mathcal{O}(m_a^{-1})$ and its effective mass is set by the string tension $\mu_s = \pi v_a^2 \ln(v_a/H)$ where we used the cut-off H^{-1}, the effective inter-string distance [171, 172]. It has topological charge

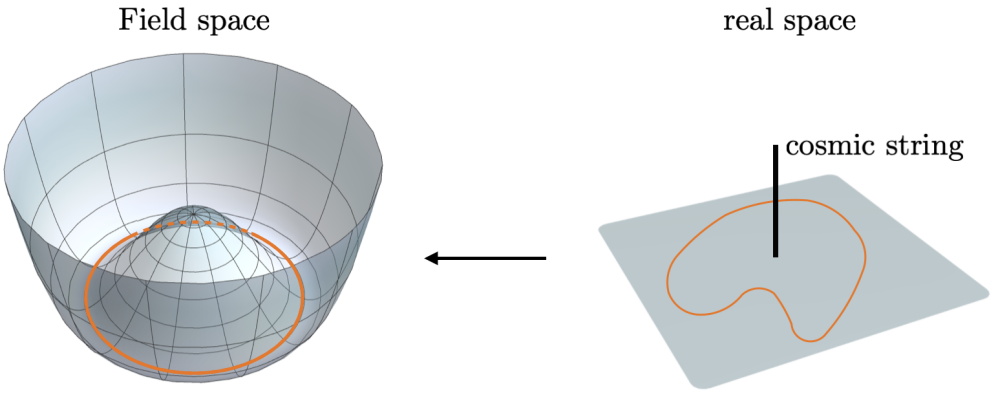

Figure 5.1: Cartoon of cosmic string production. On the left-hand side a path in real space, depicted in orange, is mapped onto a loop in field space, shown on the left. The path in field space is non-trivial, it cannot be smoothly deformed to a point without leaving the vacuum manifold, hence somewhere within the loop in real space lies a cosmic string where the field lies on top of the central peak of the potential.

given by the winding number, the number of times a closed loop around the string in real space winds around the circle in field space. This mechanism of production was discovered by Kibble and Zureck [170, 173, 174, 175].

It is believed that the interactions between axion strings is quite effective and rather quickly the network of strings is in the scaling regime where on average one has a single string per causal horizon. Two strings which encounter each other can either annihilate if their topological charges are equal and opposite or they cut each other up thereby eventually one one string remains per Hubble volume. In the scaling regime the energy density in strings scales like

$$\rho_{\text{string}} = \mu_s H(t)^2. \tag{5.29}$$

Once the universe cools below the QCD scale, each of those cosmic axion strings

is attached to $N_{\rm DW}$ domain walls [176]. Domain walls are a field configuration arising when the vacuum manifold consists of disconnected manifolds therefore a continuous path in real space may map onto a path in field space interpolating between two vacuum states - (in our case the vacuum "manifold" is simply a set of points, however the following argument still applies.) The field then necessarily leaves the vacuum in between the two end points of the path. The domain wall is usually thin, simply because a thick wall would come with a large energy density whereever the field is not in its vacuum state. The thickness is set by the scale in the problem, the axion mass m_a^{-1} [176]. Each cosmic string must now be connected to $N_{\rm DW}$ DW as the field does a full 2π change around the string and therefore passes through all $N_{\rm DW}$ vacuum states with DW interpolating between them. The domain walls effective mass is given by the wall tension $\sigma_{\rm DW} = 8.97 m_a f_{\rm PQ}^2$ [177, 27].

The string wall network behaves qualitatively different if $N_{\rm DW} = 1$ or $N_{\rm DW} > 1$. In the former case, for topological reasons, each wall connects a string with its anti-string and the wall tension pulls the two together. Once they come close they annihilate. Thus, the string wall network with $N_{\rm DW} = 1$ is unstable and annihilates almost instantly. This changes once each string is attached to more than 1 DW and the network is in principle stable. It enters a scaling regime dominated by the domain wall energy density and contributes

$$\rho_{\rm DW} = \xi \sigma_{\rm DW} H(t) \tag{5.30}$$

to the universes energy density where $\xi \sim \mathcal{O}(1)$ is the number of domain walls per Hubble patch during the scaling regime. The slow scaling of DW energy density makes it dominate the energy density of the universe quite quickly

$$t_d \leq \frac{3}{32\pi G \sigma_{\rm DW}}. \tag{5.31}$$

A universe dominated by domain walls undergoes accelerated expansion

$$\frac{\partial R(t)}{\partial t} = \sqrt{\frac{8\pi G}{3}\rho_{\rm DW}}R(t) \qquad \rightarrow \qquad R(t) \propto t^2 \tag{5.32}$$

and is inconsistent with observation. We therefore must find a mechanism to collapse the network before domination [178]. This is known as the axion domain wall problem and chapter 6 will be dedicated to it. An excellent review can be found in [179].

5.5 Bias

Let us define a second type of horizon, the Hubble horizon. It divides an expanding universe into a region in which particles are moving slower than the speed of light and one where they move faster relative to an observer. The latter happens because of the expansion of space and is not a violation of relativity. During inflation the comoving Hubble horizon shrinks and, as a result, large scales transition from being within the Hubble patch to lying outside of it, we say those scales exit the horizon. Modes which have exited the horizon are frozen by causality. This division suggests a natural basis to expand fields obeying the equation of motion

$$\frac{\partial^2 a}{\partial t^2} - \frac{\nabla^2 a}{e^{2H_i t}} + 3H_i\frac{\partial a}{\partial t} + \frac{\partial V}{\partial a} = 0 \tag{5.33}$$

as a mode expansion for sub-horizon modes and a course grained fluctuation field χ for super horizon modes around a mean over many horizon sizes $\bar{\chi}$ [180, 181, 182]

$$a(\mathbf{x},t) = \int \Theta\left(p - \varepsilon H_i e^{H_i t}\right)\left[\hat{a}_{\mathbf{p}}a_{\mathbf{p}}(t)e^{i\mathbf{p}\cdot\mathbf{x}} + h.c.\right] + \chi(\mathbf{x},t) - \bar{\chi}. \tag{5.34}$$

The fluctuation field obeys a Langevin type equation

$$\frac{\partial a}{\partial t} = \frac{1}{3H_i}\left(\frac{\nabla^2 a}{e^{2H_i t}} - \frac{\partial V}{\partial a}\right) + \eta(\mathbf{x}, t) \tag{5.35}$$

with $\eta(\mathbf{x}, t)$ acting as white noise sourced by the modes leaving the horizon, essentially causing the averaged field to random walk. The Langevin type equation can be translated into a Fokker-Planck equation for the normalized probability distribution of the field $P(\chi, \bar{\chi}, t)$

$$\frac{\partial P(\chi, \bar{\chi}, t)}{\partial t} = \frac{\partial}{\partial \chi}\left(\frac{1}{3H_i}\frac{\partial V}{\partial \chi}P(\chi, \bar{\chi}, t)\right) + \frac{H_i^3}{8\pi^2}\frac{\partial^2 P(\chi, \bar{\chi}, t)}{\partial \chi^2}. \tag{5.36}$$

The solution to this equation may be calculated as an infinite series [183]

$$P(\chi, \bar{\chi}, t) = \exp\left(-\frac{4\pi^2}{3H_i^4}V(\chi)\right)\sum_{n=0}^{\infty} a_n \Phi_n(\chi) e^{-\Lambda_n(t-t_i)} \tag{5.37}$$

with $\Phi_n(\chi)$ the eigenfunctions of

$$-\frac{1}{2}\frac{\partial^2 \Phi_n}{\partial \chi^2} + \frac{1}{2}\left(\left(\frac{4\pi^2}{3H_i^4}\frac{\partial V}{\partial \chi}\right)^2 - \frac{4\pi^2}{3H_i^4}\frac{\partial^2 V}{\partial \chi^2}\right)\Phi_n = \frac{4\pi^2 \Lambda_n}{H_i^3}\Phi_n \tag{5.38}$$

and the coefficients a_n are given by the initial condition at $t = t_i$ as

$$a_n = \int P(\chi, \bar{\chi}, t)\Phi_n(\chi)\exp\left(\frac{4\pi^2}{3H_i^4}\frac{\partial V}{\partial \chi}\right)d\chi. \tag{5.39}$$

The distribution (5.37) eventually, for late enough times, evolves towards the static limit

$$P(\bar{\chi}) = \frac{\exp\left(-\frac{4\pi^2}{3H_i^4}V(\bar{\chi})\right)}{\int \exp\left(-\frac{4\pi^2}{3H_i^4}V(\chi')\right)d\chi'} \tag{5.40}$$

the timescale of this evolution depends on the details of the potential. Each individual Hubble patch starts out with a randomly chosen average axion field drawn from

the distribution (5.40) and, as the universe expands and more and more scales exit the horizon, the distribution function for said Hubble patch becomes Gaussian with increasing width. We are effectively neglecting the effects of the potential for the random walk of each individual section of space. The solution of (5.36) in this limit is then

$$P(\chi, \bar{\chi}, t)^{V=0} = \sqrt{\frac{8\pi^3}{H_i^3 t}} e^{-\frac{2\pi^2}{H_i^3 t}(\chi - \bar{\chi})^2} \tag{5.41}$$

which is indeed a Gaussian with growing width

$$\Delta\chi = \frac{H_i^3 t}{4\pi^2}. \tag{5.42}$$

The effect of the potential enters into the average over many patches drawn each drawn from distributions (5.41). Since each Random walk is slightly biased towards the vacuum states of the potential, eventually the distribution of the average value over many Hubble patches accumulates around the vacuum states [182] and evolves towards (5.40). We thus end up with a universe divided into Hubble patches, each with a mean axion value drawn from (5.41) where the mean field over many patches $\bar{\chi}$ satisfies (5.40). Thus, when the temperature of the universe drops below the potential barrier between the different vacuum states and DW form, the field is no longer equally likely to be anywhere in field space. Adopting for a second $N_{\mathrm{DW}} = 2$ we may then define a bias in the population of one vacuum over the other as

$$b(\bar{\chi}) = \int f(\chi) P(\chi, \bar{\chi}, t)^{V=0} d\chi \tag{5.43}$$

where $f(\chi)$ is ± 1 depending on which vacuum state the field ends up in. Inflation gives access only to the probability distribution of $\bar{\chi}$, hence it is natural to translate

this into a probability of finding a bias [184]

$$P(|b| < x) = \sum_{\bar{\chi};\, b=b(\bar{\chi})} \int_{b(\bar{\chi})=-x}^{b(\bar{\chi})=x} P(\bar{\chi}) d\bar{\chi}. \tag{5.44}$$

Having established a statistical bias in the vacuum state populations, the co-moving DW network energy density decays exponentially like [185, 186, 187, 188]

$$\rho_{\rm DW} \propto \frac{\sigma_{\rm DW}}{\eta} e^{-|b|^2 \left(\frac{\eta}{\eta_{\rm form}}\right)^3} \tag{5.45}$$

where $\eta_{\rm form}$ is the conformal time at which the DW are formed. This can be understood intuitively when thinking about the actual physical implication of a statistical bias. In a $3+1$ dimensional universe, the introduction of a large bias in the distribution results in a universe with one percolating domain in the vacuum with higher occupation interrupted by bubbles of the other vacuum. The threshold probability bias to get only one vacuum percolating is $p = 0.3$. The size of those bubbles will roughly be proportional to the horizon size at formation and a function of the bias with which they are produced. Hence, when the scale of the universe becomes large enough for the bubbles to be contained within one causal patch, they will shrink and collapse due to the large surface tension. Note that, in our case, it is not false vacuum as the two states are still degenerate and we have not specified which of the $N_{\rm DW}$ vacuum states will eventually be chosen and indeed this mechanism chooses one at random. The situation for a small statistical bias is slightly different in that both vacuum states initially percolate, but eventually the disfavoured one will evolve into pockets which then again collapse due to their surface tension [185].

Chapter 6

Biased Axion Domain walls

The domain wall problem, described in section 5.4, constitutes a significant cosmological problem for many axion models. Any model with $N_{\rm DW} > 1$ quarks charged under $U(1)_{\rm PQ}$ whose PQ symmetry breaking takes place after inflation (or with sufficiently high reheat temperature) leads to cosmological disaster i.e. the universe undergoes rapid expansion driven by domain walls and is incompatible with observation. While recognised since work by Sikivie in the 1980's [176], the domain wall problem remains an interesting problem to study and there have been many attempts at its solution.

The trivial solution, rather than solving the problem, circumnavigates it by having a high energy scale at which $U(1)_{\rm PQ}$ spontaneously breaks, well above the scale of inflation. We will call this scenario the pre inflational PQ breaking. In this case our universe started off well within a Hubble patch at the scale of PQ breaking and any domain walls are trivially inflated away. That is to say that the patches of vacuum are much larger than our current horizon and play no role in the cosmological evolution after inflation. We conclude that in case the PQ symmetry spontaneously breaks before inflation and is not restored during the period of reheating, there exists no axion domain wall problem. Once we change the succession of these cosmological events however, the domain wall problem returns. For sufficiently high scale inflation

the domain wall problem even exists in the pre inflation scenario because the deSitter temperature $T_{\rm ds} \sim H_i/2\pi$ causes fluctuations in the PQ field to generate domain walls at the horizon scale [189]. This mechanism is efficient for $f_{\rm PQ} \lesssim T_{\rm ds}$.

Assuming for now that $U(1)_{\rm PQ}$ breaks after inflation, we are faced with the task to find a solution to the domain wall problem. As was discussed in chapter 5 the domain wall network is only stable when $N_{\rm DW} > 1$. Technically, we could assume the problem to be solved if we limit ourselves to axion models in which there is only a single quark charged under $U(1)_{\rm PQ}$. While not suffering from cosmological disaster, it is unsatisfying to exclude any model with $N_{\rm DW} \neq 1$. Note however that there is a case for doing so in a related but different context [190]. The argument there is that a deSitter vacuum is not consistent in a quantum theory and therefore there must not be any positive energy vacuum states [191, 192, 193]. Applied to the axion potential this excludes any $N_{\rm DW} \neq 1$ theory as higher dimensional operators will always break the degeneracy between the vacuum states and therefore leave positive energy vacuum states or deSitter vacua. There is still room for $N_{\rm DW} \neq 1$ axion UV completions if we find a mechanism under which the true vacuum is chosen fast enough, another way of saying that the domain walls must disappear fast enough.

6.1 Explicit PQ breaking

If we go beyond $N_{\rm DW} = 1$ (e.g. the DFSZ axion has $N_{\rm DW} = 6$), the traditional solution to the domain wall problem as discovered by Sikivie [176], involves a small explicit breaking of the PQ symmetry. This is accomplished by adding a term

$$\delta V = -\xi \left(\phi e^{-i\delta} + h.c. \right) \tag{6.1}$$

to the axion potential (1.18). The usual argument to get around the unnaturalness of adding such term by hand is to invoke higher order operators. These operators are

suppressed by the Planck scale $M_{\rm pl} \sim 10^{19}\,\text{GeV}$ and lead to terms [194]

$$\delta V_{\rm pl} = \frac{|g|\, e^{i\delta}}{M_{\rm pl}^{2m+n-4}} \left|\phi\right|^{2m} \phi^n + h.c. + c. \tag{6.2}$$

The constant c is chosen such that $\min V = 0$ and a great deal of fine tuning is necessary to avoid having large vacuum energy. The coupling can in general be complex introducing a phase δ with coupling strength $|g|$. The above term stems from a $2m+n$ dimensional operator with a $U(1)_{\rm PQ}$ charge n; Under $U(1)_{\rm PQ}$ the $\left|\phi\right|^{2m}$ stays invariant and ϕ^n changes by n. The whole operator is suppressed by $M_{\rm pl}^{2m+n-4}$ to guarantee its sub-dominance to lower order operators and save the perturbative expansion. We see that the inclusion of this term has indeed a similar effect like the originally proposed (6.1) and leads to a potential after spontaneous symmetry breaking of $U(1)_{\rm PQ}$ with ϕ acquiring a vev $v_a = N_{\rm DW} f_{\rm PQ}$

$$\delta V_{\rm pl} = |g|\, M_{\rm pl}^2 \left(\frac{f_{\rm PQ}}{\sqrt{2} M_{\rm pl}}\right)^{2m+n-2} f_{\rm PQ}^2 \left(1 - \cos\left(na + \delta\right)\right) \tag{6.3}$$

such that the axion field lives in the combined potential

$$V(a) = m_a^2 f_{\rm PQ}^2 \left(1 - \cos(N_{\rm DW} a)\right) + |g|\, M_{\rm pl}^2 \left(\frac{f_{\rm PQ}}{\sqrt{2} M_{\rm pl}}\right)^{2m+n-2} f_{\rm PQ}^2 \left(1 - \cos\left(na + \delta\right)\right). \tag{6.4}$$

Interestingly, there are tight constraints on such operators which bound them from above and below.

Explicitly breaking $U(1)_{\rm PQ}$ is necessarily bounded from above because in the limit of very strong breaking there was no $U(1)_{\rm PQ}$ in the first place therefore reintroducing the original strong CP problem. To avoid spoiling the PQ solution, we cannot have arbitrarily strong breaking. This is related to the axion quality problem. We can find this upper bound from the potential above. We consider the strong CP problem solved when the axion field's vacuum expectation value is smaller than the current

limit on the QCD vacuum angle $\theta < 10^{-10}$. We may find the vev as $V(a) = 0$ and obtain

$$\langle\theta\rangle = \frac{|g|\, M_{\rm pl}^2 \left(\frac{f_{\rm PQ}}{\sqrt{2}M_{\rm pl}}\right)^{2m+n-2} \frac{n}{N} \sin\delta}{m_a^2 + |g|\, M_{\rm pl}^2 \left(\frac{f_{\rm PQ}}{\sqrt{2}M_{\rm pl}}\right)^{2m+n-2} n^2 \cos\delta} \sim |g| \left(\frac{M_{\rm pl}}{m_a}\right)^2 \left(\frac{f_{\rm PQ}}{\sqrt{2}M_{\rm pl}}\right)^{2m+n-2} \frac{n}{N} \sin\delta \tag{6.5}$$

where we made use of the fact that the potential generated by the higher order operators is much smaller than the QCD potential. It is natural to assume the phase introduced from the coupling to be $\delta \sim \mathcal{O}(1)$. Thence

$$|g| \left(\frac{f_{\rm PQ}}{\sqrt{2}M_{\rm pl}}\right)^{2m+n} \frac{n}{N_{\rm DW}} < 1.6 \times 10^{-91} \tag{6.6}$$

where we made use of the equivalence between axion mass m_a and PQ scale $f_{\rm PQ}$ for the QCD axion (1.19).

To find a lower bound on the explicit PQ breaking we look at the DW problem. After appearance it takes only a short time before the walls dominate the universe's energy density, leading to accelerated expansion (5.32), incompatible with observation. Therefore, they must decay quickly enough and never come to dominate. We can set a conservative upper bound on the timescale of decay be requiring the domain walls to disappear at the latest when big bang nucleosynthesis (bbn) starts around $t_{\rm bbn} = 1\,\mathrm{s}$. Having a small explicit breaking lifts the degeneracy of the $N_{\rm DW}$ vacuum states leaving, in general, only one true vacuum and $N_{\rm DW} - 1$ false ones. A bubble of false vacuum surrounded by the true vacuum experiences a pressure causing the domain wall shell to shrink. This pressure arises due to the difference in energy density. The domain wall contributes

$$E_{\rm DW} = \sigma_{\rm DW} R^2 \tag{6.7}$$

for a bubble of size R and the energy density of the contained volume is

$$E_{\rm vol} = \delta V R^3. \tag{6.8}$$

The work done by the energy difference between the volume of false vacuum and the true vacuum at $V = 0$ is $\Delta E \sim \delta V R^3$. Then we may find the force acting on the DW $F_{\rm DW} = \delta V R^2$ and hence its acceleration

$$a = \frac{\delta V}{\sigma_{\rm DW}} \simeq 2.8 \times 10^{58}\,{\rm GeV}\,|g| \left(\frac{f_{\rm PQ}}{\sqrt{2}M_{\rm pl}}\right)^{2m+n-1} \tag{6.9}$$

where again we used (1.19) and estimated the potential difference δV to be the maximum of the potential generated by higher order operators. The true difference will be slightly smaller. This, however, does not greatly affect the argument made here. We can estimate the time of collapse to be roughly when the acceleration is fast enough to accelerate the DW close to the speed of light thereby overcoming the expansion of space leading to collapse. This leads to the requirement

$$|g| \left(\frac{f_{\rm PQ}}{\sqrt{2}M_{\rm pl}}\right)^{2m+n-1} \geq 1.2 \times 10^{-83}. \tag{6.10}$$

We may combine (6.6) and (6.10) to constrain the dimension of Planck operators which would solve the DW problem while not spoiling the PQ solution

$$8.5 \times 10^{-91} \left(\frac{f_{\rm PQ}}{10^{12}\,{\rm GeV}}\right) < |g| \left(\frac{f_{\rm PQ}}{\sqrt{2}M_{\rm pl}}\right)^{2m+n} < 1.6 \times 10^{-91} \frac{N_{\rm DW}}{n}. \tag{6.11}$$

The window for solving both problems is very narrow indeed. There does only exist a solution to the above equation if

$$f_{\rm PQ} < 1.9 \times 10^{11}\,{\rm GeV} \frac{N_{\rm DW}}{n} \tag{6.12}$$

which sets a convenient upper bound on the PQ scale. This bound is, assuming $N_{\mathrm{DW}}/n \sim \mathcal{O}(1)$ which seems natural, close to the upper bound coming from cosmology, above which axion DM overcloses the universe. Having done this rough estimate we may use the right inequality of (6.11) to find

$$2m + n < 1 + \frac{\log\left(1.2 \times 10^{-83}\right)}{\log\left(\frac{f_{\mathrm{PQ}}}{\sqrt{2}M_{\mathrm{pl}}}\right)} \tag{6.13}$$

as an upper bound on the dimension of Planck-suppressed operators. The left inequality leads, after minimal algebra, to

$$2m + n > \frac{\log\left(1.6 \times 10^{-91}\frac{N_{\mathrm{DW}}}{n}\right)}{\log\left(\frac{f_{\mathrm{PQ}}}{\sqrt{2}M_{\mathrm{pl}}}\right)}. \tag{6.14}$$

Figure 6.1 shows the available parameter space for the operator dimension as a function of f_{PQ} for $N_{\mathrm{DW}}/n \sim \mathcal{O}(1)$. A larger value makes the problem worse while a lower value is marginally better. We would generally not expect this value to be very far from 1. While for reasonable f_{PQ} there do exist operator dimensions for which both aforementioned problems are solved the solution is very unnatural. To leave the PQ solution to the strong CP problem unspoiled we must suppress lower order operators. However, in order to still have fast enough decay we must basically guarantee that the lowest dimensional operator which is allowed within the PQ solution does exist. We therefore would be tasked with having to explain how to suppress all Planck operators up to the specific order we require. We therefore are forced to conclude that explicitly breaking $U(1)_{\mathrm{PQ}}$ to get around the domain wall problem is unsatisfying. Additionally, improvement in neutron EDM measurements will tighten the constraints eventually closing the parameter space completely.

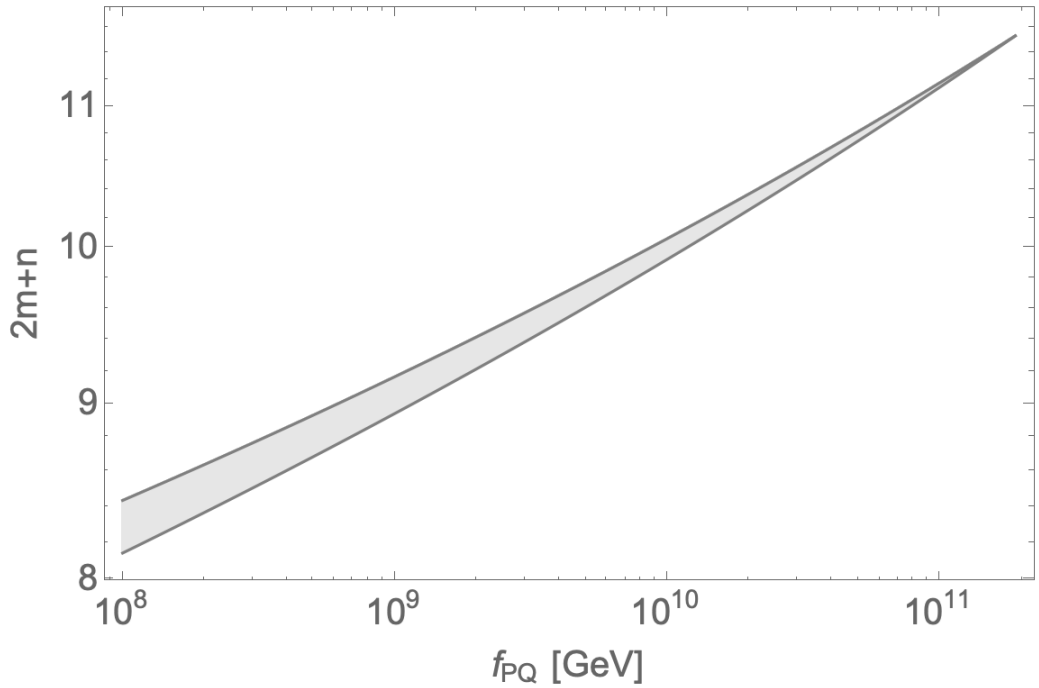

Figure 6.1: The plot shows the dimension of the Planck suppressed higher order operators as a function of PQ scale $f_{\rm PQ}$. The grey region is the allowed region based on the inequalities (6.13) and (6.14) derived in the main text. The plot ends at $f_{\rm PQ} \sim 10^{11}\,{\rm GeV} N_{\rm DW}/n$ above which there is no parameter space available.

6.2 Statistical bias

There are a number of other attempts at solving the domain wall problem and while we will mention some later on in the chapter, the list provided here is not exhaustive. We mentioned above that inflation can, provided that PQ breaks before, solve the problem. It turns out that there is another possible mechanism with which one can hope to solve the problem namely a 'bias' generated by light field dynamics during inflation as described in section 5.5. This was first proposed for Z_2 symmetries [186, 187, 184, 188] and shown to lead to exponential decay of the domain wall network. We will show how the mechanism applies to the axion potential in the rest of the chapter.

The set-up for statistical bias generation in the distribution of vacuum occupation

throughout the universe involves a few key features, as described in the introduction. The field in question must be light compared to the deSitter temperature and have a potential. The former ensures that fluctuations in the field are generated and the latter allows for accumulation of non-Gaussianity. Naturally the axion is light and therefore trivially fulfils the first requirement, the potential however limits the applicability as the axion only gets mass below the QCD scale Λ_{QCD}. This could in principle be circumvented with the addition of other fields coupling the the axion and we will revisit this case at the end of the chapter. For now, we focus on the pure axion case.

Suppose the universe is in a deSitter stage characterised by a approximately constant Hubble parameter H_i and with metric given by

$$ds^2 = a(t)\eta_{ij}dx^i dx^j. \tag{6.15}$$

The factor $a(t)$ is the scale factor of the universe and η_{ij} is the diagonal Minkowski metric with negative signature. Constant Hubble parameter by definition leads to exponential expansion, $a(t) \propto \exp(H_i t)$. The axion field's equation of motion was already established in chapter 5 but is repeated for convenience

$$\left[\left(\frac{\partial}{\partial t}\right)^2 + 3H_i\frac{\partial}{\partial t} - \frac{1}{a(t)^2}\nabla^2\right] a(x) + V'\left(a(x)\right) = 0. \tag{6.16}$$

Following the same procedure as in section 5.5 we may divide the axion field into sub-horizon modes and a course grained fluctuation field χ of super-horizon modes around a mean value $\bar{\chi}$ which is obtained by averaging over many horizon sizes. In full analogy to the discussion before we find a Fokker-Planck equation for the normalized probability distribution of the field $P(\chi, \bar{\chi}, t)$

$$\frac{\partial P(\chi,\bar{\chi},t)}{\partial t} = \frac{\partial}{\partial \chi}\left(\frac{1}{H_i}\frac{\partial V}{\partial \chi}P(\chi,\bar{\chi},t)\right) + \frac{H_i^3}{8\pi^2}\frac{\partial^2 P(\chi,\bar{\chi},t)}{\partial \chi^2} \tag{6.17}$$

whose solution is given by (5.37). For late times $t \to \infty$ the distribution evolves towards a static solution and thus we take for the average field

$$P_{\text{static}}(\bar{\chi}) = \exp\left(-\frac{4\pi^2}{3H_i^4}V(\bar{\chi})\right) / \int \exp\left(-\frac{4\pi^2}{3H_i^4}V(\chi)\right) d\chi. \tag{6.18}$$

To make further progress we must specify the potential of our axion field. For the pure axion case without addition of other degrees of freedom to the SM the axion's potential is flat down to the scale of QCD and then acquires the usual QCD potential (1.18) which, for now, we approximate, as is customary, by

$$V\left(a(x)\right) = m_a^2 f_{\text{PQ}}^2 \left(1 - \cos\left(N_{\text{DW}}\frac{a(x)}{f_{\text{PQ}}}\right)\right). \tag{6.19}$$

With this form of the potential, the above equations can be solved analytically. Starting with equation (5.38) we find a reduction to a Schrödinger type equation when dropping terms of order $(m_a/H_i)^4$. Those terms are necessarily small by our initial assumption of negligible mass compared to the Hubble scale. The resulting equation

$$\frac{\partial^2\Phi_n}{\partial\chi^2} + \left[\frac{4\pi^2}{3}\frac{N_{\text{DW}}^2 m_a^2}{H_i^4}\cos\left(N_{\text{DW}}\frac{\chi}{f_{\text{PQ}}}\right) + \frac{8\pi^2\Lambda_n}{H_i^3}\right]\Phi_n = 0 \tag{6.20}$$

is solved by a Mathieu Function

$$\Phi_n \propto M_C\left(\frac{32\pi^2 f_{\text{PQ}}^2}{N_{\text{DW}}^2 H_i^3}\Lambda_n, \frac{8\pi^2 f_{\text{PQ}}^2 m_a^2}{3H_i^4}, N_{\text{DW}}\frac{\chi}{2f_{\text{PQ}}}\right) \approx \cos\left(\sqrt{\frac{8\pi^2 f_{\text{PQ}}^2}{H_i^3}\Lambda_n}\frac{\chi}{f_{\text{PQ}}}\right) \tag{6.21}$$

where we used the smallness of $(m_a/H_i)^2$ to approximate the function as a cos. Having made this approximation it is a trivial task to find the eigenvalues

$$\Lambda_n \approx \frac{n^2}{8\pi^2}\left(\frac{H_i}{f_{\text{PQ}}}\right)^2 H_i. \tag{6.22}$$

We thus find that the static solution (6.18) is reached after

$$N_{\text{efold}} \geq 8\pi^2 \left(\frac{f_{\text{PQ}}}{H_i}\right)^2 \tag{6.23}$$

when the first temporal correction in the sum (5.37) is exponentially suppressed. We begin to see a problem namely, the required number of e-folds is very large if $f_{\text{PQ}} \gg H_i$ and we will show below that in fact in this case we recover the pre-inflational PQ breaking scenario. In the opposite limit, while the static solution is reached almost instantly, we run into problems with the axion potential. The deSitter temperature in this scenario induces fluctuations in the PQ field of order $H_i/2\pi$ larger than the central potential hill of the wine bottle potential. We therefore recover $\langle\Phi\rangle \sim 0$ and PQ symmetry is restored in this sense. The situation gets even worse when looking at the axion potential, the generation of which relies on the formation of quark bilinears. Those can only form when the timescale of QCD interactions $\Lambda_{\text{QCD}}^{-1}$ is fast enough to overcome the universes expansion H_i^{-1}. Another way of saying is that QCD should not see the curvature of space, $\Lambda_{\text{QCD}} > H_i$. This is obviously a tight constraint and impossible to fulfil when $H_i \gg f_{\text{PQ}}$.

We must therefore conclude that introduction of a statistical bias into the probability distribution, at least in the pure axion case, is limited to $H_i \leq \Lambda_{\text{QCD}} \ll f_{\text{PQ}}$ in which case the static limit is only approached after an enormous number of e-folds, effectively requiring eternal inflation. Assuming inflation lasts sufficiently long, we may calculate a measure for the DW size via the two point correlation function of the axion field [183]. Points which are correlated are in causal contact and in the same vacuum state.

The correlation length diverges for large N_{efold} which simply means that in this limit the domain walls are inflated away and the problem is circumvented. This is equivalent to the pre-inflational PQ breaking and probably not very surprising

when thinking about the large separation of scales involved. PQ breaks at a scale of $f_{\rm PQ}$ and the axion field rolls down the potential hill. The universe continues to expand with the deSitter fluctuations, making the axion field random walk around the potential resulting in an effectively flat distribution after $\sim f_{\rm PQ}/H_i$ steps. The temperature during inflation evolves like $T \propto a(t)^{-1}$, thus it takes on the order of $\ln(f_{\rm PQ}/\Lambda_{\rm QCD}) \sim 30$ e-folds to drop down to the QCD scale. After such few e-folds the random walk process has not taken the field very far away from its initial point but the size of previously causally connected regions already hugely increased. Waiting even longer until the static distribution is reached or the random walk takes the field away from its initial point by an appreciable amount will take much longer and make the domain size exponentially bigger. Hence, the problem here is really one of scales. What worked well for a Z_2 symmetry fails with the introduction of a compact field with large radius compared to the random walk step size.

We are continuing investigations of the domain wall problem, for example the inclusion of additional degrees of freedom coupling to the axion field can change the potential and might alter the conclusions.

6.3 Future direction - monopole mass

We are currently investigating the inclusion of a magnetic monopole of some dark gauge group. For example a dark $SU^D(3)$ which is broken to a dark $U^D_{em}(1)$ can result in t'Hooft-Polyakov monopoles [195, 196]. In the absence of charged particles, the Lagrangian describing the coupling of the axion to this dark version of electromagnetism is

$$\mathcal{L} \supset \frac{1}{2}\left(\partial_\mu a\right)\left(\partial^\mu a\right) - \frac{1}{4}F_{\mu\nu}F^{\mu\nu} + \frac{e^2}{32\pi^2}\frac{a}{v_a}F_{\mu\nu}\tilde{F}^{\mu\nu}, \tag{6.24}$$

analogous to the axion's coupling to SM electrodynamics described in (1.20). Here, e is the dark electric charge of the dark $U^D_{em}(1)$. For convenience we will in the following omit the word "dark" when referring to electric and magnetic quantities.

The presence of magnetic monopoles results in a potential for the axion field through the Witten effect [197]. A theory with a dark electron of charge e and a monopole of magnetic charge g must satisfy the Dirac quantisation condition [198]

$$eg = 2\pi m, \qquad m \in \mathbb{N}. \tag{6.25}$$

If the theory features two or more dyons, the condition is modified to [199, 200, 201]

$$q_1 g_2 - q_2 g_1 = 2\pi m. \tag{6.26}$$

Gauss's law for the electric field including the axion coupling reads

$$\nabla \cdot \left(\mathbf{E} + \frac{e^2}{8\pi^2} \frac{a}{v_a} \mathbf{B} \right) = 0. \tag{6.27}$$

Here $v_a = N_{\mathrm{DW}} f_{\mathrm{PQ}}$ is the vacuum expectation value of the PQ field. A magnetic monopole of charge g produces a coulomb field $\mathbf{B} = g\mathbf{r}/r^3$ and, in the presence of a non-zero axion field, it also produces an electric field

$$\mathbf{E} = -\frac{e^2}{8\pi^2} \frac{a}{v_a} \mathbf{B} = -\frac{e^2 g}{8\pi^2} \frac{a}{v_a} \frac{\mathbf{r}}{r^3}. \tag{6.28}$$

Be $\Lambda(\mathbf{x})$ a gauge transformation of the electromagnetic potential A_μ then the action of the generator of the gauge transformation must be trivial and we find

$$Q_\lambda = \int d^3\mathbf{x} \frac{\delta \mathcal{L}}{\delta \partial_0 A_\mu} \delta A_\mu = \int d^3\mathbf{x} \left(\mathbf{E} + \frac{e^2}{8\pi^2} \frac{a}{v_a} \mathbf{B} \right) \cdot \nabla \Lambda(\mathbf{x}) \tag{6.29}$$

which, for $\exp(iQ_\Lambda) \equiv 1$, implies the Witten condition [197]

$$\frac{q}{e} + \frac{eg}{8\pi^2}\frac{a}{v_a} = n \in \mathbb{N}. \tag{6.30}$$

Hence, in the presence of an axion field, a t'Hooft-Polyakov magnetic monopole with charge $g = 4\pi/e$ becomes a dyon with axion field dependent charge

$$q = ne - \frac{1}{2\pi}\frac{a}{v_a}. \tag{6.31}$$

We thus see that an axion field will be repelled by the monopole because of the large cost in electrostatic field energy

$$E_{\mathbf{E}} \equiv \frac{1}{2}\int \mathbf{E}^2 d^3\mathbf{x} = \int \frac{e^4 g^2}{32\pi^3 r^2}\left(\frac{a}{v_a}\right)^2 dr \tag{6.32}$$

where we assumed radial symmetry for the axion field $a(r)$. The energy in the combined axion-monopole system for a single monopole in a static axion background is then

$$V = \frac{1}{2}\int \left((\nabla a)^2 + \mathbf{E}^2\right) d^3\mathbf{x} = v_a \frac{e^2 g}{4\pi}\int_0^{\frac{r_0}{r_M}} \left(\left(\frac{\partial_x a}{v_a}\right)^2 + \left(\frac{a}{v_a}\right)^2\right) dx \tag{6.33}$$

with $r_0 = e^2 g/8\pi^2 v_a$ and r_M the size of the monopole. The axion field far from the monopole must approach the randomly chosen angle θ_0 and should minimise the potential energy (6.33). This is fulfilled for

$$\frac{a}{v_a} = \theta_0 \exp\left[-\frac{r_0}{r}\right], \qquad \rightarrow \qquad V_0 = v_a \frac{e^2 g}{4\pi}\theta_0^2\left(1 - \exp\left[-2\frac{r_0}{r_M}\right]\right). \tag{6.34}$$

In the limit of a large monopole size $r_M \rightarrow \infty$ we recover the self energy of a charged sphere of size r_M. If there are light fermions charged under the dark $U^D(1)_{\text{em}}$, they screen the charge of the monopole to a size $r_M \sim m_e^{-1}$ where m_e is the mass of the

lightest charged fermion [202, 203].

Assuming a number density of monopoles and antimonopoles $n_M = n_{M^+} + n_{M^-}$ the axion ground state energy (6.34) in a plasma of monopoles is

$$U \simeq n_M V_0 \sim \frac{e^4 g^2}{16\pi^3} \frac{n_M}{r_M v_a^2} \left(v_a \theta_0\right)^2 \tag{6.35}$$

which is equivalent to the axion having a monopole induced mass [204]

$$(m_a^M)^2 \equiv \frac{e^4 g^2}{8\pi^3} \frac{n_M}{r_M v_a^2}. \tag{6.36}$$

Note that if the monopoles were SM magnetic monopoles instead of originating from some dark sector and the lightest quark was massless, then $m_a^M \propto m_q^{1/2} \to 0$ as is expected since in this case the θ vacua of QCD are equivalent and no longer physical observables.

The axion field vacuum state of this potential will be such that the dyon's electric charge is cancelled, hence

$$q = ne - \frac{1}{2\pi} \frac{a}{v_a} \equiv 0 \qquad \Leftrightarrow \qquad \frac{a}{v_a} = 2\pi ne. \tag{6.37}$$

This corresponds to a single axion field value and therefore solves the domain wall problem. The axion acquires mass well before the QCD transition and gets a potential with effective domain wall number $N_{\mathrm{DW}} = 1$. Once this mass is cosmologically important, the axion field accumulates around this single vacuum state. Therefore, even if the monopoles then disappear, for example via a Higgs mechanism similar to [205, 206] where the breaking of the remaining $U(1)$ results in the connection of monopoles and antimonopoles by strings which pull the monopoles together under their tension, the axion field is localised around a single vacuum state when the temperature drops below Λ_{QCD}.

If we allow higher charged dyons with magnetic charge Z_m and electric charge Z_e, then the potential is modified to

$$U = 4\pi e^2 n_M \sum_{Z_m, Z_e} \left(\frac{\left(Z_m \frac{\theta_0}{2\pi} - Z_e \right)^2}{r_M} \frac{n_M^{Z_e, Z_m}}{n_M} \right). \tag{6.38}$$

If we ignore the dependence of r_M on the charge, we see that the potential has infinite local minima $\theta = 2\pi Z_e / Z_m$ but unless the fraction $n_M^{Z_e, Z_m}/n_M$ conspires to be the same for different charge combinations, we only expect one global minimum and the domain wall problem is still principally solved.

To fully test the viability of this idea, further investigation of the monopole parameter space is necessary in order to understand the requirements on the monopole density and properties to solve the domain wall problem and compare those to the constraints they are subjected to. In order to justify the assumption of a single global minimum of the potential when allowing multiple dyons we must further investigate the monopole production and stability of higher charged states. Depending on the cosmological epoch during which the monopole mass of the axion becomes relevant, other signals like gravitational waves from the phase transition may also be identified.

Appendix A

Asymmetric Beams

With the definition of the geometry (2.11), (2.12) we exploited the symmetry between the two beams present in the collision of two optical beams. This allowed the directions to be specified in a very simple manner. When quoting the bounds achievable by the collision of two beams at different frequencies we must drop this assumption. We may choose to fix the geometry such that the axion again propagate in the $\hat{z}$ direction. This is the case for

$$\frac{\mathbf{k}_1}{|\mathbf{k}_1|} = \frac{1}{\sqrt{\omega_1^2 + \omega_2^2 + 2\omega_1\omega_2\cos\alpha}} \left(\omega_2\sqrt{\sin^2\alpha}, 0, \sqrt{\omega_2^2\cos^2\alpha + \omega_1^2 + 2\omega_1\omega_2\cos\alpha}\right) \tag{A.1}$$

and

$$\frac{\mathbf{k}_2}{|\mathbf{k}_2|} = \frac{1}{\sqrt{\omega_1^2 + \omega_2^2 + 2\omega_1\omega_2\cos\alpha}} \left(\omega_1\sqrt{\sin^2\alpha}, 0, \sqrt{\omega_1^2\cos^2\alpha + \omega_2^2 + 2\omega_1\omega_2\cos\alpha}\right). \tag{A.2}$$

The electric and magnetic field of the electromagnetic waves are found from the requirement that they be mutually orthogonal and have $\mathbf{E}_i \cdot \mathbf{B}_j \neq 0$. We choose

$$\frac{\boldsymbol{\mathcal{E}}_1}{|\boldsymbol{\mathcal{E}}_1|} = (0, 1, 0), \tag{A.3}$$

$$\frac{\boldsymbol{\mathcal{B}}_1}{|\boldsymbol{\mathcal{B}}_1|} = \frac{-1}{\sqrt{\omega_1^2+\omega_2^2+2\omega_1\omega_2\cos\alpha}}\left(\sqrt{\omega_2^2\cos^2\alpha+\omega_1^2+2\omega_1\omega_2\cos\alpha}, 0, \omega_2\sqrt{\sin^2\alpha}\right) \tag{A.4}$$

for the first laser and for the second laser

$$\frac{\boldsymbol{\mathcal{E}}_2}{|\boldsymbol{\mathcal{E}}_2|} = \frac{1}{\sqrt{\omega_1^2+\omega_2^2+2\omega_1\omega_2\cos\alpha}}\left(\sqrt{\omega_1^2\cos^2\alpha+\omega_2^2+2\omega_1\omega_2\cos\alpha}, 0, -\omega_2\sqrt{\sin^2\alpha}\right), \tag{A.5}$$

$$\frac{\boldsymbol{\mathcal{B}}_2}{|\boldsymbol{\mathcal{B}}_2|} = (0,1,0). \tag{A.6}$$

We then evaluate $\mathcal{F} = \boldsymbol{\mathcal{E}}_1 \cdot \boldsymbol{\mathcal{B}}_2 + \boldsymbol{\mathcal{B}}_1 \cdot \boldsymbol{\mathcal{E}}_2$ to find

$$\frac{\mathcal{F}^2}{|\boldsymbol{\mathcal{E}}_1|^2|\boldsymbol{\mathcal{E}}_2|^2} = \left(\frac{\omega_1\omega_2\sin^2\alpha+2\omega_1\omega_2\cos\alpha-\sqrt{(\omega_1\cos\alpha+\omega_2)^2(\omega_2\cos\alpha+\omega_1)^2}+\omega_1^2+\omega_2^2}{\omega_1^2+\omega_2^2+2\omega_1\omega_2\cos\alpha}\right)^2. \tag{A.7}$$

For the reconversion to the electric signal field the geometry results in a source

$$\frac{|\mathbf{j}_0|^2}{\omega_\phi^2\omega_1^2|\boldsymbol{\mathcal{E}}_2|^2} = \left(\left(1-\frac{k_\phi}{\omega_\phi}\sqrt{\frac{(\omega_1\cos\alpha+\omega_2)^2}{\omega_1^2+\omega_2^2+2\omega_1\omega_2\cos\alpha}}\right)^2+\frac{k_\phi^2}{\omega_\phi^2}\frac{(\omega_1\cos\alpha+\omega_2)^2}{(\omega_1^2+\omega_2^2+2\omega_1\omega_2\cos\alpha)}\frac{1}{(k_\phi d)^2}\right) \tag{A.8}$$

where again, we chose beam 2 to be the stimulating one. This results in energy of the signal field

$$E = \frac{g_{a\gamma\gamma}^4}{256\pi^2}\frac{l^2}{d^2}\omega_\phi^2 E_1 E_2^2 \frac{\mathcal{F}^2}{|\boldsymbol{\mathcal{E}}_1|^2|\boldsymbol{\mathcal{E}}_2|^2}\frac{|\mathbf{j}_0|^2}{\omega_\phi^2\omega_1^2|\boldsymbol{\mathcal{E}}_2|^2} \tag{A.9}$$

from which we may trivially find the bounds on $g_{a\gamma\gamma}$ as indicated in 2.2.

Bibliography

[1] Konstantin Beyer, Brian Reville, Archie Bott, Hye-Sook Park, Subir Sarkar, and Gianluca Gregori. Analytical estimates of proton acceleration in laser-produced turbulent plasmas. *J. Plasma Phys.*, 84(6):905840608, 2018, astro-ph/1808.04356.

[2] B. King, B. M. Dillon, K. A. Beyer, and G. Gregori. Axion-like-particle decay in strong electromagnetic backgrounds. *JHEP*, 12:162, 2019, hep-ph/1905.05201.

[3] K. A. Beyer, G. Marocco, R. Bingham, and G. Gregori. Axion detection through resonant photon-photon collisions. *Phys. Rev. D*, 101(9):095018, 2020, hep-ph/2001.03392.

[4] K. A. Beyer, G. Marocco, C. Danson, R. Bingham, and G. Gregori. Parametric co-linear axion photon instability. 8 2021, hep-ph/2108.01489.

[5] K. A. Beyer, G. Marocco, R. Bingham, and G. Gregori. Light-shining-through-wall axion detection experiments with a stimulating laser. *Phys. Rev. D*, 105(3):035031, 2022, 2109.14663.

[6] R. D. Peccei. The Strong CP problem and axions. *Lect. Notes Phys.*, 741:3–17, 2008, hep-ph/0607268.

[7] Gerard 't Hooft. Symmetry Breaking Through Bell-Jackiw Anomalies. *Phys. Rev. Lett.*, 37:8–11, 1976.

[8] R. J. Crewther, P. Di Vecchia, G. Veneziano, and Edward Witten. Chiral Estimate of the Electric Dipole Moment of the Neutron in Quantum Chromodynamics. *Phys. Lett. B*, 88:123, 1979. [Erratum: Phys.Lett.B 91, 487 (1980)].

[9] Maxim Pospelov and Adam Ritz. Theta vacua, QCD sum rules, and the neutron electric dipole moment. *Nucl. Phys. B*, 573:177–200, 2000, hep-ph/9908508.

[10] Maxim Pospelov and Adam Ritz. Neutron EDM from electric and chromoelectric dipole moments of quarks. *Phys. Rev. D*, 63:073015, 2001, hep-ph/0010037.

[11] C. Abel et al. Measurement of the permanent electric dipole moment of the neutron. *Phys. Rev. Lett.*, 124(8):081803, 2020, hep-ex/2001.11966.

[12] Steven Weinberg. The U(1) Problem. *Phys. Rev. D*, 11:3583–3593, 1975.

[13] J. S. Bell and R. Jackiw. A PCAC puzzle: $\pi^0 \to \gamma\gamma$ in the σ model. *Nuovo Cim. A*, 60:47–61, 1969.

[14] Stephen L. Adler. Axial vector vertex in spinor electrodynamics. *Phys. Rev.*, 177:2426–2438, 1969.

[15] Kazuo Fujikawa. Path Integral for Gauge Theories with Fermions. *Phys. Rev. D*, 21:2848, 1980. [Erratum: Phys.Rev.D 22, 1499 (1980)].

[16] Gerard 't Hooft. Computation of the Quantum Effects Due to a Four-Dimensional Pseudoparticle. *Phys. Rev. D*, 14:3432–3450, 1976. [Erratum: Phys.Rev.D 18, 2199 (1978)].

[17] Curtis G. Callan, Jr., R. F. Dashen, and David J. Gross. The Structure of the Gauge Theory Vacuum. *Phys. Lett. B*, 63:334–340, 1976.

[18] A. A. Belavin, Alexander M. Polyakov, A. S. Schwartz, and Yu. S. Tyupkin. Pseudoparticle Solutions of the Yang-Mills Equations. *Phys. Lett. B*, 59:85–87, 1975.

[19] Nicola Cabibbo. Unitary Symmetry and Leptonic Decays. *Phys. Rev. Lett.*, 10:531–533, 1963.

[20] Makoto Kobayashi and Toshihide Maskawa. CP Violation in the Renormalizable Theory of Weak Interaction. *Prog. Theor. Phys.*, 49:652–657, 1973.

[21] R. D. Peccei. Reflections on the strong CP problem. *Nucl. Phys. B Proc. Suppl.*, 72:3, 1999, hep-ph/9807514.

[22] Jihn E. Kim and Gianpaolo Carosi. Axions and the Strong CP Problem. *Rev. Mod. Phys.*, 82:557–602, 2010, hep-ph/0807.3125. [Erratum: Rev.Mod.Phys. 91, 049902 (2019)].

[23] Anson Hook. TASI Lectures on the Strong CP Problem and Axions. *PoS*, TASI2018:004, 2019, 1812.02669.

[24] R. D. Peccei and Helen R. Quinn. CP conservation in the presence of pseudoparticles. *Phys. Rev. Lett.*, 38:1440–1443, Jun 1977.

[25] R. D. Peccei and Helen R. Quinn. Constraints imposed by CP conservation in the presence of pseudoparticles. *Phys. Rev. D*, 16:1791–1797, Sep 1977.

[26] Sinya Aoki et al. Review of Lattice Results Concerning Low-Energy Particle Physics. *Eur. Phys. J. C*, 74:2890, 2014, hep-lat/1310.8555.

[27] Giovanni Grilli di Cortona, Edward Hardy, Javier Pardo Vega, and Giovanni Villadoro. The QCD axion, precisely. *JHEP*, 01:034, 2016, hep-ph/1511.02867.

[28] Sz. Borsanyi et al. Calculation of the axion mass based on high-temperature lattice quantum chromodynamics. *Nature*, 539(7627):69–71, 2016, hep-lat/1606.07494.

[29] Mark Srednicki. Axion Couplings to Matter. 1. CP Conserving Parts. *Nucl. Phys. B*, 260:689–700, 1985.

[30] Howard Georgi, David B. Kaplan, and Lisa Randall. Manifesting the Invisible Axion at Low-energies. *Phys. Lett. B*, 169:73–78, 1986.

[31] Luca Di Luzio, Maurizio Giannotti, Enrico Nardi, and Luca Visinelli. The landscape of QCD axion models. *Phys. Rept.*, 870:1–117, 2020, 2003.01100.

[32] Jihn E. Kim. Weak Interaction Singlet and Strong CP Invariance. *Phys. Rev. Lett.*, 43:103, 1979.

[33] Mikhail A. Shifman, A. I. Vainshtein, and Valentin I. Zakharov. Can Confinement Ensure Natural CP Invariance of Strong Interactions? *Nucl. Phys. B*, 166:493–506, 1980.

[34] A. R. Zhitnitsky. On Possible Suppression of the Axion Hadron Interactions. (In Russian). *Sov. J. Nucl. Phys.*, 31:260, 1980.

[35] Michael Dine, Willy Fischler, and Mark Srednicki. A Simple Solution to the Strong CP Problem with a Harmless Axion. *Phys. Lett. B*, 104:199–202, 1981.

[36] P. Sikivie. Experimental Tests of the Invisible Axion. *Phys. Rev. Lett.*, 51:1415–1417, 1983. [Erratum: Phys.Rev.Lett. 52, 695 (1984)].

[37] Georg Raffelt and Leo Stodolsky. Mixing of the Photon with Low Mass Particles. *Phys. Rev. D*, 37:1237, 1988.

[38] Stephen L Adler. Photon splitting and photon dispersion in a strong magnetic field. *Annals of Physics*, 67(2):599–647, 1971.

[39] Edward Witten. Some Properties of O(32) Superstrings. *Phys. Lett.*, 149B:351–356, 1984.

[40] Asimina Arvanitaki, Savas Dimopoulos, Sergei Dubovsky, Nemanja Kaloper, and John March-Russell. String Axiverse. *Phys. Rev.*, D81:123530, 2010, hep-th/0905.4720.

[41] Pierre Sikivie. Detection Rates for 'Invisible' Axion Searches. *Phys. Rev. D*, 32:2988, 1985. [Erratum: Phys.Rev.D 36, 974 (1987)].

[42] P.A. Zyla et al. Review of Particle Physics. *PTEP*, 2020(8):083C01, 2020.

[43] Pierre Sikivie. Invisible Axion Search Methods. *Rev. Mod. Phys.*, 93(1):015004, 2021, 2003.02206.

[44] S. J. Asztalos et al. An Improved RF cavity search for halo axions. *Phys. Rev. D*, 69:011101, 2004, astro-ph/0310042.

[45] Leanne Duffy, P. Sikivie, D. B. Tanner, Stephen J. Asztalos, C. Hagmann, D. Kinion, L. J Rosenberg, K. van Bibber, D. Yu, and R. F. Bradley. Results of a search for cold flows of dark matter axions. *Phys. Rev. Lett.*, 95:091304, 2005, astro-ph/0505237.

[46] S. J. Asztalos et al. A SQUID-based microwave cavity search for dark-matter axions. *Phys. Rev. Lett.*, 104:041301, 2010, astro-ph/0910.5914.

[47] J. Hoskins et al. A search for non-virialized axionic dark matter. *Phys. Rev. D*, 84:121302, 2011, astro-ph/1109.4128.

[48] Lawrence Krauss, John Moody, Frank Wilczek, and Donald E. Morris. Calculations for Cosmic Axion Detection. *Phys. Rev. Lett.*, 55:1797, 1985.

[49] R. Bradley, J. Clarke, D. Kinion, L. J. Rosenberg, K. van Bibber, S. Matsuki, M. Muck, and P. Sikivie. Microwave cavity searches for dark-matter axions. *Rev. Mod. Phys.*, 75:777–817, 2003.

[50] S. De Panfilis, A. C. Melissinos, B. E. Moskowitz, J. T. Rogers, Y. K. Semertzidis, Walter Wuensch, H. J. Halama, A. G. Prodell, W. B. Fowler, and F. A. Nezrick. Limits on the Abundance and Coupling of Cosmic Axions at 4.5-Microev $<$ m(a) $<$ 5.0-Microev. *Phys. Rev. Lett.*, 59:839, 1987.

[51] Walter Wuensch, S. De Panfilis-Wuensch, Y. K. Semertzidis, J. T. Rogers, A. C. Melissinos, H. J. Halama, B. E. Moskowitz, A. G. Prodell, W. B. Fowler, and F. A. Nezrick. Results of a Laboratory Search for Cosmic Axions and Other Weakly Coupled Light Particles. *Phys. Rev. D*, 40:3153, 1989.

[52] C. Hagmann, P. Sikivie, N. S. Sullivan, and D. B. Tanner. Results from a search for cosmic axions. *Phys. Rev. D*, 42:1297–1300, 1990.

[53] B. M. Brubaker et al. First results from a microwave cavity axion search at 24 μeV. *Phys. Rev. Lett.*, 118(6):061302, 2017, astro-ph/1610.02580.

[54] Ben T. McAllister, Graeme Flower, Eugene N. Ivanov, Maxim Goryachev, Jeremy Bourhill, and Michael E. Tobar. The ORGAN Experiment: An axion haloscope above 15 GHz. *Phys. Dark Univ.*, 18:67–72, 2017, ins-det/1706.00209.

[55] Dmitry Budker, Peter W. Graham, Micah Ledbetter, Surjeet Rajendran, and Alex Sushkov. Proposal for a Cosmic Axion Spin Precession Experiment (CASPEr). *Phys. Rev. X*, 4(2):021030, 2014, hep-ph/1306.6089.

[56] Derek F. Jackson Kimball et al. Overview of the Cosmic Axion Spin Precession Experiment (CASPEr). *Springer Proc. Phys.*, 245:105–121, 2020, ins-det/1711.08999.

[57] Peter W. Graham and Surjeet Rajendran. New Observables for Direct Detection of Axion Dark Matter. *Phys. Rev. D*, 88:035023, 2013, hep-ph/1306.6088.

[58] Jonathan L. Ouellet et al. First Results from ABRACADABRA-10 cm: A Search for Sub-μeV Axion Dark Matter. *Phys. Rev. Lett.*, 122(12):121802, 2019, hep-ex/1810.12257.

[59] Jonathan L. Ouellet et al. Design and implementation of the ABRACADABRA-10 cm axion dark matter search. *Phys. Rev. D*, 99(5):052012, 2019, ins-det/1901.10652.

[60] E. Aprile et al. Excess electronic recoil events in XENON1T. *Phys. Rev. D*, 102(7):072004, 2020, hep-ex/2006.09721.

[61] James B. Dent, Bhaskar Dutta, Jayden L. Newstead, and Adrian Thompson. Inverse Primakoff Scattering as a Probe of Solar Axions at Liquid Xenon Direct Detection Experiments. *Phys. Rev. Lett.*, 125(13):131805, 2020, hep-ph/2006.15118.

[62] Silvia Garbari, Chao Liu, Justin I. Read, and George Lake. A new determination of the local dark matter density from the kinematics of K dwarfs. *MNRAS*, 425(2):1445–1458, September 2012, astro-ph/1206.0015.

[63] A. Halprin, C. M. Andersen, and H. Primakoff. Photonic Decay Rates and Nuclear-Coulomb-Field Coherent Production Processes. *Phys. Rev.*, 152:1295–1303, 1966.

[64] Duane A. Dicus, Edward W. Kolb, Vigdor L. Teplitz, and Robert V. Wagoner. Astrophysical Bounds on the Masses of Axions and Higgs Particles. *Phys. Rev. D*, 18:1829, 1978.

[65] Georg G. Raffelt. Astrophysical methods to constrain axions and other novel particle phenomena. *Phys. Rept.*, 198:1–113, 1990.

[66] Georg G. Raffelt. Astrophysical axion bounds. *Lect. Notes Phys.*, 741:51–71, 2008, hep-ph/0611350.

[67] John N. Bahcall and M. H. Pinsonneault. What do we (not) know theoretically about solar neutrino fluxes? *Phys. Rev. Lett.*, 92:121301, 2004, astro-ph/0402114.

[68] S. Andriamonje et al. An Improved limit on the axion-photon coupling from the CAST experiment. *JCAP*, 04:010, 2007, hep-ex/0702006.

[69] E. Arik et al. Probing eV-scale axions with CAST. *JCAP*, 02:008, 2009, hep-ex/0810.4482.

[70] S. Aune et al. CAST search for sub-eV mass solar axions with 3He buffer gas. *Phys. Rev. Lett.*, 107:261302, 2011, hep-ex/1106.3919.

[71] M. Arik et al. Search for Solar Axions by the CERN Axion Solar Telescope with ^{3}He Buffer Gas: Closing the Hot Dark Matter Gap. *Phys. Rev. Lett.*, 112(9):091302, 2014, hep-ex/1307.1985.

[72] M. Arik et al. New solar axion search using the CERN Axion Solar Telescope with ^{4}He filling. *Phys. Rev. D*, 92(2):021101, 2015, hep-ex/1503.00610.

[73] R Bernabei, P Belli, R Cerulli, F Montecchia, F Nozzoli, A Incicchitti, D Prosperi, CJ Dai, HL He, HH Kuang, et al. Search for solar axions by primakoff effect in nai crystals. *Physics Letters B*, 515(1-2):6–12, 2001.

[74] Georg G. Raffelt and David S. P. Dearborn. Bounds on Hadronic Axions From Stellar Evolution. *Phys. Rev. D*, 36:2211, 1987.

[75] Alexandre Payez, Carmelo Evoli, Tobias Fischer, Maurizio Giannotti, Alessandro Mirizzi, and Andreas Ringwald. Revisiting the SN1987A gamma-ray limit on ultralight axion-like particles. *JCAP*, 02:006, 2015, astro-ph/1410.3747.

[76] A. Burrows. Supernova explosions in the universe. *Nature*, 403:727–733, 2000.

[77] Stan Woosley and Thomas Janka. The physics of core-collapse supernovae. *Nature Phys.*, 1:147, 2005, astro-ph/0601261.

[78] Tobias Fischer, Sovan Chakraborty, Maurizio Giannotti, Alessandro Mirizzi, Alexandre Payez, and Andreas Ringwald. Probing axions with the neutrino signal from the next galactic supernova. *Phys. Rev. D*, 94(8):085012, 2016, astro-ph/1605.08780.

[79] Christopher S. Reynolds, M.C. David Marsh, Helen R. Russell, Andrew C. Fabian, Robyn Smith, Francesco Tombesi, and Sylvain Veilleux. Astrophysical limits on very light axion-like particles from Chandra grating spectroscopy of NGC 1275. *ApJ*, 890(1):59, 7 2019, hep-ph/1907.05475.

[80] M. Ajello et al. Search for Spectral Irregularities due to Photon–Axionlike-Particle Oscillations with the Fermi Large Area Telescope. *Phys. Rev. Lett.*, 116(16):161101, 2016, astro-ph/1603.06978.

[81] Mikhail V. Beznogov, Ermal Rrapaj, Dany Page, and Sanjay Reddy. Constraints on Axion-like Particles and Nucleon Pairing in Dense Matter from the Hot Neutron Star in HESS J1731-347. *Phys. Rev. C*, 98(3):035802, 2018, astro-ph/1806.07991.

[82] Núria Vinyoles, Aldo M. Serenelli, Francesco L. Villante, Sarbani Basu, Johannes Bergström, M. C. Gonzalez-Garcia, Michele Maltoni, Carlos Peña Garay, and Ningqiang Song. A new Generation of Standard Solar Models. *Astrophys. J.*, 835(2):202, 2017, astro-ph/1611.09867.

[83] Joerg Jaeckel, Eduard Masso, Javier Redondo, Andreas Ringwald, and Fuminobu Takahashi. The Need for purely laboratory-based axion-like particle searches. *Phys. Rev.*, D75:013004, 2007, hep-ph/0610203.

[84] Javier Redondo and Andreas Ringwald. Light shining through walls. *Contemp. Phys.*, 52:211–236, 2011, 1011.3741.

[85] Klaus Ehret et al. New ALPS Results on Hidden-Sector Lightweights. *Phys. Lett. B*, 689:149–155, 2010, hep-ex/1004.1313.

[86] Aaron Spector. Alps ii technical overview and status report. *arXiv preprint arXiv:1611.05863*, 2016.

[87] R. Ballou et al. New exclusion limits on scalar and pseudoscalar axionlike particles from light shining through a wall. *Phys. Rev.*, D92(9):092002, 2015, hep-ex/1506.08082.

[88] L. Maiani, R. Petronzio, and E. Zavattini. Effects of Nearly Massless, Spin Zero Particles on Light Propagation in a Magnetic Field. *Phys. Lett. B*, 175:359–363, 1986.

[89] Federico Della Valle, Aldo Ejlli, Ugo Gastaldi, Giuseppe Messineo, Edoardo Milotti, Ruggero Pengo, Giuseppe Ruoso, and Guido Zavattini. The PVLAS experiment: measuring vacuum magnetic birefringence and dichroism with a birefringent Fabry–Perot cavity. *Eur. Phys. J.*, C76(1):24, 2016, optics/1510.08052.

[90] Klaus Ehret et al. Resonant laser power build-up in ALPS: A 'Light-shining-through-walls' experiment. *Nucl. Instrum. Meth. A*, 612:83–96, 2009, ins-det/0905.4159.

[91] Stephen L. Adler, J. Gamboa, F. Mendez, and J. Lopez-Sarrion. Axions and 'Light Shining Through a Wall': A Detailed Theoretical Analysis. *Annals Phys.*, 323:2851–2872, 2008, hep-ph/0801.4739.

[92] Ariel Arza and Pierre Sikivie. Production and detection of an axion dark matter echo. *Phys. Rev. Lett.*, 123(13):131804, 2019, hep-ph/1902.00114.

[93] Ariel Arza and Elisa Todarello. The axion dark matter echo: a detailed analysis. 7 2021, hep-ph/2108.00195.

[94] V Anastassopoulos, S Aune, K Barth, A Belov, H Bräuninger, Giovanni Cantatore, JM Carmona, JF Castel, SA Cetin, F Christensen, et al. New cast limit on the axion–photon interaction. *Nature Physics*, 13(6):584, 2017.

[95] Adrian Ayala, Inma Domínguez, Maurizio Giannotti, Alessandro Mirizzi, and Oscar Straniero. Revisiting the bound on axion-photon coupling from globular clusters. *Physical review letters*, 113(19):191302, 2014.

[96] Luca Di Luzio, Federico Mescia, and Enrico Nardi. Redefining the axion window. *Physical review letters*, 118(3):031801, 2017.

[97] Akihide Nobuhiro, Yusuke Hirahara, Kensuke Homma, Yuri Kirita, Takaya Ozaki, Yoshihide Nakamiya, Masaki Hashida, Shunsuke Inoue, and Shuji Sakabe. Extended search for sub-eV axion-like resonances via four-wave mixing with a quasi-parallel laser collider in a high-quality vacuum system. *PTEP*, 2020(7):073C01, 2020, hep-ex/2004.10637.

[98] William L. Kruer. *The physics of laser plasma interactions [electronic resource]*. Boca Raton, 1st edition, 2019.

[99] J. F. Drake, P. K. Kaw, Y. C. Lee, G. Schmid, C. S. Liu, and Marshall N. Rosenbluth. Parametric instabilities of electromagnetic waves in plasmas. *Physics of Fluids*, 17(4):778–785, April 1974.

[100] Selym Villalba-Chavez and Antonino Piazza. Axion-induced birefringence effects in laser driven nonlinear vacuum interaction. *JHEP*, 11:136, 2013, hep-ph/1307.7935.

[101] H. Terças, J. D. Rodrigues, and J. T. Mendonça. Axion-plasmon polaritons in strongly magnetized plasmas. *Phys. Rev. Lett.*, 120(18):181803, 2018, hep-ph/1801.06254.

[102] J. T. Mendonça, J. D. Rodrigues, and H. Terças. Axion production in unstable magnetized plasmas. *Phys. Rev. D*, 101(5):051701, 2020, plasm-ph/1901.05910.

[103] J. T. Mendonca. Axion excitation by intense laser fields. *EPL*, 79(2):21001, 2007, hep-ph/0702091.

[104] John David Jackson. *Classical electrodynamics*. Wiley, New York ; Chichester, 3rd ed. edition, 1999.

[105] Ariel Arza. Production of massive bosons from the decay of a massless particle beam. 9 2020, hep-th/2009.03870.

[106] J. A. Armstrong, N. Bloembergen, J. Ducuing, and P. S. Pershan. Interactions between Light Waves in a Nonlinear Dielectric. *Phys. Rev.*, 127:1918–1939, 1962.

[107] Jin Woo Yoon, Yeong Gyu Kim, Il Woo Choi, Jae Hee Sung, Hwang Woon Lee, Seong Ku Lee, and Chang Hee Nam. Realization of laser intensity over 10 23 w/cm2. *Optica*, 8(5):630–635, May 2021.

[108] Colin N. Danson, Constantin Haefner, Jake Bromage, Thomas Butcher, Jean-Christophe F. Chanteloup, Enam A. Chowdhury, Almantas Galvanauskas, Leonida A. Gizzi, Joachim Hein, David I. Hillier, and et al. Petawatt and exawatt class lasers worldwide. *High Power Laser Science and Engineering*, 7:54, 2019.

[109] R. J. Shalloo, C. Arran, A. Picksley, A. von Boetticher, L. Corner, J. Holloway, G. Hine, J. Jonnerby, H. M. Milchberg, C. Thornton, R. Walczak, and

S. M. Hooker. Low-density hydrodynamic optical-field-ionized plasma channels generated with an axicon lens. *Physical Review Accelerators and Beams*, 22(4):041302, April 2019, plasm-ph/1902.05596.

[110] A. Picksley et al. Meter-Scale, Conditioned Hydrodynamic Optical-Field-Ionized Plasma Channels. *Phys. Rev. E*, 102(5):053201, 2020, acc-ph/2008.13683.

[111] Donna Strickland and Gerard Mourou. Compression of amplified chirped optical pulses. *Optics communications*, 55(6):447–449, 1985.

[112] Fritz Sauter. Uber das Verhalten eines Elektrons im homogenen elektrischen Feld nach der relativistischen Theorie Diracs. *Z. Phys.*, 69:742–764, 1931.

[113] W. Heisenberg and H. Euler. Consequences of Dirac's theory of positrons. *Z. Phys.*, 98(11-12):714–732, 1936, physics/0605038.

[114] Julian S. Schwinger. On gauge invariance and vacuum polarization. *Phys. Rev.*, 82:664–679, 1951.

[115] D. L. Burke et al. Positron production in multi - photon light by light scattering. *Phys. Rev. Lett.*, 79:1626–1629, 1997.

[116] C. Bamber et al. Studies of nonlinear QED in collisions of 46.6-GeV electrons with intense laser pulses. *Phys. Rev. D*, 60:092004, 1999.

[117] Thomas Heinzl and Anton Ilderton. A Lorentz and gauge invariant measure of laser intensity. *Opt. Commun.*, 282:1879–1883, 2009, class-ph/0807.1841.

[118] V. I. Ritus. Quantum effects in the interaction of elementary particles with an intense electromagnetic field. *Moscow Izdatel Nauka AN SSR Fizicheskii Institut Trudy*, 111:5–151, January 1979.

[119] Howard R. Reiss. Absorption of light by light. *Journal of Mathematical Physics*, 3(1):59–67, 1962, https://doi.org/10.1063/1.1703787.

[120] A. I. Nikishov and V. I. Ritus. Quantum Processes in the Field of a Plane Electromagnetic Wave and in a Constant Field 1. *Sov. Phys. JETP*, 19:529–541, 1964.

[121] B. King. Electron-seeded ALP production and ALP decay in an oscillating electromagnetic field. *Phys. Lett. B*, 782:737–743, 2018, hep-ph/1802.07507.

[122] David A. Burton and Adam Noble. Plasma-based wakefield accelerators as sources of axion-like particles. *New J. Phys.*, 20(3):033022, 2018, hep-ph/1710.01906.

[123] Barry M. Dillon and Ben King. ALP production through non-linear Compton scattering in intense fields. *Eur. Phys. J. C*, 78(9):775, 2018, hep-ph/1802.07498.

[124] B. M. Dillon and B. King. Light scalars: coherent nonlinear Thomson scattering and detection. *Phys. Rev. D*, 99(3):035048, 2019, hep-ph/1809.01356.

[125] M. Marklund and Padma Kant Shukla. Nonlinear collective effects in photon-photon and photon-plasma interactions. *Rev. Mod. Phys.*, 78:591–640, 2006, hep-ph/0602123.

[126] Holger Gies. Strong laser fields as a probe for fundamental physics. *Eur. Phys. J. D*, 55:311–317, 2009, hep-ph/0812.0668.

[127] A. Di Piazza, C. Muller, K. Z. Hatsagortsyan, and C. H. Keitel. Extremely high-intensity laser interactions with fundamental quantum systems. *Rev. Mod. Phys.*, 84:1177, 2012, hep-ph/1111.3886.

[128] A. Di Piazza and A. I. Milstein. Quasiclassical approach to high-energy QED processes in strong laser and atomic fields. *Phys. Lett. B*, 717:224–228, 2012, atom-ph/1204.2502.

[129] N. B. Narozhny and A. M. Fedotov. Extreme light physics. *Contemp. Phys.*, 56(3):249–268, 2015.

[130] E. M. Riordan et al. A Search for Short Lived Axions in an Electron Beam Dump Experiment. *Phys. Rev. Lett.*, 59:755, 1987.

[131] J. D. Bjorken, S. Ecklund, W. R. Nelson, A. Abashian, C. Church, B. Lu, L. W. Mo, T. A. Nunamaker, and P. Rassmann. Search for Neutral Metastable Penetrating Particles Produced in the SLAC Beam Dump. *Phys. Rev. D*, 38:3375, 1988.

[132] D. M. Wolkow. Uber eine Klasse von Losungen der Diracschen Gleichung. *Z. Phys.*, 94:250–260, 1935.

[133] J. Bergou and S. Varro. Wavefunctions of a free electron in an external field and their application in intense field interactions. II. Relativistic treatment. *Journal of Physics A Mathematical General*, 13(8):2823–2837, August 1980.

[134] W. H. Furry. On Bound States and Scattering in Positron Theory. *Phys. Rev.*, 81:115–124, 1951.

[135] Paul A. M. Dirac. Forms of Relativistic Dynamics. *Rev. Mod. Phys.*, 21:392–399, 1949.

[136] T. W. B. Kibble, Abdus Salam, and J. A. Strathdee. Intensity Dependent Mass Shift and Symmetry Breaking. *Nucl. Phys. B*, 96:255–263, 1975.

[137] Victor Dinu, Tom Heinzl, Anton Ilderton, Mattias Marklund, and Greger Torgrimsson. Vacuum refractive indices and helicity flip in strong-field QED. *Phys. Rev. D*, 89(12):125003, 2014, hep-ph/1312.6419.

[138] Frank W. J. Olver. *Asymptotics and special functions*. Computer science and applied mathematics. Academic Press, New York ; London, 1974.

[139] V. B Berestetskiĭ, E. M Lifshits, L. P Pitaevskiĭ, J. B Sykes, and J. S Bell. *Quantum electrodynamics [electronic resource]*. Landau, L. D. (Lev Davidovich), 1908-1968. Teoreticheskaia fizika (Izd. 2-e). English ; v. 4. Butterworth-Heinemann, Oxford, 2nd ed. edition, 1982.

[140] C. N. Harvey, A. Ilderton, and B. King. Testing numerical implementations of strong field electrodynamics. *Phys. Rev. A*, 91(1):013822, 2015, plasm-ph/1409.6187.

[141] A. Di Piazza, M. Tamburini, S. Meuren, and C. H. Keitel. Improved local-constant-field approximation for strong-field QED codes. *Phys. Rev. A*, 99(2):022125, 2019, hep-ph/1811.05834.

[142] A. Ilderton, B. King, and D. Seipt. Extended locally constant field approximation for nonlinear Compton scattering. *Phys. Rev. A*, 99(4):042121, 2019, hep-ph/1808.10339.

[143] A. M. Fedotov. Qualitative considerations in Intense Field QED. *arXiv e-prints*, page arXiv:1507.08512, July 2015, optics/1507.08512.

[144] Ruth Jacobs. LUXE: A new experiment to study non-perturbative QED in e^--laser and γ-laser collisions. In *28th International Workshop on Deep Inelastic Scattering and Related Subjects*, 7 2021, hep-ex/2107.10026.

[145] Anthony Hartin, Andreas Ringwald, and Natalia Tapia. Measuring the Boiling Point of the Vacuum of Quantum Electrodynamics. *Phys. Rev. D*, 99(3):036008, 2019, hep-ph/1807.10670.

[146] Arno A. Penzias and Robert Woodrow Wilson. A Measurement of excess antenna temperature at 4080-Mc/s. *Astrophys. J.*, 142:419–421, 1965.

[147] R. H. Dicke, P. J. E. Peebles, P. G. Roll, and D. T. Wilkinson. Cosmic Black-Body Radiation. *Astrophys. J.*, 142:414–419, 1965.

[148] Nathan J. Secrest, Sebastian von Hausegger, Mohamed Rameez, Roya Mohayaee, Subir Sarkar, and Jacques Colin. A Test of the Cosmological Principle with Quasars. *Astrophys. J. Lett.*, 908(2):L51, 2021, astro-ph/2009.14826.

[149] Roya Mohayaee, Mohamed Rameez, and Subir Sarkar. Do supernovae indicate an accelerating universe? *Eur. Phys. J. ST*, 230(9):2067–2076, 2021, astro-ph/2106.03119.

[150] Mark Trodden and Sean M. Carroll. TASI lectures: Introduction to cosmology. In *Theoretical Advanced Study Institute in Elementary Particle Physics (TASI 2002): Particle Physics and Cosmology: The Quest for Physics Beyond the Standard Model(s)*, 1 2004, astro-ph/0401547.

[151] Edwin Hubble. A relation between distance and radial velocity among extra-galactic nebulae. *Proc. Nat. Acad. Sci.*, 15:168–173, 1929.

[152] G. Steigman. Cosmology Confronts Particle Physics. *Ann. Rev. Nucl. Part. Sci.*, 29:313–338, 1979.

[153] Subir Sarkar. Big bang nucleosynthesis and physics beyond the standard model. *Rept. Prog. Phys.*, 59:1493–1610, 1996, hep-ph/9602260.

[154] L. D Landau, E. M Lifshits, L. P Pitaevskiĭ, J. B Sykes, and M. J. Kearsley. *Statistical physics. Volume 5 of Course of theoretical physics. Part 1 [electronic resource].* Landau, L. D. (Lev Davidovich), 1908-1968. Teoreticheskaia fizika (Izd. 3-e). English ; v. 5. Oxford, England ; New York, third edition, revised and enlarged / by e.m. lifshitz and l.p. pitaevskii. edition, 1980.

[155] E. R. Harrison. Standard model of the early universe. *Ann. Rev. Astron. Astrophys.*, 11:155–186, 1973.

[156] C. L. Bennett, D. Larson, J. L. Weiland, N. Jarosik, G. Hinshaw, N. Odegard, K. M. Smith, R. S. Hill, B. Gold, M. Halpern, E. Komatsu, M. R. Nolta, L. Page, D. N. Spergel, E. Wollack, J. Dunkley, A. Kogut, M. Limon, S. S. Meyer, G. S. Tucker, and E. L. Wright. Nine-year Wilkinson Microwave Anisotropy Probe (WMAP) Observations: Final Maps and Results. *The Astrophysical Journal Supplement Series*, 208(2):20, October 2013, astro-ph/1212.5225.

[157] N. Aghanim et al. Planck 2018 results. V. CMB power spectra and likelihoods. *Astron. Astrophys.*, 641:A5, 2020, astro-ph/1907.12875.

[158] Daniel Baumann. Inflation. In *Theoretical Advanced Study Institute in Elementary Particle Physics: Physics of the Large and the Small*, 7 2009, hep-th/0907.5424.

[159] Daniel Baumann. Primordial Cosmology. *PoS*, TASI2017:009, 2018, hep-th/1807.03098.

[160] Richard Lynn Davis. Cosmic Axions from Cosmic Strings. *Phys. Lett. B*, 180:225–230, 1986.

[161] Alexander Vilenkin and Tanmay Vachaspati. Radiation of Goldstone Bosons From Cosmic Strings. *Phys. Rev. D*, 35:1138, 1987.

[162] R. L. Davis and E. P. S. Shellard. DO AXIONS NEED INFLATION? *Nucl. Phys. B*, 324:167–186, 1989.

[163] Diego Harari and P. Sikivie. On the Evolution of Global Strings in the Early Universe. *Phys. Lett. B*, 195:361–365, 1987.

[164] C. Hagmann and P. Sikivie. Computer simulations of the motion and decay of global strings. *Nucl. Phys. B*, 363:247–280, 1991.

[165] Marco Gorghetto, Edward Hardy, and Giovanni Villadoro. More axions from strings. *SciPost Phys.*, 10(2):050, 2021, hep-ph/2007.04990.

[166] Sanghyeon Chang, C. Hagmann, and P. Sikivie. Studies of the motion and decay of axion walls bounded by strings. *Phys. Rev. D*, 59:023505, 1999, hep-ph/9807374.

[167] Michael Dine, Nicolas Fernandez, Akshay Ghalsasi, and Hiren H. Patel. Comments on Axions, Domain Walls, and Cosmic Strings. 12 2020, hep-ph/2012.13065.

[168] Peter W. Graham and Adam Scherlis. Stochastic axion scenario. *Phys. Rev. D*, 98(3):035017, 2018, hep-ph/1805.07362.

[169] Fuminobu Takahashi, Wen Yin, and Alan H. Guth. QCD axion window and low-scale inflation. *Phys. Rev. D*, 98(1):015042, 2018, hep-ph/1805.08763.

[170] T W B Kibble. Topology of cosmic domains and strings. *Journal of Physics A: Mathematical and General*, 9(8):1387–1398, aug 1976.

[171] A. Vilenkin and A. E. Everett. Cosmic Strings and Domain Walls in Models with Goldstone and PseudoGoldstone Bosons. *Phys. Rev. Lett.*, 48:1867–1870, 1982.

[172] Alexander Vilenkin. Cosmic Strings and Domain Walls. *Phys. Rept.*, 121:263–315, 1985.

[173] T. W. B. Kibble. Some Implications of a Cosmological Phase Transition. *Phys. Rept.*, 67:183, 1980.

[174] W. H. Zurek. Cosmological Experiments in Superfluid Helium? *Nature*, 317:505–508, 1985.

[175] W. H. Zurek. Cosmological experiments in condensed matter systems. *Phys. Rept.*, 276:177–221, 1996, cond-mat/9607135.

[176] P. Sikivie. Of Axions, Domain Walls and the Early Universe. *Phys. Rev. Lett.*, 48:1156–1159, 1982.

[177] M. C. Huang and P. Sikivie. The Structure of Axionic Domain Walls. *Phys. Rev. D*, 32:1560, 1985.

[178] Ya. B. Zeldovich, I. Yu. Kobzarev, and L. B. Okun. Cosmological Consequences of the Spontaneous Breakdown of Discrete Symmetry. *Zh. Eksp. Teor. Fiz.*, 67:3–11, 1974.

[179] Pierre Sikivie. Axion Cosmology. *Lect. Notes Phys.*, 741:19–50, 2008, astro-ph/0610440.

[180] Alexei A. Starobinsky. Dynamics of Phase Transition in the New Inflationary Universe Scenario and Generation of Perturbations. *Phys. Lett.*, 117B:175–178, 1982.

[181] Alexei A. Starobinsky. *Field Theory, Quantum Gravity and Strings*, volume 1 of *246*. Springer-Verlag Berlin Heidelberg, 1 edition, 1986. Proceedings of a Seminar Series Held at DAPHE, Observatoire de Meudon, and LPTHE, Université Pierre et Marie Curie, Paris, Between October 1984 and October 1985.

[182] Zygmunt Lalak and Steven Thomas. Domain wall formation in the postinflationary universe. *Phys. Lett.*, B306:10–18, 1993, hep-ph/9303250.

[183] Alexei A. Starobinsky and Jun'ichi Yokoyama. Equilibrium state of a self-interacting scalar field in the de sitter background. *Phys. Rev. D*, 50:6357–6368, Nov 1994.

[184] Horacio Casini and Subir Sarkar. No cosmological domain wall problem for weakly coupled fields. *Phys. Rev.*, D65:025002, 2002, hep-ph/0106272.

[185] D. Coulson, Z. Lalak, and Burt A. Ovrut. Biased domain walls. *Phys. Rev. D*, 53:4237–4246, 1996.

[186] Sebastian E. Larsson, Subir Sarkar, and Peter L. White. Evading the cosmological domain wall problem. *Phys. Rev.*, D55:5129–5135, 1997, hep-ph/9608319.

[187] Mark Hindmarsh. Analytic scaling solutions for cosmic domain walls. *Phys. Rev. Lett.*, 77:4495–4498, 1996, hep-ph/9605332.

[188] Mark Hindmarsh. Level set method for the evolution of defect and brane networks. *Phys. Rev.*, D68:043510, 2003, hep-ph/0207267.

[189] Andrei D. Linde and David H. Lyth. Axionic domain wall production during inflation. *Phys. Lett. B*, 246:353–358, 1990.

[190] Gia Dvali, Cesar Gomez, and Sebastian Zell. A Proof of the Axion? 11 2018, hep-th/1811.03079.

[191] Gia Dvali and Cesar Gomez. Quantum Compositeness of Gravity: Black Holes, AdS and Inflation. *JCAP*, 01:023, 2014, hep-th/1312.4795.

[192] Gia Dvali and Cesar Gomez. Quantum Exclusion of Positive Cosmological Constant? *Annalen Phys.*, 528:68–73, 2016, hep-th/1412.8077.

[193] Gia Dvali, Cesar Gomez, and Sebastian Zell. Quantum Break-Time of de Sitter. *JCAP*, 06:028, 2017, hep-th/1701.08776.

[194] Marc Kamionkowski and John March-Russell. Planck scale physics and the Peccei-Quinn mechanism. *Phys. Lett. B*, 282:137–141, 1992, hep-th/9202003.

[195] Gerard 't Hooft. Magnetic Monopoles in Unified Gauge Theories. *Nucl. Phys. B*, 79:276–284, 1974.

[196] Alexander M. Polyakov. Particle Spectrum in Quantum Field Theory. *JETP Lett.*, 20:194–195, 1974.

[197] Edward Witten. Dyons of Charge e theta/2 pi. *Phys. Lett. B*, 86:283–287, 1979.

[198] Paul Adrien Maurice Dirac. Quantised singularities in the electromagnetic field,. *Proc. Roy. Soc. Lond. A*, 133(821):60–72, 1931.

[199] Daniel Zwanziger. Quantum field theory of particles with both electric and magnetic charges. *Phys. Rev.*, 176:1489–1495, 1968.

[200] Julian S. Schwinger. Magnetic charge and quantum field theory. *Phys. Rev.*, 144:1087–1093, 1966.

[201] Julian S. Schwinger. Sources and magnetic charge. *Phys. Rev.*, 173:1536–1544, 1968.

[202] Frank Wilczek. Remarks on Dyons. *Phys. Rev. Lett.*, 48:1146, 1982.

[203] Curtis G. Callan, Jr. Dyon-Fermion Dynamics. *Phys. Rev. D*, 26:2058–2068, 1982.

[204] Willy Fischler and John Preskill. DYON - AXION DYNAMICS. *Phys. Lett. B*, 125:165–170, 1983.

[205] Paul Langacker and So-Young Pi. Magnetic Monopoles in Grand Unified Theories. *Phys. Rev. Lett.*, 45:1, 1980.

[206] Yasunori Nomura, Surjeet Rajendran, and Fabio Sanches. Axion Isocurvature and Magnetic Monopoles. *Phys. Rev. Lett.*, 116(14):141803, 2016, 1511.06347.